



McGill

Faculty of
Dentistry

**Mechanistic Studies on MGP-Deficient Mice: A Model
for Keutel Syndrome**

Juliana Marulanda Montoya

Faculty of Dentistry

McGill University

Montreal, Canada

A thesis submitted to McGill University in partial fulfillment of the requirements of
the degree of Doctor of Philosophy in Craniofacial Health Sciences

© **Juliana Marulanda Montoya 2018**

Dedication

I dedicate this thesis to my husband Pablo, for his unconditional support, love and endless trust in me. And to my son Samuel; I could not have asked for better company and motivation while writing this thesis.

Acknowledgments

First, I would like to express my most sincere gratitude to my supervisor Dr. Monzur Murshed for been a great mentor to me. I immensely admire his dedication, commitment toward his students and most of all, devotion to science. Your example inspires me every day. Thank you for showing me the path towards science, I will be forever grateful.

My gratitude goes to my co-supervisor Dr. Elaine C. Davis and supervisory committee members Dr. Svetlana Komarova, Dr. Dieter Reinhardt and Dr. John Mort for their suggestions and encouragement. Also, I would like to thank the current and past colleagues from Murshed's lab for their support, memories and friendship, especially Dr. Jingjing Li, Garthiga Manickam, Abhinav Parashar, Awatef Enagrat, Haitham AlQuorain, Zohreh Khavandgar and Sharifa Alebrahim.

I would also like to thank other colleges that helped me during this time, especially Ophélie Gourgas for our productive collaborations, to Marin Pellicelli for his training and troubleshooting in micro-CT, Kaushar Jahan for translating the abstract to French and Mark Lepik for his enthusiastic help in generating beautiful images.

My appreciation goes to the Shriners Hospital for Children's staff for making my days better, for your help when needed and for your daily smiles. Especial thanks to the animal facility technicians Mia Esser and Louise Marineau, your work is impeccable.

Also, I would like to thank my "Faculty of Dentistry" friends Betty Hoac, Valerie Khayat, Iris Boraschi, Dimitra Athanasiadou and Hadil Al-Jallad for making this journey even more enjoyable, and Maria Palumbo for her continuous help throughout these years.

Lastly, I want to thank my parents for their unconditional love, for supporting every decision I make and for always believing in me. What I am now is thanks to you both. And to my husband for been the best friend in this crazy ride, I simply couldn't have done it without you, and of course, for giving me the best graduation present I could have ever asked, my son.

Table of Contents

Dedication -----	2
Acknowledgments -----	3
List of figures and tables -----	9
List of abbreviations -----	10
Abstract -----	14
Resumé -----	16
Contribution of authors -----	19
Chapter 1: -----	22
General Introduction and Literature Review -----	22
1.1. Keutel syndrome -----	23
1.2. Matrix Gla Protein -----	23
<i>1.2.1. Protein description and post-translational modifications</i> -----	<i>23</i>
1.3. MGP-deficient mouse model -----	25
<i>1.4.1. Key determinants of ECM mineralization</i> -----	<i>30</i>
<i>1.4.2. Mechanisms of vascular calcification</i> -----	<i>38</i>
<i>1.4.3. Vascular calcification in human pathology</i> -----	<i>41</i>
1.5. Bone development and remodeling -----	45
<i>1.5.1. Skeletal development is a multi-step process</i> -----	<i>45</i>
<i>1.5.2. Current understanding of skeletal ECM mineralization</i> -----	<i>46</i>
<i>1.5.3. Bone remodeling</i> -----	<i>47</i>
<i>1.5.4. Matrix Gla protein in the skeletal tissues</i> -----	<i>50</i>
<i>1.5.5. Vascular calcification and osteoporosis</i> -----	<i>51</i>
1.6. Craniofacial development -----	52
<i>1.6.1 Development of the facial skeleton</i> -----	<i>53</i>
<i>1.6.2. Midface hypoplasia</i> -----	<i>55</i>
<i>1.6.3. Chondrocranium and craniofacial growth</i> -----	<i>57</i>
1.7. Rational, overall goal and aims of the current thesis -----	58
<i>1.7.1. Overall goal</i> -----	<i>58</i>
<i>1.7.2. Specific aims</i> -----	<i>58</i>
Chapter 2: -----	59
Vascular Calcification in MGP-Deficient Mice: A Phosphate and Elastin Story -----	59
2.1. Abstract -----	61
2.2. Introduction -----	62
2.3. Results -----	66

2.3.1. Ablation of <i>Smpd3</i> in <i>Mgp</i> ^{-/-} VSMCs does not prevent vascular calcification in vivo -----	66
2.3.2. Increased circulating FGF23 corrects the vascular calcification phenotype in <i>Mgp</i> ^{-/-} mice-----	67
2.3.3. A high phosphorus diet induces rapid vascular calcification in <i>Mgp</i> ^{-/-} ; <i>ApoE-Fgf23</i> mice -----	68
2.3.4. Comparative analyses of arterial elastin content in compound models expressing mouse and human elastin orthologs -----	68
2.3.5. Arterial mineral deposition is affected by elastin content, but not by ortholog combination -----	69
2.3.6. Prevention of vascular calcification in <i>Mgp</i> ^{-/-} ; <i>Eln</i> ^{-/-} ; <i>ELN</i> ^{+/+} mice -----	70
2.3.7. Mineral characterization in the aged <i>Mgp</i> ^{-/-} ; <i>Eln</i> ^{-/-} ; <i>ELN</i> ^{+/+} mice -----	71
2.4. Discussion -----	73
2.5. Materials and methods -----	82
2.5.1. Mouse models -----	82
2.5.2. Genotyping PCR-----	82
2.5.3. Micro-CT and mineral quantification-----	82
2.5.4. Histology and tissue imaging -----	83
2.5.5. Gene expression analysis -----	83
2.5.6. Serum biochemistry -----	84
2.5.7. Tissue biochemistry -----	84
2.5.8. Skeletal preparations-----	85
2.5.9. Raman spectroscopy -----	85
2.5.10. Scanning electron microscopy (SEM) and energy-dispersive X-ray spectroscopy (EDS)-----	85
2.6. Data analysis -----	86
2.7. Acknowledgements -----	86
Chapter 3: -----	95
Prevention of Arterial Calcification Corrects the Low Bone Mass Phenotype in MGP-Deficient Mice ----	95
3.1. Abstract -----	97
3.2. Introduction -----	98
3.3. Results -----	101
3.3.1. MGP deficiency leads to a low bone mass phenotype-----	101
3.3.2. Impaired osteoblast function in <i>Mgp</i> ^{-/-} mice-----	101
3.3.3. Abnormal vasculature in <i>Mgp</i> ^{-/-} bones -----	102
3.3.4. Early differentiation markers are normal in <i>Mgp</i> ^{-/-} osteoblasts -----	102
3.3.5. Restoration of <i>Mgp</i> expression in VSMCs normalizes bone mass in <i>Mgp</i> ^{-/-} ; <i>SM22-Mgp</i> mice -----	103
3.3.6. Prevention of arterial calcification independent of <i>Mgp</i> expression corrects the low bone mass phenotype in <i>Mgp</i> ^{-/-} ; <i>Eln</i> ^{+/-} mice -----	104
3.4. Discussion -----	105
3.5. Materials and methods -----	109

3.5.1. Mice	109
3.5.2. Primary osteoblast culture	109
3.5.3. Alkaline phosphatase and Alamar blue reduction assay	109
3.5.4. Quantification of <i>in vitro</i> mineralization	110
3.5.5. Gene expression analysis	110
3.5.6. Micro-CT analysis	111
3.5.7. Histomorphometric analysis	112
3.5.8. Serum analysis	112
3.6. Data analysis	113
3.7. Acknowledgments	113
Chapter 4:	122
Matrix Gla Protein Deficiency Impairs Nasal Septum Growth, Causing Midface Hypoplasia	122
4.1. Abstract	124
4.2. Introduction	125
4.3. Results	128
4.3.1. <i>Mgp</i> deficiency causes midface hypoplasia	128
4.3.2. Ectopic calcification of the cartilaginous nasal septum in MGP-deficient mice	129
4.3.3. Local expression of MGP in the cartilage corrects midface hypoplasia in MGP-deficient mice	130
4.3.4. MGP-deficient mice have a shorter nasal septum with apoptotic chondrocytes	131
4.3.5. Chondrocyte hypertrophy is not a prerequisite for nasal septum calcification in MGP-deficient mice	132
4.3.6. Amorphous calcium phosphate as a main mineral species in MGP-deficient nasal septum	133
4.3.7. Prevention of nasal septum mineralization in <i>Mgp</i> ^{-/-} ; <i>Hyp</i> mice	133
4.4. Discussion	135
4.5. Materials and methods	142
4.5.1. Mice	142
4.5.2. Skeletal preparation	142
4.5.3. Radiography and X-ray micro-computer tomography (micro-CT)	143
4.5.4. Cephalometric analysis	143
4.5.5. Histology and tissue imaging	143
4.5.6. TUNEL assay	144
4.5.7. Alkaline phosphatase activity	144
4.5.8. X-gal staining	145
4.5.9. Gene expression analysis	145
4.5.10. Electron microscopy	146
4.5.11. Electron diffraction	146

4.5.12. X-ray diffraction-----	146
4.6. Data analysis -----	147
4.7. Acknowledgements-----	147
Chapter 5:-----	158
General Discussion -----	158
5.1. General discussion -----	159
5.2. Implications and Future directions -----	170
Conclusion -----	174
References -----	175
Appendix I: Other papers published -----	189

List of figures and tables

Figure 1.1. Vitamin K-dependent γ -glutamyl carboxylation cycle.....	25
Figure 1.2. Intima vs media aortic calcification	27
Figure 1.3. Key determinants and the current understanding of the mechanisms of vascular calcification	29
Figure 1.4. Determinants of bone mineralization	46
Figure 1.5. Bone remodeling.....	50
Figure 1.6. Nasal septum and related anatomical structures	54
Table 1.1. Developmental diseases associated with midface hypoplasia.....	56
Figure 2.1. Ablation of <i>Smpd3</i> in <i>Mgp</i> ^{-/-} VSMCs does not prevent vascular calcification in vivo.....	87
Figure 2.2. Increased circulating FGF23 corrects the vascular calcification phenotype in <i>Mgp</i> ^{-/-} mice.....	89
Figure 2.3. A high phosphorus diet induces rapid vascular calcification in <i>Mgp</i> ^{-/-} ; <i>ApoE</i> - <i>Fgf23</i> mice.....	90
Figure 2.4. Comparative analyses of arterial elastin content in compound models expressing mouse and human elastin orthologs.	91
Figure 2.5. Arterial mineral deposition is affected by elastin content, but not by ortholog combination.....	92
Figure 2.6. Prevention of vascular calcification in <i>Mgp</i> ^{-/-} ; <i>Eln</i> ^{-/-} ; <i>ELN</i> ^{+/+} mice.....	93
Figure 2.7. Mineral characterization in the aged <i>Mgp</i> ^{-/-} ; <i>Eln</i> ^{-/-} ; <i>ELN</i> ^{+/+} mice.....	94
Figure 3.1. MGP deficiency leads to a low bone mass phenotype.....	114
Figure 3.2. Osteoblast function is affected in <i>Mgp</i> ^{-/-} mice.....	115
Figure 3.3. Abnormal vasculature in <i>Mgp</i> ^{-/-} bones	116
Figure 3.4. Early differentiation markers are normal in <i>Mgp</i> ^{-/-} osteoblasts.....	117
Figure 3.5. Restoration of <i>Mgp</i> expression in the arteries of <i>Mgp</i> ^{-/-} ; <i>SM22</i> - <i>Mgp</i> mice rescues the low bone mass phenotype.....	119
Figure 3.6. <i>Eln</i> haploinsufficiency delaying arterial calcification significantly improves bone mass in <i>Mgp</i> ^{-/-} ; <i>Eln</i> ^{+/-} mice	121
Figure 4.1. Ablation of <i>Mgp</i> , but not <i>Bglap</i> causes craniofacial malformations.....	148
Figure 4.2. MGP deficiency causes midface hypoplasia.....	149
Figure 4.3. Ectopic calcification of the cartilaginous nasal septum in MGP-deficient mice.....	150
Figure 4.4. Progressive ectopic mineralization of MGP-deficient nasal septum.....	151
Figure 4.5. Local expression of <i>Mgp</i> in the cartilage corrects the midface hypoplasia in MGP-deficient mice.....	152
Figure 4.6. MGP-deficient mice have a shorter nasal septum.....	153
Figure 4.7. MGP-deficient septal chondrocytes undergo apoptosis	154
Figure 4.8. Chondrocyte hypertrophy is not a prerequisite for ectopic mineralization of the nasal septum in MGP-deficient mice.....	155
Figure 4.9. Amorphous calcium phosphate as main mineral species in MGP-deficient nasal septum.....	156
Figure 4.10. Prevention of nasal septum mineralization in <i>Mgp</i> ^{-/-} ; <i>Hyp</i> mice.....	157

List of abbreviations

ABVG: Alcian blue - Van Gieson

ACP: Amorphous calcium phosphate

ALPL: Alkaline phosphatase

BAC: Bacterial artificial chromosome

BFR/BS: Bone formation rate over bone surface

BGLAP: Bone Gla protein

BMD: Bone mineral density

BV/TV: Bone volume over tissue volume

Ca²⁺: Calcium

CHA: Carbonated hydroxyapatite

CKD: Chronic kidney disease

ECM: Extracellular matrix

EDS: Energy-dispersive X-ray spectroscopy

ELN: Elastin

ESRG: End-stage renal disease

FGF23: Fibroblast growth factor 23

GACI: Generalized arterial calcification of Infancy

GGCX: γ -glutamyl carboxylase

HA: Hydroxyapatite

ISS: Intersphenoidal synchondrosis

MAPKs: Mitogen activated protein kinases

MAR: Mineral apposition rate

MGP: Matrix Gla protein

Micro-CT: Micro-computed tomography

MSCs: Mesenchymal stem cells

MVs: Matrix vesicles

NEXAF: Near-edge X-ray absorption fine structure spectroscopy

NFATc1: Nuclear factor of activated T-cells cytoplasmic 1

NF- κ B: Nuclear factor - κ B

Ob/B.Pm: Osteoblasts per bone perimeter

Ob/T.Ar: Osteoblasts per tissue area

Oc/B.Pm: Osteoclasts per bone perimeter

OCP: Octacalcium phosphate

OPG: Osteoprotegerin

OPN: Osteopontin

PHEX: Phosphate-regulating gene with homologies to endopeptidases on the X chromosome

P_i: Inorganic phosphate

PP_i: Pyrophosphate

qRT-PCR: Quantitative real-time PCR

RANKL: Receptor activator of NF-κB ligand

SEM: Scanning electron microscopy

SMPD3: Sphingomyelin phosphodiesterase 3

SOS: Spheno-occipital synchondrosis

TB: Toluidine blue

TEM: Transmission electron microscopy

TNRF: Tumor necrosis factor receptor

TRAP: Tartrate resistant acid phosphatase

VKORC1: Vitamin K epoxide reductase

VKVG: von Kossa and van Gieson

VSMCs: Vascular smooth muscle cells

XPS: X-Ray photoelectron Spectroscopy

Abstract

Matrix Gla protein (MGP) is an extracellular matrix (ECM) protein with a potent anti-mineralization function, it is highly expressed in chondrocytes and vascular smooth muscle cells (VSMCs). Genetic mutations in *MGP* lead to Keutel syndrome, a rare autosomal disorder hallmarked by ectopic cartilage calcification, midface hypoplasia, peripheral pulmonary stenosis and vascular calcification. The *Mgp*^{-/-} mice recapitulate the phenotypic traits of Keutel syndrome, albeit with a more severe vascular calcification phenotype. Although MGP is one of the most potent inhibitors of ectopic calcification *in vivo*, the molecular mechanisms of its mode of action are still unknown. Here, we investigated the epistatic effects of several genetic regulators of ECM mineralization on the vascular calcification phenotype of *Mgp*^{-/-} mice. We show that transgenic augmentation of circulating fibroblast growth factor 23 (FGF23), a phosphaturic hormone, prevents the vascular calcification caused by MGP deficiency. Using a humanized mouse model, we showed that a 40% reduction of medial content of elastin, a protein abundant in the arterial media, completely prevented vascular calcification in *Mgp*^{-/-} mice until 3 weeks of age. These findings demonstrate that the severity of medial calcification in MGP-deficient mice depends on the serum phosphate levels and the elastin content in the arterial walls. Also, we observed a progressive loss of body weight in *Mgp*^{-/-} mice. Considering the paradigm linking metabolic regulators of energy metabolism and body mass to that of bone remodeling, we studied the bone volume in *Mgp*^{-/-} mice. We noticed a decrease of bone volume in *Mgp*^{-/-} mice caused by an impaired osteoblast function. We examined whether the prevention of arterial calcification in *Mgp*^{-/-} mice could correct the low bone mass phenotype. The bone mass of two different genetic models: *Mgp*^{-/-};*SM22-Mgp* and *Mgp*^{-/-};*Eln*^{+/-} mice were examined. In the former strain, vascular calcification was fully rescued by transgenic restoration of *Mgp* in the VSMCs, while in the latter, elastin haploinsufficiency significantly impeded the deposition of minerals in the arterial walls. In both

models, the low bone mass phenotype seen in *Mgp*^{-/-} mice was rescued. Our data support the hypothesis that the arterial calcification, not MGP deficiency itself, is the primary cause of the low bone mass phenotype in *Mgp*^{-/-} mice, and provides evidence that arterial calcification affects bone remodeling. Lastly, we studied the craniofacial phenotype in *Mgp*^{-/-} mice. Our comparative cephalometric analyses revealed a severe midface hypoplasia in *Mgp*^{-/-} mice. *In vivo* reporter studies demonstrated that the *Mgp* promoter is highly active at the cranial sutures, cranial base synchondroses and nasal septum. We found the nasal septum to be abnormally mineralized and shortened in *Mgp*^{-/-} mice. Transgenic restoration of *Mgp* expression in chondrocytes fully corrected the craniofacial anomalies caused by MGP deficiency, suggesting a local role for MGP in the developing nasal septum. Of note, systemic reduction of inorganic phosphate level was sufficient to prevent abnormal mineralization of the nasal septum in *Mgp*^{-/-};*Hyp* compound mutants. Our work provides evidence that modulation of local and systemic factors regulating ECM mineralization can be possible therapeutic strategies to prevent ectopic cartilage calcification and some forms of congenital craniofacial anomalies in humans.

As a whole, our mechanistic studies to investigate the phenotypic traits of MGP-deficient mice have provided a deeper understanding of the pathophysiology of Keutel syndrome. This knowledge will be useful to further understand the general mechanism soft tissue calcification in humans and may serve as a basis for the novel therapeutic approaches to prevent its initiation and/or progression.

Resumé

Protéine Gla de la matrice (MGP) est une protéine de la matrice extracellulaire (MEC) ayant une fonction d'anti-minéralisation. Elle est fortement exprimée dans les chondrocytes et les cellules musculaires lisses vasculaires (CMLV). Des mutations génétiques de *MGP* se manifestent par le syndrome de Keutel, une maladie génétique rare transmise sur le mode autosomique. Cette maladie est caractérisée par une calcification diffuse des cartilages, une dysmorphie faciale, des sténoses des branches périphériques de l'artère pulmonaire et une calcification vasculaire. Les souris *Mgp*^{-/-} présentent le même phénotype que le syndrome de Keutel, avec toutefois un niveau de calcification vasculaire plus élevé. Bien que MGP soit l'un des inhibiteurs les plus puissants de la calcification ectopique *in vivo*, les mécanismes moléculaires de son mode d'action sont encore inconnus. Nous avons étudié les effets épistatiques de plusieurs régulateurs génétiques de la minéralisation de la MEC sur le phénotype de la calcification vasculaire des souris *Mgp*^{-/-}. Nous démontrons ici que l'augmentation transgénique d'une hormone phosphaturique circulante, le facteur de croissance des fibroblastes 23 (FGF23), prévient la calcification vasculaire causée par une déficience en MGP. En utilisant un modèle de souris humanisé, nous avons prouvé qu'une réduction de 40% en élastine, une protéine abondante dans les milieux artériels, empêchait complètement la calcification vasculaire chez les souris *Mgp*^{-/-} jusqu'à l'âge de 21 jours. Ces résultats démontrent que la sévérité de la calcification médiale chez les souris déficientes en MGP dépend des taux de phosphate sérique et de la teneur en élastine dans les parois artérielles. De plus, nous avons observé une perte progressive de poids corporel chez les souris *Mgp*^{-/-}. Considérant le modèle reliant les régulateurs métaboliques du métabolisme énergétique et de la masse corporelle à celui du remodelage osseux, nous avons étudié le volume osseux chez les souris *Mgp*^{-/-}. Nous avons remarqué une diminution du volume osseux chez les souris *Mgp*^{-/-} causée par une altération de la fonction des ostéoblastes. Nous avons examiné si la prévention de la

calcification artérielle chez les souris *Mgp*^{-/-} pouvait corriger le phénotype de la faible masse osseuse. Les masses osseuses de deux différents modèles génétiques, des souris *Mgp*^{-/-};*SM22-Mgp* et *Mgp*^{-/-};*Eln*^{+/-}, ont été comparées. Dans la première lignée, la calcification vasculaire a été entièrement préservée par la restauration transgénique de *Mgp* dans les CMLV, tandis que dans la seconde, l'haploinsuffisance en élastine a empêché de manière significative le dépôt de minéraux dans les parois artérielles. Dans les deux modèles, le phénotype de faible masse osseuse observé chez les souris *Mgp*^{-/-} a été corrigé. Nos données soutiennent l'hypothèse que la calcification artérielle, et non pas la carence en MGP, est la principale cause du phénotype de la faible masse osseuse chez les souris *Mgp*^{-/-} et fournit aussi des preuves que la calcification artérielle affecte le remodelage osseux. Enfin, nous avons étudié le phénotype crâniofacial des souris *Mgp*^{-/-}. Nos analyses comparatives céphalométriques ont révélé une sévère hypoplasie faciale médiane chez les souris *Mgp*^{-/-}. Les études *in vivo* du gène rapporteur ont démontré que le promoteur *Mgp* est très actif au niveau des sutures crâniennes, des synchondroses à base crânienne et de la cloison nasale. Nous avons constaté que la cloison nasale était anormalement minéralisée et raccourcie chez les souris *Mgp*^{-/-}. La restauration transgénique de l'expression de *Mgp* dans les chondrocytes a complètement corrigé les anomalies craniofaciales causées par une déficience en MGP, suggérant un rôle local pour la MGP dans le septum nasal pendant le développement. Il est important de noter que la réduction systémique du taux de phosphate inorganique était suffisante pour empêcher la minéralisation anormale de la cloison nasale chez les mutants du composé *Mgp*^{-/-};*Hyp*. Notre recherche prouve que la modulation des facteurs locaux et systémiques régulant la minéralisation de la MEC peut être une stratégie thérapeutique pour prévenir la calcification du cartilage ectopique et certaines formes d'anomalies craniofaciales congénitales chez l'humain. Dans l'ensemble, nos études sur les traits phénotypiques des souris déficientes en MGP ont permis de mieux comprendre la physiopathologie du syndrome de Keutel. Cette connaissance sera utile pour mieux comprendre le mécanisme général de la calcification des tissus mous chez l'humain et pourra servir de

base aux nouvelles approches thérapeutiques pour prévenir l'initiation et/ou la progression de la calcification des tissus mous.

Contribution of authors

Chapter 1:

- **Marulanda J**, Alqarni S, Murshed M. Mechanisms of Vascular Calcification and Associated Diseases. *Curr Pharm Des.* 2014; 20(37):5801-10

Marulanda J: Prepared the initial draft of the review paper

Alqarni S: Performed literature search for the paper and proof read

Murshed M: Organized the sections, corrected the text and approved the final version

- **Marulanda J**, Murshed M. Role of Matrix Gla protein in midface development: Recent Advances. *Oral Diseases*, (Accepted). DOI: 10.1111/odi.12758

Marulanda J: Prepared the initial draft of the review paper

Murshed M: Approved the final version

Chapter 2:

- **Marulanda J**, Parashar A, Gourgas O, Bai X, Karaplis AC, Mecham R, Cerruti M, Brinckmann J Murshed M. Vascular calcification in MGP-deficient mice: A phosphate and elastin story. Unpublished

Marulanda J: Contributed to the research experimental design, conducted experiments, analyzed data, and prepared the manuscript

Parashar A: Conducted experiments, analyzed data, and prepared the manuscript

Gourgas O: Performed mineral characterization, and contributed to writing

Bai X: Contributed to the generation of *ApoE-Fgf23* mice

Karaplis AC: Provided the *ApoE-Fgf23* mice

Mecham R: Provided the *Eln-/-;ELN+/+* mice

Cerruti M: Supervised O. Gourgas for mineral characterization

Brinckmann J: Performed amino acid analysis

Murshed M: Contributed to the research experimental design, conducted experiments, analyzed data, and approved the final version of the manuscript

Chapter 3:

- **Marulanda J,** Gao C, Roman H, Henderson J, Murshed M. Prevention of arterial calcification corrects the low bone mass phenotype in MGP-deficient mice. *Bone*. 2013 Dec;57(2):499-508

Marulanda J: Contributed to the research experimental design, conducted experiments, analyzed data, and prepared the manuscript.

Gao C: Generated the micro-CT data

Henderson J: Contributed to micro-CT data and

Murshed M: Contributed to the research experimental design, conducted experiments, analyzed data, and approved the final version of the manuscript

Chapter 4:

- **Marulanda J,** Eimar H, McKee M, Berkvens M, Nelea V, Roman H, Borrás T, Tamimi F, Ferron M, Murshed M. Matrix Gla Protein Deficiency Impairs Nasal Septum Development Causing Midface Hypoplasia. *The Journal of Biological Chemistry*. 2017; 292(27):11400-11412

Marulanda J: Contributed to the research experimental design, conducted experiments, analyzed data, and prepared the manuscript

Eimar H: Performed the initial micro-CT scans and cephalometric analysis

McKee M.D: Conducted the EM, mineral characterization experiments and contributed to manuscript preparation

Berkvens M: Contributed to the analysis of the phenotype of *Mgp*^{-/-};*Col2a1-Mgp* mice

Nelea V: Conducted mineral characterization experiments and proofread the manuscript

Roman H: Generated the *Col2a1-Mgp* mice

Borrás T: Generated the *Mgp-Cre;Gtrosa6tm1Sor* mice

Tamimi F: Contributed to the micro-CT analyses and proofread the manuscript

Ferron M: Provided the *Bglap*^{-/-} mice and contributed to the experimental design

Murshed M: Contributed to the research experimental design, conducted experiments, analyzed data and prepared the final version of the manuscript

Chapter 1:

General Introduction and Literature Review

1.1. Keutel syndrome

In 1972, Keutel J. described the first case of Keutel syndrome as an autosomal recessive syndrome with peripheral pulmonary stenosis, brachytelephalangism, neural hearing loss and abnormal cartilage calcification/ossification [1]. Later, in 1984, Fryns *et al* described a 13 year old girl with the exact same phenotype, confirming the existence of Keutel syndrome with a probable autosomal recessive inheritance as stated before [2].

Munroe, in 1999 through a genome search using homozygosity mapping in two consanguineous families of Turkish origin identified *MGP* as the candidate gene. Then, mutational analysis of *MGP* was performed on genomic DNA from the probands and their families, identifying mutations that predict an absent or non-functional MGP [3]. Further characterization of new probands identified a typical facial appearance described as midface hypoplasia, subnormal IQ, repeated respiratory infections and otitis media. Long-term follow up of Keutel syndrome patients revealed mainly complications involving the respiratory system. Also, permanent skin rashes, asthma, severe arterial hypertension and short memory loss have been reported [4].

Post-mortem examination of two siblings revealed concentric calcification of coronary, pulmonary, hepatic, renal, meningeal and cerebral arteries [5]. Later, the first case of aortic calcification was reported in a 6-year old female patient [6].

1.2. Matrix Gla Protein

1.2.1. Protein description and post-translational modifications

Matrix Gla protein (MGP), was first isolated from demineralized bovine bone matrix and was reported to have vitamin-k dependent modified amino acids, γ -carboxyglutmic acid (Gla) at positions 37, 41, 48

and 52. It is a 14 kDa protein which amino acid composition includes one disulfide bond [7]. Its sequence homology with Bone Gla protein (BGP/osteocalcin) indicate that these proteins arose by gene duplication and subsequent divergent evolution [8].

In humans, MGP has 5 glutamic acid residues that seem to play a role in its ability to bind to calcium phosphate crystals and bone morphogenetic protein. The glutamate residues are converted to Gla-residues during a post-translational modification carried out by a vitamin-K dependent carboxylase. Upon oxidation of the co-factor – vitamin K hydroquinone (KH₂), the introduction of an extra carboxyl group takes place at the γ -position of a glutamate residue. After reduction, vitamin K can be recycled by the vitamin K epoxide reductase (VKOR), which oxidizes it to reinitiate the cycle. The synthesis of Gla proteins can be blocked by 4-hydroxycoumarin derivatives that block the VKOR enzyme, such as Warfarin, a commonly prescribed anticoagulant. Additionally, MGP undergoes serine phosphorylation at the serine residues at positions 3, 6 and 9. Phosphorylation of ECM proteins has been recognized as a mechanism of activity regulation, however, the precise function of such modifications in MGP's anti-mineralization function is still unclear [9]. Also, the kinase that phosphorylates the serine residues in MGP is still unknown.

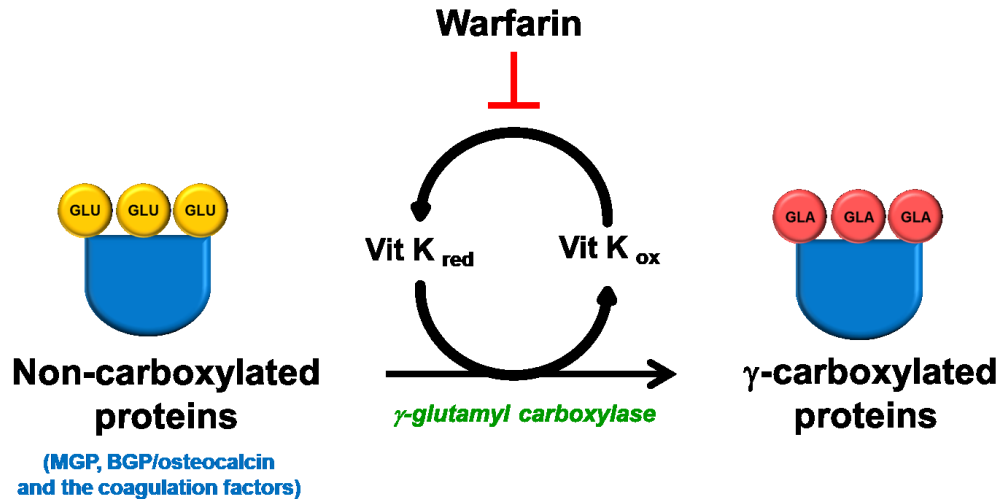


Figure 1.1. Vitamin K-dependent γ -glutamyl carboxylation cycle

Schematic representation of the γ -carboxylation of Gla proteins such as MGP and osteocalcin; and coagulation factors such as II, VII, IX, X, proteins C,S and Z [10]. The enzymatic reaction is carried out by the γ -glutamyl carboxylase (GGCX), using vitamin K as a co-factor. The oxidation and reduction of vitamin K is a continuous process dependent on the vitamin K epoxide reductase (VKORC) and can be inhibited by warfarin (taken from Dr. Murshed’s lecture slides).

1.3. MGP-deficient mouse model

Mgp^{-/-} mice were generated by Karsenty’s lab in 1997 in order to help in the understanding of ECM calcification and the molecular determinants that regulate this process. MGP had been described as a small extracellular protein of 14 kDa, which is synthesized by VSMCs and chondrocytes. Gene targeting at the *Mgp* locus in embryonic stem cells resulted in the replacement of a 3.4 kb region containing the proximal promoter, exons 1,2 and 3 and most of exon 4. *Mgp*-null mice developed severe arterial calcification, ectopic mineralization of cartilaginous tissues and died within two months of age due to the cardiovascular phenotype. Also, short stature, fractures and osteopenia were reported [11].

1.4. Vascular calcification

Deposition of minerals in the organic matrices is a physiologic process in bones, cartilage and teeth. However, the mineralization of soft tissues, such as blood vessel walls, is a pathologic condition associated with a variety of genetic and metabolic conditions.

Calcific deposits of minerals in the cardiovascular system or vascular calcification has been traditionally considered as a passive process, a corollary of aging or degenerative diseases such as advanced atherosclerosis, chronic kidney disease (CKD) and type II diabetes [12-14]. More recently, however, advanced imaging techniques, noninvasive diagnostic methods and the availability of genetically modified mouse models have proven the 'passive process' concept of vascular calcification invalid. According to the current view, vascular calcification is considered as an active and regulated process that shares many common regulators with bone mineralization [15]. The physiologic concentration of two mineral ions—calcium (Ca^{2+}) and inorganic phosphate (P_i), a suitable extracellular mineral scaffolding matrix and an environment free of mineralization inhibitors have been identified as the major players in bone mineralization [16, 17]. While these common factors also govern the initiation and progression of mineral deposition in the arterial tissues, the exact mechanism may differ depending on the type of vascular calcification.

Conventionally, vascular calcification has been classified according to the histological deposits of the hydroxyapatite ($\text{Ca}_{10}(\text{PO}_4)_6(\text{OH})_2$) crystals within the arteries and their anatomic localization within the cardiovascular system [15, 18]. The calcification occurring in the intima layer of the artery is commonly associated with atherosclerotic plaques, the fatty deposits that can be both stable and unstable. Two patterns of calcification have been described that are associated with the atherosclerotic plaques— a punctate pattern of minerals in the basal region of the intima layer adjacent to the media,

and a diffused pattern all over the intima, less likely to be diagnosed by the imaging tests. The inflammatory process triggered by the lipoproteins trapped in the subendothelial extracellular matrix (ECM) prompts the secretion of many factors by several different cell types, which may in turn facilitate the initiation and progression of the calcification process [19]. On the contrary, medial calcification or Mönckeberg sclerosis occurs independent of atherosclerotic lesions and is more prevalent in CKD and diabetic patients. This type of calcification is characterized by thickening of the medial layer and disruption of the elastic laminae, the concentric elastic ECM rich in elastin and associated fibrillar proteins. The hydroxyapatite (HA) crystals are deposited within and around the elastic lamina and can lead to hypertension and heart failure [12, 15, 20].

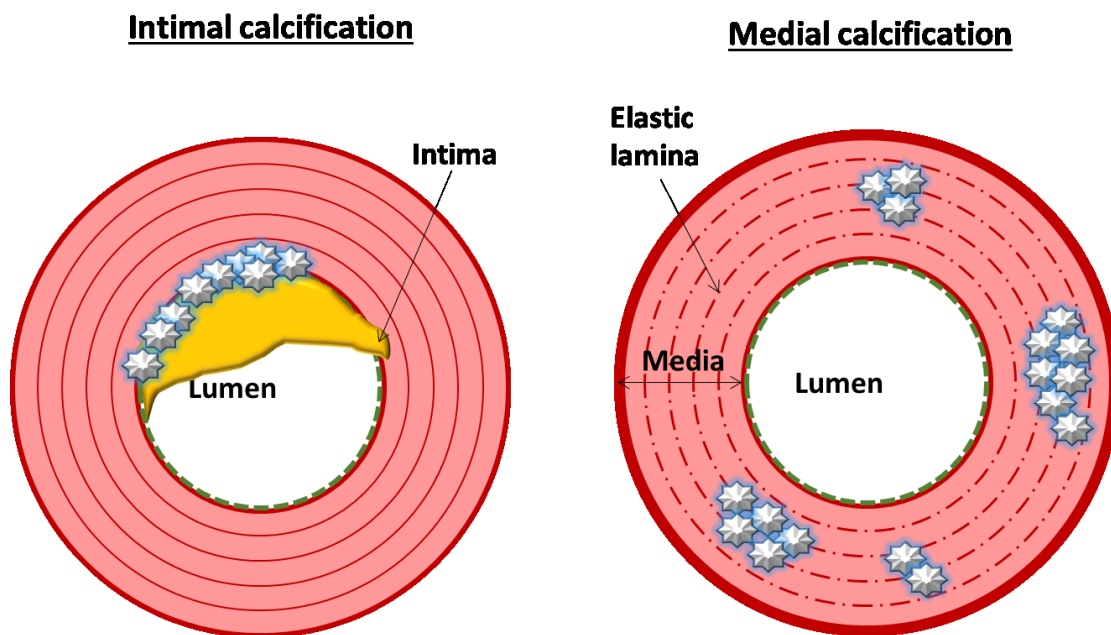


Figure 1.2. Intima vs media aortic calcification

Schematic representation of intima and medial calcification. Minerals deposit on the intima layer in association with the atherosclerotic plaque in intima calcification. In media calcification, mineral crystals are deposited on the elastic lamina. Also, thickening of the media and fragmentation of the elastic lamina is observed (Adapted from Dr. Murshed's lecture slides).

Apart from the arteries, calcification can occur in the heart valves. Calcific valve disease (CVD) is a common condition, affecting 25% of the individuals over 65 years and 52% of individuals over 85 years and occurs in response to mechanical stress and inflammation [21, 22]. According to the degree of dysfunction of the valve leaflet due to the calcification, CVD is divided into two stages: Aortic sclerosis when mobility is not compromised and stenosis when the valve mobility is impeded, causing high systolic pressures. Both conditions have been associated with increased morbidity and mortality [22]. Additionally, vascular calciphylaxis may lead to partial calcification of the soft tissues, often observed when the calcium phosphate concentration is unbalanced. Clinically, when the serum calcium phosphate product exceeds $60\text{mg}^2/\text{dl}^2$, ectopic calcification of soft tissue can occur, occluding the small vessels. The malfunction of certain systemic extracellular matrix mineralization inhibitors such as Fetuin-A and pyrophosphate (PP_i) seem to be a common cause of such disorders. Vascular calciphylaxis is frequent in CKD, diabetes or other metabolic diseases [18, 23].

The current understanding of vascular calcification has been greatly benefited by our understanding of bone mineralization. As evident by many studies, there are common links between bone mineralization and vascular calcification [18, 24]. A recurring theme explaining the spatial restriction of physiologic mineralization in bone suggests that the mineralization of bone ECM can be explained, in part, by the unique co-expression of tissue-nonspecific genes in bone forming osteoblasts [16]. Based on our understanding of bone mineralization and the identification of the common regulators of the ECM mineralization in general, several theories, not necessary mutually exclusive, have been proposed to explain the possible mechanisms for vascular calcification (**Figure 1.3.**).

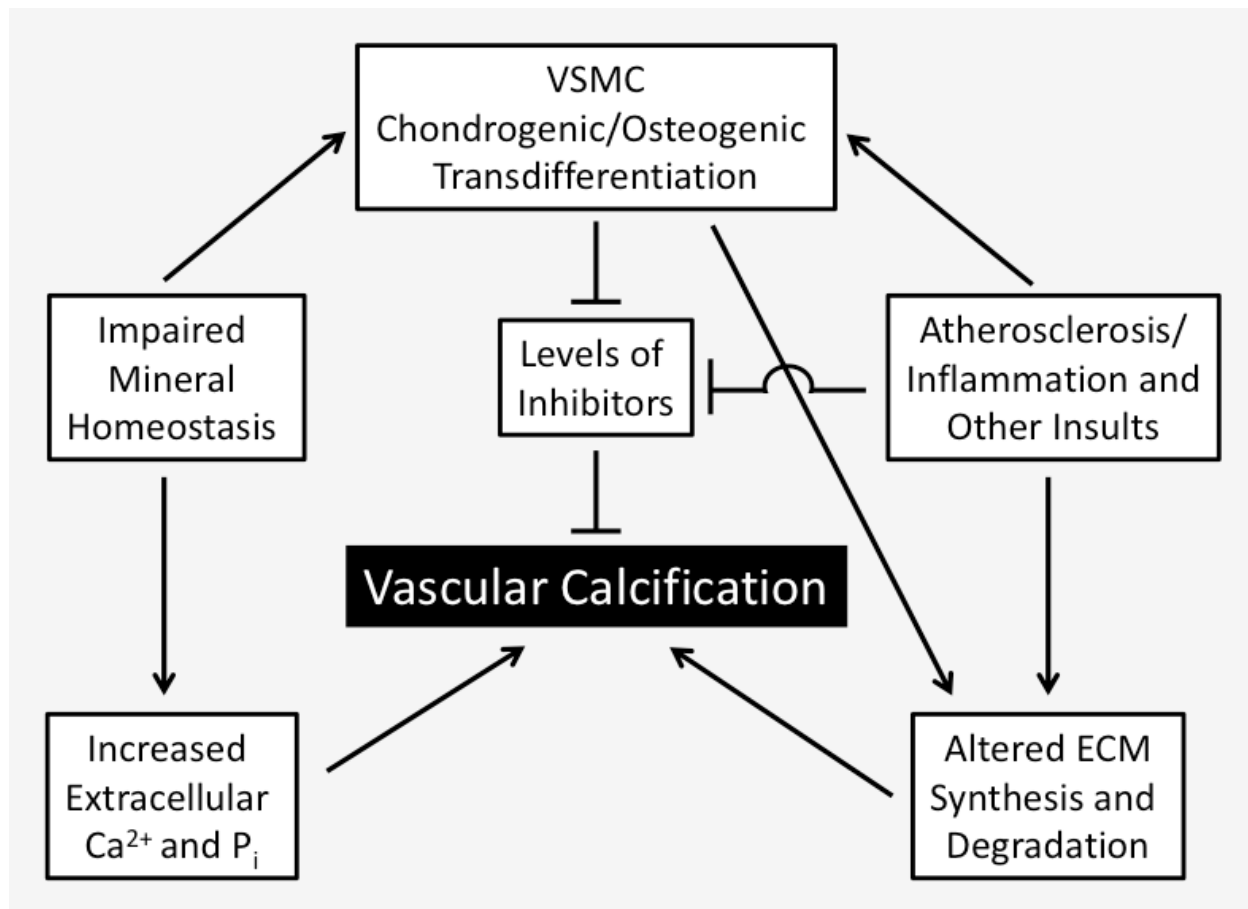


Figure 1.3. Key determinants and the current understanding of the mechanisms of vascular calcification

The extracellular levels of two mineral ions Ca^{2+} and P_i , presence of a suitable mineral-scaffolding extracellular matrix (ECM) and the absence of mineralization inhibitors are the basic determinants of vascular calcification. These factors, autonomously or mutually, may regulate the initiation and progression of calcific mineral deposition in the arterial walls. For example, in mice; the loss of mineralization inhibitor Matrix Gla protein (MGP) alone is sufficient to initiate severe arterial calcification, without any requirement of chondrogenic or osteogenic differentiation of the vascular smooth muscle cells (VSMCs). However, arterial calcification caused by MGP deficiency is affected by the extracellular P_i levels and the elastin gene dosage showing the critical interplay among various factors regulating vascular calcification. As shown in the scheme, impaired mineral homeostasis and inflammatory responses triggered by atherosclerosis or other insults may directly affect the major determinants of vascular calcification. These pathologic conditions may also induce chondrogenic or osteogenic transdifferentiation of VSMCs that may in turn promote the initiation and/or progression of vascular calcification.

1.4.1. Key determinants of ECM mineralization

Mineral ions: As shown by numerous studies, extracellular levels of ionized Ca and P_i , are indispensable for ECM mineralization. Alteration in serum Ca and P_i levels by genetic, metabolic or therapeutic means are now identified as important determinants of vascular calcification [25].

Serum P_i levels play a critical role in bone mineralization. Genetic diseases in mice and humans with reduced serum P_i levels as seen in vitamin D-deficient rickets or X-linked hypophosphatemia, lead to decreased bone mineralization or osteomalacia [26-29]. On the other hand, elevated extracellular levels of P_i have been associated with ectopic medial calcification. As a possible mechanism, it has been suggested that the increase of circulating P_i levels may promote the chondro/osteogenic transdifferentiation of the vascular smooth muscle cells (VSMCs) in the arterial media, which in turn may induce vascular calcification [13, 30]. Further, P_i may promote the progression of mineral deposition by inducing VSMC apoptosis and matrix degradation [31].

In agreement with the cardinal role of P_i in the regulation of vascular calcification, a reduced serum P_i level (hypophosphatemia) can prevent vascular calcification in mice lacking matrix Gla protein (MGP), a potent inhibitor of vascular calcification (*see below*)[16]. The severe vascular calcification phenotype and the associated abnormalities seen in *Mgp*^{-/-} mice are completely absent in *Mgp*^{-/-};*Hyp* compound mutants, that show hypophosphatemia caused by the *Phex* mutation [26]. A more recent study suggests that PHEX may regulate ECM mineralization independent of P_i levels, via its ability to degrade osteopontin [32].

Inactivation of *Phex* leads to an increase of fibroblast growth factor 23 (FGF23), a P_i regulating hormone in the serum. FGF23 acts on kidney proximal tubule cells to decrease the expression of type II Na/ P_i transporters resulting in renal P_i wasting [33, 34]. The role of serum FGF23 in P_i homeostasis has

been demonstrated in a liver-specific FGF23 expressor transgenic line, which recapitulated the *Hyp* phenotype [35].

Although the role of extracellular P_i in ECM mineralization is already established, how this process is affected by the intracellular P_i levels *in vivo* is still unknown. This aspect of ECM mineralization demands further exploration, thanks to a number of studies describing the revival of a controversial mechanism explaining ECM mineralization– the matrix vesicle (MV)-mediated initiation of mineral deposition in the hard tissues [36]. MVs are small cellular vesicles which bud off from the mineralizing cell bodies. Within the protected microenvironment of the MVs, the transport of P_i from the extracellular space and the enzymatic release of P_i from various phospholipids, phosphoproteins and polyphosphates have been thought to act as the major rheostat for the initiation of mineral precipitation [37, 38]. Interestingly, P_i -induced osteogenic differentiation of human VSMCs was prevented by knocking-down PiT-1, a Type III sodium-phosphate transporter, the most abundant transporter of P_i in human and rat VSMCs. Overexpression of mouse PiT-1 in this cell culture model restored the osteogenic phenotype and the *in vitro* ECM mineralization [39]. *In vivo*, however, the VSMC-specific ablation of *PiT-1* did not prevent the arterial calcification phenotype in a mouse model of vascular calcification, suggesting a compensatory role by PiT-2, a complementary type III sodium-phosphate cotransporter [40]. Considering the available *in vitro* and *in vivo* data, a more definitive role of P_i transport in the initiation and progression of vascular calcification can be best studied using a Pit-1/Pit-2 conditional knockout mouse model in which both the transporters can be ablated in the VSMCs. The induction of vascular calcification by a genetic, pharmacologic or diet-based approach in this model can provide a more definitive proof in this regard.

In patients, Ca has been shown to prevent cardiovascular disease by lowering blood cholesterol levels by inhibiting the absorption of fatty acids, to regulate blood pressure by downregulating the renin-angiotensin system and to improve insulin secretion from the pancreas. Calcium regulates the

sodium-potassium balance and has anti-obesity effects [41]. However, the hypercalcemia, along with the elevated serum P_i levels typically found in CKD patients seems to be the cause of vascular calcification [42]. Human vascular smooth muscle cells appear to calcify in presence of elevated levels of Ca, and Ca- P_i in an *in vitro* model [31].

Mineral scaffolding matrix: Often hydroxyapatite crystals are deposited on and around a suitable mineral scaffolding ECM. In bone, fibrillar type I collagen acts as a mineral scaffold [25, 43]. Type I collagen is composed of three peptide chains; two α -1 and one α -2 chains forming the triple helix that are stacked and covalently linked within the collagen fibrils. The deposition of hydroxyapatite crystals can take place both within the collagen fibrils and in the intrafibrillar spaces[25]. The *in vitro* mineralization of the demineralized collagen-rich organic matrix suggests a mineral scaffolding role for collagen. Further, genetic experiments suggest that reduced collagen synthesis by bone forming osteoblasts results in lower amount of mineralized bone[43] [44]. The most abundant mineral nucleating protein in the blood vessel walls however appears to be elastin that is a major constituent of the medial elastic laminae [45]. In medial calcification, hydroxyapatite crystals are often deposited along the elastic lamina and thought to be associated with abnormal elastin degradation. More recently, it has been shown that the initiation and progression of medial calcification can be significantly delayed by decreasing the elastin gene dosage [46].

Mineralization inhibitors: For a proper mineralization of hard tissue ECM, an environment free of mineralization inhibitors is mandatory [16]. In the contrary, these inhibitors are needed to prevent the spontaneous soft tissue calcification. Connective tissues that carry suitable mineral scaffolding ECMs require mineralization inhibitors as the extracellular levels of Ca and P_i are high enough to result in their spontaneous precipitation as calcium phosphate salts. Considering their importance in the

prevention of vascular calcification, a detailed description of several key mineralization inhibitors is provided below:

Inorganic pyrophosphate (PP_i): More than forty years ago, it was shown that PP_i, a chemical derivative of P_i, can inhibit ECM mineralization. PP_i is formed by two P_i groups joined by an ester bond [47]. Due to its ability to bind the nascent calcium-containing crystals and inhibit further crystal growth, PP_i is considered as one of the most potent inhibitors of ECM mineralization that can prevent the formation of both hydroxyapatite and calcium oxalate crystals [47, 48].

Enpp1 and *Ank*, two genes important for the maintenance of extracellular PP_i levels, are abundantly expressed. ENPP1 belongs to a group of ectoenzymes that produce PP_i from a variety of nucleotides [49, 50]. ANK is a transmembrane protein that transports PP_i to the extracellular space [51]. Mutations in these two genes in both mice and humans lead to abnormal calcification of soft tissue including blood vessels [52]. Interestingly, in bone, both *Enpp1* and *Ank* are highly expressed by osteoblasts, the cell type involved in the secretion of bone ECM and its subsequent mineralization [16]. This apparently paradoxical observation suggests that a regulatory mechanism must exist to limit the extracellular levels of PP_i in the mineralizing tissues. In fact, a cell membrane bound enzyme known as tissue nonspecific alkaline phosphatase (ALPL) is produced by bone and tooth cells, which cleaves PP_i to generate P_i [27]. This ALPL enzymatic activity may alter the local P_i to PP_i ratio to favor mineral precipitation. The importance of ALPL during skeletal ECM mineralization was formally demonstrated by the identification of a broad spectrum of missense mutations and deletions of *Alpl* in hypophosphatasia patients possessing defects in bone and tooth mineralization. The generation and analysis of ALPL-deficient mice further confirmed the requirement of this gene for the proper mineralization of these tissues [29, 53].

The induction of ALPL activity in the vascular tissues has been shown to induce ectopic calcification in animal models [16, 53]. This has been proposed as a possible mechanism for vascular calcification that is caused by chondrogenic/osteogenic transdifferentiation of VSMCs in response to various stimuli. ALPL activity may serve a dual role — it can degrade PP_i , a mineralization inhibitor and in the process, generate two molecules of P_i , a mineral ion that promotes ECM mineralization [54]. The importance of PP_i metabolism in vascular calcification has been further elucidated by human mutation analysis showing that the *ENPP1* gene is associated with idiopathic infantile arterial calcification, a genetic disease characterized by calcification of the elastic lamina of muscular arteries and stenosis [55]. More recently, *in vitro* experiments have suggested the role of PP_i , not just as a restrictor of hydroxyapatite crystal growth, but as a regulator of cell phenotype in mesenchymal precursors, since its deficiency promotes transdifferentiation of VSMC into chondrocytes, thereby, promoting arterial calcification [52]. Moreover, low levels of serum PP_i have been identified in hemodialysis patients and end-stage renal disease, where arterial calcification is a common complication [56, 57].

Matrix Gla protein (MGP): MGP is a 14 kDa protein that belongs to a family of gamma-carboxylated glutamic acid (Gla)-containing proteins [58]. In mice, four Gla-residues in MGP are modified by a vitamin K-dependent gamma-carboxylase [59]. The gamma-carboxyglutamic acid residues bind to Ca^{2+} ions and may prevent the seeding and further growth of the nascent hydroxyapatite crystals [59, 60]. Genetic mutations in *MGP* lead to Keutel syndrome, a rare autosomal disorder hall marked by ectopic cartilage calcification, skeletal hypoplasia and peripheral pulmonary stenosis [3]. More recently, aortic, intracerebral and renal arterial calcification has been reported in these patients [6, 61].

MGP-null mice (*Mgp*^{-/-} mice) recapitulate most of the phenotypic abnormalities of the Keutel syndrome patients, albeit with a more severe vascular calcification phenotype. At birth, however, there

is no apparent mineral deposition in the arteries of *Mgp*^{-/-} mice. The first traces of vascular calcification in the thoracic aorta appear around day 8 and shortly thereafter, the homozygous mutant mice start growing slower than their wild type (WT) littermates [11, 62-64]. All *Mgp*^{-/-} mice die within two months due the severity of vascular calcification and other associated abnormalities. Radiography and whole-mount Alizarin red staining for Ca²⁺ containing minerals revealed extensive calcification of the elastic and muscular arteries in *Mgp*^{-/-} mice [11, 63, 65].

Although MGP is one of the most potent inhibitors of ectopic calcification *in vivo*, the molecular mechanisms of its mode of action are still unknown. We showed earlier that the anti-mineralization function of MGP requires 4 Gla-residues [65]. Native MGP with 4 Gla-residues, when overexpressed in bone caused severe mineralization defects; while overexpression of MGP lacking all 4 Gla-residues did not affect bone mineralization. Interestingly, the presence of Gla-residues in osteocalcin, another Gla protein was not sufficient to prevent arterial calcification in *Mgp*^{-/-} mice, suggesting that additional feature(s) in MGP protein is/are necessary for its anti-mineralization function [65]. In a separate study, O'Young *et al* based on their atomistic molecular dynamics data, suggested that MGP prevents soft tissue calcification by adsorbing directly to the growing HA crystal. The central region of the MGP molecule is rich in Gla sites that undergo γ -carboxylation, and moreover, the N-terminus, with three sites of serine, goes phosphorylation in order to become active and exert its anti-mineralization function [66]. These findings are yet to be proven in cell culture and animal models.

Fetuin-A: Fetuin-A, is a 60 kDa glycoprotein synthesized in the liver and secreted into the blood, where it exerts its systemic anti-mineralization function. It is shown to have high affinity for calcium phosphates, forming a soluble colloidal particle that encloses fetuin, Ca²⁺ and P_i [67, 68]. In conformity with its affinity towards calcium phosphate minerals, fetuin accumulates in bone and sites of ectopic calcification e.g. atherosclerotic plaques [67]. The Fetuin-A knockout mice (*Ahsg*^{-/-} mice) display a

severe calcification phenotype when fed with a diet rich in minerals and vitamin D, or when generated on the DBA/2 genetic background prone to ectopic calcification. The phenotype of *Ahsg*^{-/-} mice consists of severe calcification of various organs, including myocardial, pulmonary and renal calcification [68]. These mice show cardiac fibrosis, diastolic dysfunction and impaired tolerance to ischemia and ectopic calcification in various tissues including kidney, lung, skin, brown fat, and pancreas. Interestingly, these mice do not show calcification of the vascular walls and their phenotype is not lethal, as seen in the *Mgp*^{-/-} mice. Despite the presence of a prolonged vascular calcification phenotype, there has been no report of the presence of chondrocytes or osteoblasts in the calcified soft tissues, suggesting the existence of an additional mechanism [68].

So far, no null-Fetuin-A mutations have been identified in humans, but interestingly, low levels of circulating Fetuin-A have been identified in patients with vascular calcification and CKD [69, 70]. At the same time, the serum levels of Fetuin-A are reduced in patients suffering from Pseudoxanthoma elasticum (PXE), a genetic disease caused by a mutation in the *Abcc6* gene. The ectopic calcification seen in PXE is localized primarily in skin, eyes and cardiovascular system [71]. The overexpression of Fetuin-A in a mouse model for PXE (*Abcc6*^{-/-} mice), which recapitulates the late onset and progressive soft tissue mineralization seen in humans, reduces the soft tissue mineralization by a 70% at 12 weeks of age [72]. These compelling experimental data place Fetuin-A as an important systemic mineralization inhibitor, but its exact role in the prevention of arterial calcification is still unresolved and needs further investigation.

RANK/RANKL/OPG: These cytokines/cytokine receptors make part of the Tumor Necrosis Factor (TNF) superfamily and are key regulators of bone remodeling. Receptor activator of nuclear factor kappa B (RANK) is a membrane protein expressed in the osteoclast surface and is activated upon the binding to its ligand (RANKL), expressed by the osteoblasts. The binding of RANKL to RANK on

osteoclast precursors promote osteoclastogenesis. Osteoprotegerin (OPG) is a decoy receptor for RANKL that interferes with the RANK-RANKL interaction and acts as a negative regulator of osteoclast differentiation [73, 74]. The triad RANK/RANKL/OPG is widely recognized as major regulators of bone remodeling. Recently, this triad has been linked to the inflammatory response of endothelial cells and VSMCs during pathologic calcification, especially in the chronic inflammation seen in the arterial walls in the course of atherosclerosis, and has been proposed as one of the possible mechanisms for the given vascular pathology [74, 75].

Currently, there are two separate mouse models in which *Opg* has been ablated (*Opg*^{-/-} mice) [75, 76]. Both of these models show a marked osteoporotic phenotype caused by a significant increase of bone resorption by osteoclasts. One of these models showed the presence of arterial calcification in the aorta and large renal artery [75]. This unexpected finding provided a clue that the OPG/RANK/RANKL triad could play an important role in atherosclerotic arterial calcification. Panizo *et al*, showed that the *in vitro* incubation of VSMCs treated with RANKL causes calcification in a dose dependent manner [77]. Furthermore, the addition of OPG and the knockdown of RANK by shRNA in the presence of RANKL can prevent arterial calcification. Subsequent analyses identified an upregulation of BMP-4 in the VSMCs, a signaling molecule previously involved in the osteogenic transformation of VSMCs that leads to vascular calcification [77, 78]. Although interesting, these data need to be interpreted with caution as no vascular calcification has been reported in the *Opg*^{-/-} mice that were generated by a Japanese group [76]. In these mice arterial calcification can be induced by feeding a high phosphorus diet in combination with calcitriol (1 α 25-dihydroxyvitamin D3) [79]. Also, contradictory findings fail to link the OPG/RANKL/RANK triad directly as an independent mechanism for vascular calcification as OPG knocked-down-human-VSMCs treated with RANKL failed to demonstrate increased proliferation, upregulation of calcification-associated genes and *in vitro*

calcification as claimed by other groups [80]. Additionally, although serum OPG levels are strongly associated with increased cardiovascular risk and mortality in nonuremic and uremic patients, so far, no such association linking serum levels of RANKL to vascular calcification has been reported [81, 82].

1.4.2. Mechanisms of vascular calcification

At present, the predominant hypothesis on the mechanism of vascular calcification suggests that the chondro/osteogenic transdifferentiation of the VSMCs is a prerequisite for vascular calcification. A variety of factors including genetic mutations, apoptosis, renal abnormalities causing altered mineral homeostasis, chronic inflammation and secondary effects of age related metabolic diseases may induce the transdifferentiation of VSMCs into osteoblast or chondrocyte-like cells. These cells then acquire the abilities to modulate the levels of basic regulators of ECM mineralization to initiate vascular calcification.

Calcified arteries of human patients undergoing renal transplantation have shown to express the chondro/osteogenic transcription factor RUNX2 followed by the upregulation of other osteoblast markers such as type I collagen, osteopontin (SPP1), bone sialoprotein (IBSP1) and ALPL [83, 84]. Osteogenic differentiation of VSMCs was also reported in the aortas of transgenic mice, ubiquitously expressing *Msx2* (encodes an osteoblast-specific transcription factor), which were fed with a high-fat diet. High-fat diet leads to vascular calcification in these transgenic mice, but not in their non-transgenic littermates. In this model, *Msx2* expression in aortic adventitia can induce expression of WNT ligands and downregulate its canonical antagonist DKK1, eventually leading to upregulation of ALPL in the VSMCs in a paracrine manner [18, 85].

The phenotypic plasticity of the VSMCs, as well as their differentiation and proliferation have been shown to be regulated by BMPs, secreted cytokines that belong to the transforming growth factor (TGF- β) superfamily. BMP2 seems to have an inhibitory effect on the VSMCs, whereas BMP7 seem to promote the VSMC phenotype. The regulation of BMPs seems to be a critical step in the mechanism of

arterial calcification [86]. It has been proposed that MGP-deficiency leads to the differentiation of multipotent mesenchymal progenitors or transdifferentiation of VSMCs present in the vascular walls into chondro/osteogenic precursors [87]. This view is supported by the presence of large chondrocyte-like cells seen in the histological sections prepared from the calcified *Mgp*^{-/-} aorta [63]. Zebboudj et al. suggested that MGP binds to bone morphogenetic proteins (BMPs), signaling molecules that are required for both chondrocyte and osteoblasts differentiation. These investigators proposed that an intermediate level of MGP leads to a strong inhibition of BMP osteoinductive function by inhibiting the phosphorylation of SMAD-1, a regulatory transcription factor in BMP signaling pathway [88].

A more recent study showed that the expression of RUNX2, an early chondrogenic/osteogenic transcription factor, is upregulated in the VSMCs of MGP-deficient arteries. Using a genetic model, Speer *et al.* confirmed that the cells with chondrocyte-like morphology are actually of VSMC origin. They used the VSMC-specific expression of a reporter gene to genetically trace the chondrocyte-like cells and showed that these cells had lost the smooth muscle lineage markers before expressing the chondrogenic/osteogenic marker RUNX2 [87]. Although interesting, this study raises some important questions, which demand further clarification. It is not clear whether the suggested chondrogenic differentiation takes place before the initiation of mineral deposition on the elastic lamina. Speer *et al.* showed that RUNX2 upregulation can be detected at two weeks of age in the arterial tissues; however, previous studies showed extensive arterial mineralization at this age in *Mgp*^{-/-} mice [63]. Although this study showed an upregulation of RUNX2, no other chondrogenic markers seemed to be induced. During endochondral bone formation, only hypertrophic chondrocytes are involved in growth plate cartilage mineralization; considering this observation, question can be raised whether an early chondrogenic differentiation of VSMCs in MGP-deficient aorta is sufficient to cause massive calcification seen in this tissue.

More recently, Khavandgar *et al* showed that the chondrogenic/osteogenic transdifferentiation of VSMC is not an indispensable mechanism for arterial calcification in *Mgp*^{-/-} mice. In young MGP-deficient mice, prior to arterial calcification, no upregulation of chondro-osteogenic markers was detected. Although, in older mice, there were upregulations of chondrogenic markers SOX9 and aggrecan, this was detectable only in heavily calcified arteries. Moreover, there was no significant upregulation of ALPL activity in the MGP-deficient arteries and ablation of *Alpl* in the *Mgp*^{-/-};*Alpl*^{-/-} compound mutants had no effect on the vascular calcification phenotype. Considering that *Alpl* expression is regulated primarily by the BMP signaling pathway, these data suggest that the vascular calcification seen in MGP-deficient mice may not involve an induction of BMP signaling [46]. In agreement with these findings, a previous study showed that the levels of *Runx2* mRNA was not altered in rat VSMCs treated with neither BMP-2, warfarin (a MGP antagonist) nor BMP antagonist Noggin. Additionally, the treatment with Noggin did not prevent the arterial calcification induced by warfarin, which prevents the activation of MGP through gamma-carboxylation of its glutamic residues [89].

Abnormal remodeling of medial ECM may cause vascular calcification. Elastin and microfibrils form the elastic fibers within the tunica media. The degradation of elastin, the most abundant protein in the elastic fibers, by MMPs leads to elastic lamina calcification [90]. Further supporting these observations, it has been reported that there are shared genetic bases for the disruption of arterial elastic lamina and medial calcification [91]. Elastin-containing elastic fibers are prone to calcification in a number of pathologic conditions including heart valve calcification [92].

Khavandgar *et al*, demonstrated that the elastin content in arteries is critical for the initiation and progression of vascular calcification in *Mgp*^{-/-} mice. The amounts of accumulated minerals differ within the same MGP-deficient artery depending on the content of elastin: the thoracic segment been more mineralized consistent with its higher elastin composition, when compared with the abdominal segment that has lower elastin content. This correlation was further confirmed by the reduction of

elastin gene dosage in *Mgp*^{-/-};*Eln*^{+/-} mice. The loss of one *Eln* allele delays significantly the initiation and progression of arterial calcification in the compound mutants. Taken together, these findings suggest that MGP might protect the mineral nucleation sites in the elastic lamina and thereby prevent vascular calcification [46].

Apart from the modalities described above, it is believed that cell death can lead to matrix vesicle-mediated calcification. *In vitro* studies using human VSMCs have shown that these cells form nodules spontaneously, that calcify after 28 days of culture, and matrix vesicles have been identified within the nodules with electron microscopy. Proudfoot *et al*, demonstrated that the prevention of apoptosis in VSMCs prevents the calcification of the cell nodules in culture, and likewise, the stimulation of apoptosis increases nodule calcification. Additionally, they showed that the apoptotic cell bodies can nucleate and crystallize Ca²⁺ [93]. More recently, autophagy, a protective mechanism of VSMCs to prevent P_i-mediated calcification, is believed to regulate matrix vesicle release [94].

1.4.3. Vascular calcification in human pathology

Atherosclerosis: Atherosclerosis is a chronic inflammatory condition of the blood vessels which involves increased cellular proliferation, lipid accumulation, ulceration, hemorrhage, thrombosis and vascular calcification. Atherosclerotic plaques in the arteries consist of aggregates of plasma lipids, mostly cholesterol, different cell populations, such as VSMCs, and monocytes/macrophages, collagen fibers and proteoglycans coming from the surrounding extracellular matrix [95]. As the disease progresses, retention of lipoproteins in the subendothelial extracellular matrix initiates an inflammatory response. The adjacent endothelial cells start to secrete adhesion molecules that later recruit monocytes from the circulating blood stream. This process becomes chronic with the incorporation of new cells and the secretion of extracellular matrix, which eventually decreases the arterial lumen diameter and reduces blood flow. This chronic process can become acute at any point, by the matrix

metalloproteinases (MMPs) secreted by macrophages that start degrading the tissue surrounding the plaque, releasing thrombogenic components to the blood stream, resulting in arterial thrombosis [19].

Ectopic mineral deposition in the atherosclerosis lesions is a common complication. Currently, the osteogenic differentiation of VSMC resulting in the upregulation of several osteogenic genes and the loss of mineralization inhibitors like MGP and Fetuin-A are the most accepted mechanism to explain the mechanism of arterial calcification in atherosclerosis plaque. However, the increase of collagen-rich fibrous matrix and upregulation of MMPs may independently affect the initiation and progression of mineral deposition in the atherosclerotic plaques.

Chronic Kidney Disease (CKD): In 2002, CKD was defined by the National Kidney Foundation as glomerular filtration rate (GFR) levels less than 60ml/min/1.73m² and the severity was classified in 5 stages, where stage 1 is kidney damage without changes in the GFR, and level 5 as end-stage renal disease. CKD has been associated with aging, hypertension and diabetes [96, 97]. Accelerated vascular calcification has been widely reported among the aggravating factors of CKD, which worsens their already elevated risk of cardiovascular mortality [97].

Arterial calcification in CKD patients has been strongly associated with their characteristic dysregulated mineral metabolism, causing elevated P_i levels in serum and transient hypercalcemia. In early stages of CKD, the serum P_i levels are maintained by the upregulation of fibroblast growth factor-23 (FGF23) and parathyroid (PTH) hormones. Both hormones promote P_i waste by modulating the renal P_i reabsorption, downregulating the sodium-phosphate transporters type II (NPTII) in the renal proximal tubule. PTH also regulates bone remodeling, which serves as an active reservoir for serum P_i [13]. As the renal function decreases in late stages of CKD, the GFR also decreases, resulting in hyperphosphatemia. High serum P_i levels as a consequence of inefficient urinary P_i excretion, altered

bone remodeling, and the ingestion of diet rich in P_i , can directly affect the VSMCs, promoting vascular calcification [19, 30].

The proposed mechanisms for the induction of arterial calcification associated with elevated P_i levels in serum are chondro-osteogenic differentiation of VSMCs, loss of mineralization inhibitors and matrix remodeling. High levels of uncarboxylated-dephosphorylated MGP have been found in CKD patients, which increase progressively as the renal damage and the vascular calcification aggravate [98]. Additionally, thinning and fragmentation of the medial elastic fibers have been identified in arteries of uremic patients, along with a significant upregulation of MMP-2 and MMP-9 activities. These later findings are consistent with the elastin and matrix remodeling promoted mechanism of vascular calcification [46, 99].

Diabetes mellitus type II: Diabetes mellitus type II (DMTII) is a common disease found in 6.2% of the population. Diabetes predisposes to kidney disease and accounts for the main cause of end stage CKD. Interestingly, cardiovascular disease is the main cause of death in diabetic patients with end stage CKD. Atherosclerosis and medial calcification are common findings in DMTII, and media calcification has been identified as an important independent predictor of cardiovascular disease and mortality, stroke and amputation in these patients [14, 100].

The proposed mechanisms for arterial calcification in DMTII are similar to the ones discussed before for CKD. Additionally, animal and human studies point towards hyperglycemia generating osmotic, metabolic and oxidative stresses as triggering factors for vascular calcification[18]. These factors are believed to upregulate osteogenic transcription factors such as RUNX2 and ALPL in VSMCs[100]. Diabetic arteries are shown to upregulate MMP activities, which lead to increased degradation of elastic fibers, thus, elastic-derived peptides, an end-product of elastic degradation are

known to be detected in serum of diabetic patients. Elastin-degraded arterial calcification can be exacerbated in the presence of high glucose, as shown by Sinha, *et al* [101].

Osteoporosis: Osteoporosis is an old age disease characterized by decreased bone mass, strength and microarchitecture along with increased risk of bone fractures. The pathophysiology of osteoporosis involves the imbalanced bone formation by osteoblasts and bone resorption by osteoclasts [102]. A number of clinical studies show a strong association between vascular calcification and risk of osteoporotic fractures, and between osteoporosis and cardiovascular events. Low bone mineral density BMD has been shown to be correlated with coronary Ca^{2+} score and atherosclerosis, whereas an augmented osteoporotic bone phenotype was seen in menopausal women with arterial calcification [36]. Interestingly, the standard treatment for osteoporosis with bisphosphonates seems to reduce arterial calcification while improving the BMD [103, 104].

It has been suggested that the same molecular signals that regulate bone remodeling may also cause soft tissue calcification. According to a widely suggested theory the triad RANK/RANKL/OPG relates osteoporosis to arterial calcification. OPG inhibits bone resorption by scavenging RANKL and preventing its binding to RANK leading to impaired osteoclastogenesis. It is believed that in osteoporotic patients higher RANKL to OPG ratio increases systemic levels of P_i and Ca that in turn can be redeposited in the blood vessels [105, 106].

Pseudoxanthoma elasticum: Pseudoxanthoma elasticum (PXE) is a rare autosomal recessive genetic disease caused by mutations in the *ABCC6* gene. It is characterized by ectopic mineralization and fragmentation of elastic fibers with resulting clinical manifestations in the skin, eyes and cardiovascular system. The estimated prevalence ranges between 1:25,000 to 1:100,000 [107, 108].

The cardiovascular phenotype in patients with PXE includes calcification and fragmentation of the elastic fibers in the internal and medial elastic lamina and adventitia layers of aorta and medium-size arteries, endocardium, pericardium and vascular structures of the heart. Moreover, the high prevalence of atherosclerosis leads to an increased risk of cardiovascular disease, stroke and gastrointestinal hemorrhage [109]. To date, not exact mechanism has been proposed to explain the arterial calcification phenotype characteristic of PXE, however, its connection with the elastin degradation and matrix remodeling mechanism is evident.

1.5. Bone development and remodeling

1.5.1. Skeletal development is a multi-step process

Skeletal development in vertebrates involves concerted functions of three major cell types—chondrocytes in cartilage, and osteoclasts and osteoblasts in bone. The spatiotemporal distribution of the precursor stem cells that gives rise to these cell types, their proliferation, differentiation and programmed death determines the growth, shape and load-bearing capacity of the future skeleton [110, 111]. Developmentally, bones can be categorized into two types: endochondral and intramembranous bones. A cartilage ‘precast’ (anlagen) is essential for endochondral bone formation while it is not needed for the formation of intramembranous bones. However, the formation of both bone types is initiated by the condensation of mesenchymal stem cells (MSC) that first proliferate and differentiate into chondrocytes in the case of endochondral bones or osteoblasts in the case of intramembranous bones.

A cluster of chondrocytes within the core of the developing endochondral bones differentiate first to form a well-defined structure known as the growth plate. The growth plate has four distinct zones: 1) a resting zone of chondrocyte precursors; 2) a proliferative zone with small chondrocytes that synthesize ECM proteins including type II collagen; and 3) a zone of prehypertrophic and 4)

hypertrophic chondrocytes. The hypertrophic zone possesses terminally differentiated chondrocytes that secrete a cartilaginous matrix rich in type X collagen. Eventually, the matrix becomes vascularized and mineralized, presumably leading to the apoptosis of the hypertrophic chondrocytes. The mineralized cartilage matrix is then replaced by a type I collagen-rich bone matrix through the concerted resorptive and formative activities of osteoclasts and osteoblasts, respectively [111, 112].

1.5.2. Current understanding of skeletal ECM mineralization

Mineralized ECM is a salient feature of the skeletal tissues. According to a well-accepted model, when present at physiologic concentrations, two mineral ions – P_i and Ca^{2+} – will promote hydroxyapatite crystal growth within and between newly synthesized collagen fibrils in the skeletal ECM [17]. More than fifty years ago, it was shown that inorganic pyrophosphate (PP_i), a chemical derivative of P_i , can inhibit the mineralization process [47, 48]. The presence of a scaffolding matrix and a defined extracellular ratio of P_i to PP_i are two critical determinants of ECM mineralization. In bone, tissue nonspecific alkaline phosphatase (TNAP/ALPL), an ectoenzyme bound to the osteoblast cell membrane, cleaves PP_i to generate P_i [113]. ALPL enzymatic activity may alter the local P_i to PP_i ratio to favor mineral precipitation [54].

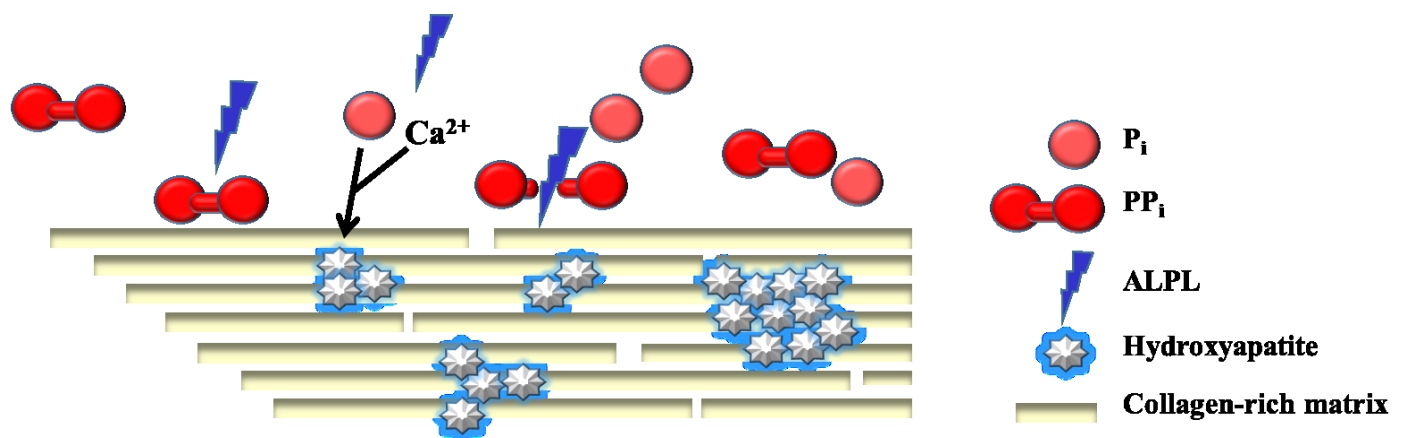


Figure 1.4. Determinants of bone mineralization

The key determinants of hard tissue mineralization consist of the mineral ions P_i and Ca^{2+} , a mineral scaffolding collagen matrix, and the absence of mineralization inhibitors such as pyrophosphate. Alkaline phosphatase (ALPL) promotes bone mineralization by cleaving PP_i (Adapted from Dr. Murshed's lecture slides).

1.5.3. Bone remodeling

Bone is a dynamic tissue that has important functions throughout life, such as attain and preserve skeletal size and shape, maintain its structural integrity and regulate mineral homeostasis. Bone modeling is a process by which the bone grows and reshapes according to mechanical stimuli; and involves bone formation and resorption independently, at distinct anatomical locations. On the contrary, bone remodeling is the tightly coordinated event, responsible for bone repair of damaged tissue and mineral homeostasis, which involves bone formation and resorption at the same anatomical site to preserve the bone mass. A brief discussion on the major cell types that participate in bone remodeling is presented below:

Osteoclasts: Osteoclasts are terminally differentiated myeloid cells with the unique capacity to remove mineralized bone. These cells are multinucleated and express tartrate-resistant acid phosphatase. An important cytokine required for osteoclast survival, expansion and differentiation is RANKL (receptor activator of NF- κ B ligand [114]. RANKL is secreted by the osteoblasts and osteocytes. RANKL binds to its receptor RANK, localized on the surface of the osteoclast precursor cell. Its activation results in the commitment of monocyte/macrophage precursor cells to the osteoclast lineage and the activation of mature osteoclasts. RANK is a member of the tumor necrosis factor receptor (TNFR) superfamily. It recruits adaptor molecules that activate downstream signaling molecules like mitogen activated protein kinases (MAPKs) and nuclear factor- κ B (NF- κ B) [115]. Mice lacking RANK (*Rank*^{-/-} mice) show a severe disorder in bone resorption and remodeling, as well as in growth plates during endochondral bone formation due to a lack on osteoclasts. Also, they display absence of teeth, associated with the osteopetrotic phenotype [116].

The RANKL/RANK complex induces the trimerization of RANK, inducing the binding of an adaptor protein TRAF6 that activates a downstream signaling cascade. This adaptor protein stimulates NF- κ B, a signaling molecule essential for osteoclastogenesis [115] and the nuclear factor of activated T-cells cytoplasmic 1 (NFATc1). NFATc1 is a transcription factor that acts in the late-signaling stage, regulating the multinucleation process and bone resorption function by the osteoclast. For example, NFATc1 upregulates the osteoclast-specific genes that encode proteins involved in osteoclast function, such as Cathepsin K and tartrate-resistant acid phosphatase (TRAP)[115]. Osteoclast-specific NFATc1 knockout mice show severe osteopetrosis due to an inhibition of osteoclastogenesis [117]. Additionally, NFATc1 has been shown to regulate osteoblasts and immune cells [115]. An additional modulator of osteoclastogenesis secreted by the osteoblasts is OPG. It is a soluble decoy receptor produced for RANKL, that prevents the activation of RANK, through a competition with RANKL.

Osteoblasts: Osteoblasts are the bone-forming cells that play several important roles in bone remodeling: Induction of osteoclastogenesis during the early differentiation stage, and production of ECM proteins and mineralization during the late differentiation stage. Osteoblasts derive from pluripotent mesenchymal stem cells that have the potential to differentiate into myocytes, chondrocytes, adipocytes and osteoblasts, process that depend on a cascade of regulatory transcription factors.

The first transcription factor and the master regulator of osteoblast differentiation is the Runt-related transcription factor 2 or RUNX2. Its expression in common chondro/osteoprogenitors is controlled by different homeodomain transcription factors and suppressors. RUNX2 not only plays a critical role in the early stages of development, but regulates bone formation beyond this phase [118, 119]. In differentiating osteoblasts, RUNX2 induces the expression of Osterix (OSX/SP7) an

osteoblast-specific transcription factor. In genetic experiments, *Osx* inactivation in mice results in perinatal lethality, undifferentiated osteoblasts and complete absence of endochondral and intramembranous bone formation [120, 121]. Once committed, preosteoblasts become functional mainly because of ATF4 transcriptional activity which regulates the synthesis and secretion of type I collagen [44, 122]. Genetic mutations leading to impaired osteoblastogenesis have been associated with several human diseases. A heterozygous mutation of the human *RUNX2* gene causes Cleidocranial dysplasia (CCD), condition characterized by a delay in fontanelles closure and hypoplastic clavicles [123]. Recently, a single base pair mutation in the *SP7/OSX* gene was associated to a form of non-collagenous osteogenesis imperfecta characterized mainly by facial dysmorphism and frequent bone fractures, whereas a loss-of-function mutation in the *RSK2* gene leads to Coffin-Lowry syndrome, an X-linked condition that displays mental retardation and skeletal abnormalities in the affected males [124, 125].

Osteocytes: During osteoid mineralization, some terminally differentiated osteoblasts become embedded in the matrix, becoming osteocytes. They form a network that extends throughout the bone. This network contains dendrite-like processes that interact with other osteocytes and with osteoblasts in the bone surface. Osteocytes respond to mechanical load, and their network allows them to detect mechanical strain and microdamage that occur during normal skeletal function. It is now known that osteocytes initiate the repair process [114]. These cells modulate the functions of both osteoclasts and osteoblasts by releasing soluble factors e.g. RANKL and sclerostin, respectively.

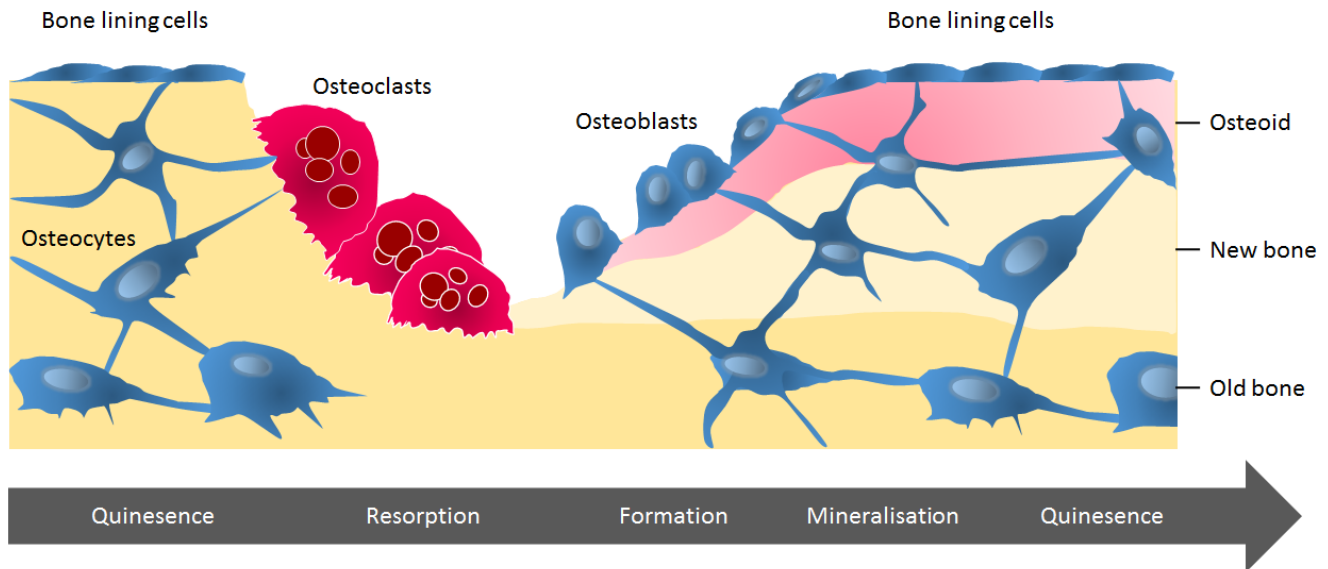


Figure 1.5. Bone remodeling

During bone remodeling, terminally differentiated osteoclasts resorb old bone, whereas osteoblasts precursors are recruited. Then, these cells proliferate and differentiate into mature osteoblasts that secrete new bone matrix (osteoid). Later, the osteoblasts mineralize the osteoid, engulfing some cells into the newly secreted ECM, becoming osteocytes.

1.5.4. Matrix Gla protein in the skeletal tissues

Until now, there is no clear understanding whether MGP is expressed by osteoblasts in bone, and thus, its direct role in bone mineralization and homeostasis is still speculative. As mentioned earlier, Price *et al* isolated MGP for the first time from urea extracts of demineralized bovine bone matrix. In the original report, they described it as “The first matrix-associated Gla containing protein to be purified from bone” [7]. Later, it was also isolated from the vertebral cartilage of the soupfin shark (*Galeorhinus galeus*), accounting for ~40% of the total protein of the calcified cartilage, which carried minerals comparable to the that of bovine bones [126]. On the other hand, the initial report on the *Mgp*^{-/-} mice describes *Mgp* expression by *in situ* hybridization in vascular tissues (except in myocardium), trachea and in the growth plate cartilage. It detects strong signal in proliferative chondrocytes and to a lesser extent in late hypertrophic chondrocytes, but not in bone. However, an osteopenic phenotype was

reported on these mice [11]. These findings raised the question whether the isolated MGP from bovine bone reported by Price, *et al* is secreted locally by osteoblasts, or whether it is coming from the vasculature, since bone is a highly vascularized tissue. It is also possible that the circulating MGP is accumulated in bones as it binds to the mineralized ECM via its Gla-residues. Additionally, a direct contamination from the vasculature's ECM proteins while preparing the bone extracts can not be fully ruled out. At this point, there are no reports on the bone phenotype of Keutel syndrome patients, thus, the question whether MGP plays a direct role in bone mineralization and/or remodeling, still needs to be investigated.

1.5.5. Vascular calcification and osteoporosis

Osteoporosis and cardiovascular diseases; more specifically vascular calcification, were seen as independent entities for long time. However, long-scale epidemiological studies have linked them with incontrovertible evidence. Not only they share conventional risk factors such as menopause, smoking, sedentarism and diabetes, but both pathologies share cytokines and growth factors that affect them [127].

For example, it has been suggested that the osteoclast differentiation regulator OPG may mediate vascular calcification. Numerous studies have reported that upregulated OPG levels are associated with poorer cardiovascular outcomes, such as coronary diseases, aortic aneurisms and cardiovascular mortality. It has been shown that OPG prevents mineral crystal nucleation and growth, inhibiting vascular calcification *in vitro*. Additionally, high levels of OPG have been detected in cases of ectopic calcification such as atherosclerosis [128]. It has been recently reported that FGF23, a phosphaturic hormone, upregulates OPG with no effect on RANKL expression in VSMCs. At the same

time, OPG downregulates the expression of osteogenic markers such as BMP2/4, RUNX2 and ALPL, thus, limiting the vascular calcification process [129].

Also, release of proinflammatory and proresorptive cytokines such as tumor necrosis factor α (TNF α) and interleukin IL-6 by VSMCs, endothelial cells and macrophages during the atherosclerotic event, result in the recruitment of macrophages and monocytes that can differentiate into osteogenic cells, inducing calcification of the plaque. Also, these cytokines are known as potent promoters of bone resorption in post menopausal women.

It was recently reported that two polymorphisms in the *MGP* gene in men were associated with the progression of aortic calcification and bone loss in the femoral neck. Single nucleotide polymorphisms (SNPs) -138T>C, -7G>A, and Thr83Ala were genetically associated with a decrease bone mineral density (BMD) in men. No effect was observed in women [130].

1.6. Craniofacial development

Congenital anomalies or birth defects are a major cause of perinatal lethality affecting 2-3% of all newborns [131]. A significant number of these infants show abnormal craniofacial development. Such abnormalities often affect the overall body functions in the surviving individuals and may lead to long-term disabilities [132]. Some of these defects are very common, such as oral clefts, which occur approximately 1 in every 700 live births, while others can be relatively rare, such as facial hypoplasia seen in Keutel syndrome or Chondrodysplasia punctata [3, 132-134].

Craniofacial development is a complex process that involves interactions among cells of multiple developmental origins, their migration, proliferation and differentiation. Both genetic and epigenetic factors regulating the concerted morphogenesis of two different craniofacial tissues, bone and cartilage, may affect the craniofacial growth and patterning. Impairment of the cellular and

extracellular events regulating the development of any of these tissues may result in birth defects of the craniofacial complex [135, 136]. The primary causes of these deformities are genetic, however, maternal exposure to toxic substances and nutritional status during pregnancy may also lead to these developmental abnormalities [137-139]. Although the functions of many different protein mediators of cartilage and bone development are well-known, their molecular mechanism of action and how they cross-talk with each other is still unknown. A lack of understanding of how these mediators work at the molecular levels and insufficient information on their interplay during bone and cartilage formation are seriously hampering the development of novel therapeutics, diagnostic approaches and management of congenital skeletal abnormalities in children.

1.6.1 Development of the facial skeleton

The skeletal elements in the whole body and the skull particularly, are formed by two different mechanisms, intramembranous and endochondral ossification. Formation of both bone types initiate with the condensation of mesenchymal stem cells (MSC), which first proliferate and then differentiate into mature cells. During endochondral ossification, condensations of precursor cells take place in the exact space and shape of the future bone, providing a cartilage template (anlagen) for its formation. Chondrocytes within the core of the developing endochondral bones eventually differentiate to form two distinct growth plates at both ends. At the center, chondrocytes become hypertrophic, undergo apoptosis and the mineralized matrix secreted by them is resorbed by osteoclasts. Osteoblasts then secrete the bone matrix and the primary spongiosa is formed. Most of the skeletal bones are formed throughout this mechanism, including all the long bones (limbs) and the chondrocranium in the skull. On the other hand, the intramembranous ossification involves the condensation of mesenchymal precursors that differentiate immediately into bone without the need of a cartilaginous template. The flat bones of the skull, the maxillomandibular bones and the clavicles are formed through the

intramembranous ossification. Around the fourth month of embryonic life (E14.5 in mice), the ossification of intramembranous bones appears before the cartilaginous bones in the appendicular skeleton. The clavicle is the first bone to ossify, followed immediately by the cranial bones [110, 140].

The embryonic tissues that give rise to the skull derive from the neural crest, mesoderm and ectoderm. Around the 4th week of embryonic life the structures that give rise to the face appear as prominences: one frontonasal, two maxillary and two mandibular prominences [141]. The development of the upper face occurs in two stages accompanying complex morphogenetic movements [142]. The early phase gives rise to the lip and a later phase gives rise to the secondary palate. In human embryos (E11.5 in mice), the upper lip and primary palate is formed before the 10th week of gestation. The maxillary prominences, the lateral and medial nasal processes fuse to form the upper lip. If this fusion is interrupted, cleft lip can occur, potentially affecting the development of the secondary palate. Next, the medial nasal prominences merge along the midline and differentiate into the nasal septum. When fully formed, the nasal septum divides the nasal cavity into two separate chambers [135, 136, 143].

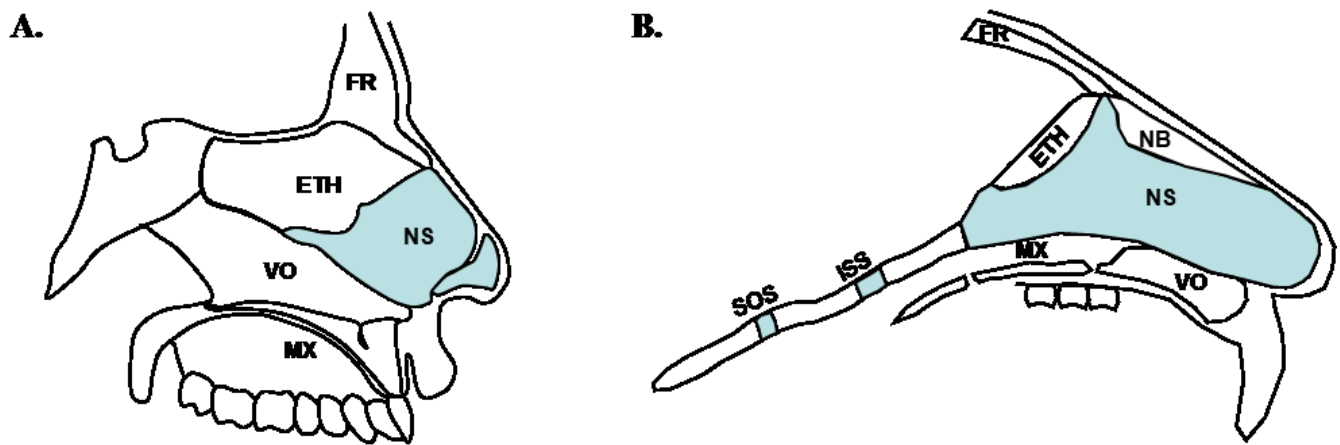


Figure 1.6. Nasal septum and related anatomical structures

Schematic representation of **A.** human and **B.** mouse craniofacial complex showing the anatomical localization of the cartilaginous part of the nasal septum (NS) that remains unmineralized throughout life. ETH: Perpendicular plane of the ethmoid, FR: Frontal bone, MX: Maxillary bone, VO: Vomer, ISS: Intersphenoidal synchondrosis, SOS: Spheno-occipital synchondrosis, NB: Nasal bone.

1.6.2. Midface hypoplasia

Midface hypoplasia is a developmental anomaly in which the nasal, maxillary and zygomatic bones in the cheek grow slower than other facial structures [144]. Genetic mutations, epigenetic factors or traumatic injuries during the early stage of life may lead to midface hypoplasia. A mild form of this disorder is usually considered as a harmless developmental anomaly of the face, while a severe form may seriously affect the health. The complications of a severe midface hypoplasia may include breathing problems while sleeping (sleep apnea), misalignment of the jaw and eyelids, dental malocclusion, chewing and swallowing difficulties and overall disfigurement of the face [145-147]. Apart from the psychological burden, the patients may have insomnia, high blood pressure, persistent dry eyes, speech and chewing difficulties [145]. The available treatments for these problems rely on both symptomatic interventions and surgical procedures.

Congenital diseases associated with midface hypoplasia

Patients with several different craniofacial syndromes and disorders such as cleft palate and achondrodysplasia may show the signs of midface hypoplasia. Some of these conditions are presented in the table below:

Disease	Mutation	Description
Crouzon syndrome	Autosomal dominant; <i>FGFR2</i> and <i>FGFR3</i>	Affects the branchial/pharyngeal arch, which gives rise to the maxilla and mandible, leading to an impaired growth of the maxilla. The most common feature is craniosynostosis, the abnormal fusion of the sutures (Meyers, Orlow, Munro, Przylepa, & Jabs, 1995; Reardon et al., 1994).
Apert syndrome	Most cases sporadic, but autosomal dominant cases are reported; <i>FGFR2</i>	Allelic to Crouzon syndrome. In addition to midface hypoplasia and craniosynostosis during development, patients show characteristic hand deformities caused by syndactyly (Wilkie et al., 1995).
Pfeiffer syndrome	Autosomal dominant; <i>FGFR1</i> , <i>FGFR2</i> and unknown	Patients show craniosynostosis with an underdeveloped upper jaw and beak-shaped nose and characteristic anomalies of the hands and feet (Lajeunie et al., 1995; Schell et al., 1995).
Chondrodysplasia punctata	X-linked recessive <i>ARSE</i>	Occurs almost exclusively in males. Patients show short stature, short finger tips and toes and midface hypoplasia. Mutation in arylsulfatase E has been thought to affect the post translational gamma carboxylation of the Gla proteins. Similar features seen in Warfarin Embryopathy (Parenti et al., 1997).
Keutel syndrome	Autosomal recessive; <i>MGP</i>	Patients show abnormal calcification of all cartilaginous tissues, short stature, and severe midface hypoplasia with class III malocclusion. Similar features seen in Warfarin Embryopathy (Fryns, van Fleteren, Mattelaer, & van den Berghe, 1984; Munroe et al., 1999).
Warfarin Embryopathy	-	Seen in children born to mothers treated with warfarin, an anti-coagulant. Developmental abnormalities are similar to Chondrodysplasia Punctata and Keutel syndrome (Starling, Sinha, Boyd, & Furck, 2012; Wainwright & Beighton, 2010).

Table 1.1. Developmental diseases associated with midface hypoplasia

1.6.3. Chondrocranium and craniofacial growth

The role of the chondrocranium and particularly the role of the nasal septum during facial development has been a matter of controversy during the last 65 years. Scott, in 1951 proposed that the nasal septum, as all other primary cartilages acts as a growth center, separating the facial structures allowing the sagittal growth of the face [148]. This observation was supported by the findings that the nasal septum has intrinsic growth ability and responds to hormones and growth factors. Additionally, animal studies demonstrated that the extirpation of the nasal septum impaired the midface development in rats and rabbits [149, 150]. However, such experimental approaches were criticized, as facial development occurs slowly in humans in comparison to the animal models used and the observed midface malformations were then attributed to the surgical trauma during nasal septum resection. Moss, in 1968, proposed the nasal septum as a passive structure that serves a supportive role for the other craniofacial structures [151]. However, *in vitro* studies show that the intrinsic growth capacity of the nasal septum is comparable to that of epiphyseal cartilages and a more recent study demonstrates this finding *in vivo* [152, 153]. Furthermore, the early corrections of nasal septum deformities in infants with cleft lips and palates or other facial defects show a greater effect on the correction of the overall craniofacial irregularities [154].

Similarly, the cartilaginous portions of the cranial base, such as the intersphenoidal synchondrosis (ISS) and the spheno-occipital synchondrosis (SOS), play a crucial role during early and late craniofacial development. Particularly, the SOS has been defined as a growth center and a guide for the longitudinal growth of the maxilla, midface and mandible [155]. Of interest, the SOS is the last synchondrosis to fuse in the cranial base. Its closure occurs around the pubertal spurt, thus, fusing earlier in girls than in boys [155]. Premature fusion of the SOS causes craniofacial malformations, including midface hypoplasia, as seen in Apert, Crouzon and Pfeiffer syndromes [156-159]. Recent studies demonstrate that indeed, the SOS fuses earlier in syndromic patients than in healthy controls

and suggests that the early fusion is correlated with a more severe midface hypoplasia, which has become of great interest in regards of treatment planning [160].

1.7. Rational, overall goal and aims of the current thesis

The anti-mineralization function of MGP in skeletal and soft tissues is well established. However, several key questions remain unanswered, such as whether modification of elastin levels in the cardiovascular system can completely prevent arterial calcification, whether MGP affects bone formation directly, and the cause of midface hypoplasia in Keutel syndrome patients. Thus, the current work is directed towards answering these questions in order to advance the field of pathologic soft tissue calcification.

1.7.1. Overall goal

The analysis of the phenotypic traits of MGP-deficient mice as a model for human Keutel syndrome.

1.7.2. Specific aims

1.7.2.1. Investigate the mechanism of arterial calcification in MGP-deficient mice.

1.7.2.2. Study the bone phenotype in MGP-deficient mice.

1.7.2.3. Examine the role of MGP in craniofacial development.

Chapter 2:

Vascular Calcification in MGP-Deficient Mice: A Phosphate and
Elastin Story

Vascular Calcification in MGP-deficient Mice: A Phosphate and Elastin Story

Juliana Marulanda¹, Abhinav Parashar¹, Ophélie Gourgas², Xiuying Bai³, Andrew C. Karaplis³, Robert P. Mecham⁴, Marta Cerruti², Juergen Brinckmann^{5,6} Monzur Murshed^{1,3,7}

¹Faculty of Dentistry, McGill University, Montreal, Quebec, Canada

²Materials Engineering, McGill University, Montreal, Québec, Canada

³Division of Endocrinology, Department of Medicine, McGill University, Montreal, Quebec, Canada

⁴Department of Cell Biology and Physiology, Washington University School of Medicine, St. Louis, MO, United States

⁵Department of Dermatology, University of Luebeck, Luebeck, Germany

⁶Institute of Virology and Cell Biology, University of Luebeck, Luebeck, Germany

⁷Shriners Hospital for Children, Montreal, Quebec, Canada

Manuscript Submitted

2.1. Abstract

Vascular calcification is a pathologic condition in which calcium phosphate minerals deposit in the cardiovascular tissues. Calcific deposits in the arterial media have been associated with a number of metabolic and genetic disorders including diabetes, chronic kidney disease and generalized arterial calcification of infancy. While medial calcification and physiologic hard tissue mineralization in the skeleton are both regulated by several common determinants, emerging data suggest that there might be fundamental differences in the mechanisms underlying these two processes. In the current study, we investigated the epistatic effects of several genetic regulators of extracellular matrix (ECM) mineralization on the vascular calcification phenotype of matrix Gla protein-deficient (*Mgp*^{-/-}) mice, a model of human Keutel syndrome. We show that sphingomyelin phosphodiesterase 3 (SMPD3), an enzyme essential for skeletal hard tissue mineralization, is dispensable for the initiation and progression of vascular calcification in *Mgp*^{-/-} mice. On the other hand, transgenic augmentation of circulating fibroblast growth factor 23 (FGF23), a phosphaturic hormone which negatively regulates skeletal ECM mineralization, prevented vascular calcification caused by MGP deficiency. When the FGF23-induced hypophosphatemia was corrected using a diet-based approach, there was a rapid calcification of vascular tissues in this model. Finally, using a humanized mouse model, we showed that a 40% reduction of medial content of elastin, a protein absent in bones, but abundant in the arterial media, completely prevented vascular calcification in *Mgp*^{-/-} mice at least until 3 weeks of age. These mice lived normally and only a punctate mineral deposition was observed when they become one-year-old. Taken together, our findings demonstrate that the severity of medial calcification in MGP-deficient mice depends on the serum P_i levels and the elastin content in the arterial walls. Although FGF23-Pi axis regulates both skeletal mineralization and medial calcification, there are specific determinants for these two processes.

2.2. Introduction

Abnormal mineral deposition in the vascular tissues, commonly described as vascular calcification, is essentially an ectopic event. The pathologic calcific deposits may affect both major and peripheral arteries and the heart valves [161]. In rare cases, the veins are also found to be calcified [162].

Vascular calcification has been traditionally considered as a passive process, a corollary of aging or degenerative diseases such as advanced atherosclerosis, chronic kidney disease (CKD) and type II diabetes [12, 14, 163]. However, more recent views consider vascular calcification as an active and regulated process that shares many common determinants with the physiologic mineralization process of bones and teeth [17]. Nevertheless, physiologic mineralization and different types of vascular calcification can be regulated by specific determinants which are mutually exclusive.

Depending on the anatomical location, vascular calcification in the blood vessels has been classified into two types: intimal calcification, and medial calcification. The former is typically associated with atherosclerosis, showing dispersed, punctuate or patchy mineral crystals associated with the necrotic core of the atheroma [164, 165]. On the contrary, medial calcification occurs independent of atherosclerotic lesions and the minerals are deposited within and around the elastic lamina, the concentric and inter-connected elastic extracellular matrix (ECM) rich in elastin and associated microfibrillar proteins [12, 20]. It is believed that both types of vascular calcification can be regulated by some common determinants; however more detailed studies will be needed to fully understand how different determinants may affect the initiation and progression of vascular calcification at various sites.

The main focus of the current study is to investigate the initiation and progression of medial calcification caused by matrix Gla protein (MGP) deficiency under the epistatic effects of several known genetic regulators of ECM mineralization. More specifically, we investigated the effects of

sphingomyelin phosphodiesterase 3 (SMPD3), fibroblast growth factor 23 (FGF23) and elastin on medial calcification. Using complex genetic models, we examined how genetic modifications involving the ablation or overexpression of these genes may change the severity of medial calcification phenotype in MGP deficient (*Mgp*^{-/-}) mice.

MGP is among the most potent and abundant mineralization inhibitors expressed mainly in the vascular and cartilaginous tissues [11]. Mutations in the *MGP* gene in humans leads to Keutel syndrome, a rare disease hallmarked by abnormal cartilage and vascular calcification [3, 5, 6, 166]. The *Mgp*^{-/-} mice (*Mgp*-null) recapitulates most of these traits and have been used as a model of medial calcification in several landmark studies [11, 16, 167-170]. The presence of calcific deposits in arterial tissues of these mice can be detected as early as 5 days after birth, and after that, the amount of deposited minerals increases progressively [11, 170]. Unlike the Keutel syndrome patients, all the *Mgp*^{-/-} mice die by two months of age [11, 170].

Until recently, various types of vascular calcification have been grouped together as ectopic bone formation [171]. However, our previous work has demonstrated that early phases of medial calcification in *Mgp*^{-/-} mice do not require any upregulation of chondrogenic/osteogenic genes in the aorta [170]. As reported in this study, chondrocyte-like cells appear only during the later phases of medial calcification. This late stage differentiation of VSMCs to chondrocytes may play a role in the progression of medial calcification in *Mgp*^{-/-} arteries. Although such a possibility exists, until now, no genetic analyses have been performed to investigate this.

In the developing growth plates of the skeleton, the hypertrophic chondrocytes release specialized membrane-bound bodies called matrix vesicles (MVs) that originate from the plasma membrane. These vesicles serve as nucleation sites for the hydroxyapatite (HA) crystals [172]. Sphingomyelin phosphodiesterase 3 (SMPD3), a lipid-metabolizing enzyme has been proposed to be

involved in MV-mediated mineralization of the cartilaginous growth plate mineralization. Indeed, the growth plate mineralization was significantly delayed in mice lacking functional SMPD3 [173]. Interestingly, in a cell culture model of vascular calcification, upregulation of *Smpd3* expression in VSMCs was found to induce the secretion of calcifying exosomes (MVs) *in vitro*. Furthermore, the chemical inhibition of SMPD3 prevented mineral deposition in these cultures [174]. However, whether SMPD3 has any role to play in the progression of medial calcification in MGP-deficient mice is yet to be investigated.

Systemic inorganic P_i levels have been shown to be crucial for the development of vascular calcification [175]. For instance, elevated serum P_i levels in patients with CKD are commonly associated with medial calcification [176, 177]. Phosphate-regulating gene with homologies to endopeptidase on the X chromosome (*PHEX*) has been shown to be a critical regulator of P_i homeostasis as *PHEX* mutations in humans and mice lead to severe hypophosphatemia [178, 179]. In a previous work, our group showed that *Mgp*^{-/-};*Hyp* mice with null mutations in both *Mgp* and *Phex* (*Hyp* mice) do not develop any medial calcification [16]. *PHEX* mutation upregulates the expression of the phosphaturic hormone FGF23 in osteoblasts/osteocytes [180], which in turn, downregulates the type II sodium-phosphate co-transporters in the kidneys and prevents P_i reabsorption. However, newer evidence demonstrates that *PHEX* cleaves the mineralization inhibitor Osteopontin in the bone ECM [32]. This study raised the possibility that in addition to a FGF23/P_i-dependent mechanism, *PHEX* may regulate ECM mineralization via a P_i-independent pathway [32]. At this point, the effects these pathways on medial calcification is not well understood.

Arterial elastin content has been shown as a critical determinant of medial calcification in *Mgp*^{-/-} mice [170]. As demonstrated by this study, the reduction of the elastin gene dosage in *Mgp*^{-/-};*Eln*^{+/-} mice caused a delay of mineral deposition in their media [170]. However, the progressive increase of

deposited minerals continued and eventually these mice succumb to this phenotype. The question remains whether further reduction of elastin content would lead to a complete prevention of vascular calcification.

In the current study, we have addressed several pertinent questions related to vascular calcification in *Mgp-null* mice, which have been raised by several recent advancements in the field. We demonstrated that SMPD3 does not play a significant role in medial vascular calcification in *Mgp^{-/-}* mice. Our genetic data shows that vascular calcification in *Mgp^{-/-}* mice can be prevented by raising the circulating levels of FGF23. Lastly, we were able to completely prevent the initiation of vascular calcification in *Mgp^{-/-}* mice for up to 3 weeks merely by reducing the medial elastin content by ~40%. This study will have important effects on our understanding of the mechanisms regulating various forms of vascular calcification.

2.3. Results

2.3.1. Ablation of *Smpd3* in *Mgp*^{-/-} VSMCs does not prevent vascular calcification in vivo

In order to understand the role of SMPD3 in the initiation and progression of medial calcification in *MGP*-deficient mice, we first performed immunohistochemistry on the WT and *Mgp*^{-/-} arterial sections. We detected the presence of SMPD3 along the elastic laminae of the *Mgp*^{-/-} arteries but not on those from the WT arteries (**Figure 1A**). This finding raised the possibility that in the calcified arteries, the upregulation of SMPD3 may promote the progression of mineral accumulation. This observation prompted us to conditionally ablate *Smpd3* in the VSMCs. For this purpose, we used the *Smpd3*^{fllox/fllox} mice already generated and characterized by us [181]. The *Smpd3*^{fllox/fllox} mice were first mated with *SM22-Cre* mice to obtain *Smpd3*^{+fllox};*SM22-Cre* mice in the F1 generation, which were then backcrossed to *Smpd3*^{fllox/fllox} mice to generate *Smpd3*^{fllox/fllox};*SM22-Cre* mice. **Figure 1B** shows the schematic representation of the targeted locus before and after the Cre recombinase-mediated deletion of the ‘floxed’ DNA. PCR analyses using the depicted primer pair resulted in a band of 212bp upon Cre recombinase activity, confirming the deletion event inactivating SMPD3 in the *Smpd3*^{fllox/fllox};*SM22-Cre* mice [181] (**Figure 1C**).

We then mated *Smpd3*^{fllox/fllox};*SM22-Cre* mice with *Mgp*^{+/-} mice to eventually generate *Mgp*^{-/-};*Smpd3*^{fllox/fllox};*SM22-Cre* mice via sequential breeding of the offspring. The thoracic skeleton with the descending aorta of the resultant mice were examined by micro-CT. Interestingly, scans and mineral quantification of the thoracic aorta of 5-week-old *Mgp*^{-/-};*Smpd3*^{fllox/fllox};*SM22-Cre* mice showed no statistical difference in mineral content when compared to that of *Mgp*^{-/-} age-matched controls (**Figure 1D**). These data were further supported by histological analyses of the aorta samples. VKVG staining demonstrated comparable mineralization of both *Mgp*^{-/-} and *Mgp*^{-/-};*Smpd3*^{fllox/fllox};*SM22-Cre* aorta sections (**Figure 1E**).

2.3.2. Increased circulating FGF23 corrects the vascular calcification phenotype in *Mgp*^{-/-} mice

We showed earlier that vascular calcification was prevented in the *Mgp*^{-/-};*Hyp* mice [16]. We next investigated whether this rescue is caused by the increased circulating FGF23 levels seen in *Hyp* mice. For this purpose, we generated the *Mgp*^{-/-};*ApoE-Fgf23* compound mutants, that misexpress *Fgf23* in the liver; resulting in excessive presence of FGF23 in the circulation and increased renal P_i wasting [35].

The visual examination of *Mgp*^{-/-};*ApoE-Fgf23* mice revealed the absence of the common phenotypic traits, e.g. ruffled fur and hunched posture, associated with *Mgp*^{-/-} young adults. All the *Mgp*^{-/-} mice, die by 6 weeks of age, while the *Mgp*^{-/-};*ApoE-Fgf23* mice survived the entire length of the study (**Figure 2A**). As expected, the serum P_i levels were reduced by half in the *Mgp*^{-/-};*ApoE-Fgf23* mice when compared to the WT and *Mgp*^{-/-} littermates, whereas the serum Ca²⁺ levels remained unchanged. Recapitulating what has been reported in the patients with X-linked hypophosphatemia and *Hyp* mice [16, 182], we observed that there was also a significant increase in the circulating alkaline phosphatase levels in the newly generated *Mgp*^{-/-};*ApoE-Fgf23* compound mutants (**Figure 2B**). All the biochemical analyses were performed at 5-weeks of age.

We next performed the 3D reconstructions of micro-CT scans of the thoracic region which revealed a severe aorta calcification in the *Mgp*^{-/-} mice at 5 weeks of age. However, the age-matched *Mgp*^{-/-};*ApoE-Fgf23* mice showed a complete correction of the calcification phenotype, which was comparable to that of the *Mgp*^{-/-};*Hyp* double mutants. We observed a mild deposition of minerals in the arteries of *Mgp*^{-/-};*ApoE-Fgf23* mice at 10 months of age (**Figure 2C**). VKVG staining of the histological sections prepared from the thoracic aortae of all these mice confirmed the micro-CT results above (**Figure 2D**). Alcian blue and van Gieson (ABVG) staining of the aorta sections from 4-weekold *Mgp*^{-/-} mice showed intense blue staining indicating the presence of a proteoglycan-rich cartilage

matrix in these heavily calcified aortas. As is the case with the WT sections, the sections from the age-matched *Mgp*^{-/-};*ApoE-Fgf23* remained unstained (**Figure 2E**).

2.3.3. A high phosphorus diet induces rapid vascular calcification in *Mgp*^{-/-};*ApoE-Fgf23* mice

We next interrogated whether increased circulating levels of P_i would be sufficient to induce vascular calcification in our rescue model, the *Mgp*^{-/-};*ApoE-Fgf23* mice. Thus, we fed these mice a high (2%) phosphorus diet for 10 days, which resulted in a severe calcification of the thoracic aorta as shown by Alizarin red staining (**Figure 3A**). VKVG staining further confirmed these findings. No vascular calcification was detected in controls, WT and *ApoE-Fgf23* mice on the same high phosphorus diet (**Figure 3A**). As expected, the serum P_i level in *Mgp*^{-/-};*ApoE-Fgf23* mice increased and were comparable to that of WT mice and *ApoE-Fgf23* on the same diet. Serum Ca²⁺ levels remained unchanged (**Figure 3B**).

2.3.4. Comparative analyses of arterial elastin content in compound models expressing mouse and human elastin orthologs

In order to examine the effects of elastin orthologs and content on the initiation and progression of medial calcification, we used several genetic models expressing mouse and/or human elastin at various dosages. We first analyzed the precursor mouse strains which include 1) WT mice, carrying both copies of mouse elastin gene (*Eln*), 2) The haploinsufficient *Eln*^{+/-} mice carrying only one allele of *Eln*, 3) The *Eln*^{+/-};*ELN*^{+/+} (*Eln*^{+/-},*BACHELN*) mice, carrying one allele of *Eln* and two alleles of human elastin (*ELN*) transgene, and 4) The *Eln*^{-/-};*ELN*^{+/+} mice, containing two alleles of *ELN* only. PCR analyses revealed that our breeding program resulted in all the above genotypes (**Figure 4A**).

We interrogated whether the genetic models with mouse and human elastin orthologs express the protein at a level corresponding to the gene dosages they carry. Aortic extracts of WT, *Eln*^{+/-},

Eln^{+/-};*ELN*^{+/+} and *Eln*^{-/-};*ELN*^{+/+} mice were analyzed by amino acid analysis for elastin, collagen and non-elastin/non-collagen protein quantification. We detected an increased collagen to elastin ratio in the *Eln*^{-/-};*ELN*^{+/+} mice as reported before [183] (**Figure 4B**). This finding is supported by the increased hydroxylysine to hydroxyproline ratio in the latter mouse model (**Figure 4C**). Analysis of non-collagenous/non-elastin proteins showed an increase in *Eln*^{+/-} and *Eln*^{-/-};*ELN*^{+/+} arteries when compared to that of WT mice (**Figure 4D**). The arterial elastin content in the *Eln*^{-/-};*ELN*^{+/+} mice was the lowest. As is the case with the collagen to elastin ratio, there was an increase of collagen content over the total protein content (**Figure 4E and F**). We also noticed that elastin content in the *Eln*^{-/-};*ELN*^{+/+} aorta was slightly lower to that of WT mice, but higher than *Eln*^{+/-} mice (**Figure 4E**). In general, the relative elastin amounts present in the arteries of various genotypes used correspond to the pattern of their gene dosages.

2.3.5. Arterial mineral deposition is affected by elastin content, but not by ortholog combination

The milder vascular calcification trait in Keutel syndrome patients in comparison to the genetic model prompted us to investigate whether mouse and human elastin orthologs can promote medial calcification in a comparable manner. Earlier, we demonstrated that *Mgp*^{-/-};*Eln*^{+/-} mice with a single allele of *Eln* could delay the mineralization in the arterial walls [170]. Based on the data presented in **Figure 4E**, elastin content in this model is expected to be approximately 25% lower than normal. In the current study, we examined whether the expression of the human ortholog in the arteries of *Eln*^{+/-} mice, compensating for the loss of the endogenous protein can accelerate vascular calcification.

We bred the *Eln*^{+/-};*ELN*^{+/+} mice with *Mgp*^{+/-} mice to eventually generate *Mgp*^{-/-};*Eln*^{+/-};*ELN*^{+/+} mice. The thoracic skeleton with the descending aortae from these and control *Mgp*^{-/-} and *Mgp*^{-/-};*Eln*^{+/-} were scanned and analyzed by micro-CT at 3-weeks of age (**Figure 5A**). As reported by us previously, we observed a reduction of the deposited minerals in the *Mgp*^{-/-};*Eln*^{+/-} aorta in

comparison to that of *Mgp*^{-/-} aorta [170]. Interestingly, we observed more mineral deposition in the *Mgp*^{-/-};*Eln*^{+/-};*ELN*^{+/+} aorta in comparison to that of *Mgp*^{-/-};*Eln*^{+/-} aorta. In fact, the severity of the mineral deposition in the *Mgp*^{-/-};*Eln*^{+/-};*ELN*^{+/+} and *Mgp*^{-/-} aortae were visually indistinguishable. A quantitative analysis performed on the scanned images confirmed our qualitative observation (**Figure 5B**). We also observed a comparable mineralization of the elastic lamina by VKVG staining performed on histological sections of the aorta samples collected from the *Mgp*^{-/-}, *Mgp*^{-/-};*Eln*^{+/-} and *Mgp*^{-/-};*Eln*^{+/-};*ELN*^{+/+} mice (**Figure 5C**).

2.3.6. Prevention of vascular calcification in *Mgp*^{-/-};*Eln*^{-/-};*ELN*^{+/+} mice

The comparable abilities of mouse and human elastin orthologs to affect medial calcification established the humanized model (*Eln*^{-/-};*ELN*^{+/+} mice) developed by Hirano *et al.* [183] as a valid tool for further mechanistic studies. Considering that the arterial elastin content is the lowest in these mice in comparison to the rest of the genetic models used by us, we decided to examine how this would affect the severity of medial calcification. The homozygous *Mgp*-null mutations were introduced to the humanized model to generate the *Mgp*^{-/-};*Eln*^{-/-};*ELN*^{+/+} mice.

Remarkably, the *Mgp*^{-/-};*Eln*^{-/-};*ELN*^{+/+} mice survive at least up to 10 months, the experimental end point of our survival study (**Figure 6A**) and beyond that period. Alizarin red and Alcian blue staining of the thoracic aorta revealed a complete absence of calcification in these mice at 3-weeks of age, while the aorta was heavily calcified in the age-matched *Mgp*^{-/-} mice (**Figure 6B**). VKVG staining of thoracic aorta sections confirmed the absence of mineral deposition in the *Mgp*^{-/-};*Eln*^{-/-};*ELN*^{+/+} mice. Additionally, the typical widening of the arterial wall seen in *Mgp*^{-/-} aortas was also absent in the *Mgp*^{-/-};*Eln*^{-/-};*ELN*^{+/+} aortas. However, we observed an increase of the collagen staining adjacent to the elastic laminae in the latter genotype. Hart's staining showed that the elastic laminae were thinner, but more in number in comparison to the WT mice. Additionally, we also observed an

increased cell number in the *Mgp*^{-/-};*Eln*^{-/-};*ELN*^{+/+} mice (**Figure 6C**). We next examined the overall status of vascular calcification in these mice at 1 year of age. 3D reconstruction of micro-CT scans of the thoracic region of these aged mice revealed a mild and punctate mineralization throughout the thoracic aorta and in the coronary and intercostal arteries. In comparison, all these arteries are already heavily calcified by 5-week of age in *Mgp*^{-/-} mice (**Figure 6D**). These findings were further confirmed by VKVG staining of the thoracic aorta sections using 1-year-old *Eln*^{-/-};*ELN*^{+/+} aorta sections as controls. Hart's staining of the elastic laminae revealed elastic fiber fragmentation and medial widening in the calcified *Mgp*^{-/-};*Eln*^{-/-};*ELN*^{+/+} aortas (**Figure 6E**).

2.3.7. Mineral characterization in the aged *Mgp*^{-/-};*Eln*^{-/-};*ELN*^{+/+} mice

We next examined the mineral deposits present in the mouse arteries by combining Raman spectroscopy with scanning electron microscopy (SEM) and energy-dispersive x-ray spectroscopy (EDS). Raman spectra of *Mgp*^{-/-} arteries show the presence of carbonated hydroxyapatite (CHA) by the ν_1 P_i band between 959 and 962 cm⁻¹ (**Figure 7A**). In calcified *Mgp*^{-/-};*Eln*^{-/-};*ELN*^{+/+} aortas, Raman spectroscopy shows other mineral phases in addition to CHA (see the several ν_1 P_i vibration bands between 942 and 987 cm⁻¹ on **Figure 7A**). Although Raman spectroscopy reveals only the presence of apatite in *Mgp*^{-/-} samples, we previously showed by using X-ray photoelectron spectroscopy (XPS) and near-edge x-ray absorption fine structure spectroscopy (NEXAF) that the mineral deposits are actually a mixture of precursor phases, such as amorphous calcium phosphate (ACP) and Octacalcium phosphate (OCP), and apatite phases (HA and CHA) [184]. The difference in Raman sensitivity for detecting the precursor phases suggests that the amount of those phases is likely much less prevalent in *Mgp*^{-/-} than in *Mgp*^{-/-};*Eln*^{-/-};*ELN*^{+/+} mice.

To further characterize the calcified arteries, we estimated the degree of crystallinity of the minerals by measuring the full width at half maximum (FWHM) of the ν_1 P_i peak (**Figure 7B**). The FWHM of this peak inversely correlates with mineral crystallinity. As previously reported [184], in

Mgp^{-/-} mice the FWHM values significantly decrease over time, suggesting an increase in mineral crystallinity. Significantly higher FWHM values are found in *Mgp*^{-/-};*Eln*^{-/-};*ELN*^{+/+} mice compared to those found in 5 week-old *Mgp*^{-/-} mice while there is no significant difference with the FWHMs found in 1 week-old *Mgp*^{-/-} mice (**Figure 7B**). This suggests that the crystallinity of the minerals in the *Mgp*^{-/-};*Eln*^{-/-};*ELN*^{+/+} mice is similar to the one of *Mgp*^{-/-} mice at 1 week.

By integrating the area of the ν_1 P_i peak and dividing the value by the area of the peak at 1440 cm^{-1} , which is relative to the stretching of the CH_2 and CH_3 groups of the organic part (δ as CH_2 , CH_3), we estimated the amount of inorganic deposits relative to the amount of organic material found in the calcified aortas, i.e. mineralization extent (ME) (**Figure 7C**)[185]. In agreement with our previous work [184], from 1 to 5 week, the MEs significantly increase in *Mgp*^{-/-} mice, indicating an overall increase in mineral deposition over time. The ME values in *Mgp*^{-/-};*Eln*^{-/-};*ELN*^{+/+} mice are comparable to the values found in 1 week-old *Mgp*^{-/-} mice and are significantly lower than the ones found at 5 week in *Mgp*^{-/-} samples. This suggests that the amount of minerals in *Mgp*^{-/-};*Eln*^{-/-};*ELN*^{+/+} samples are similar to the amount found at 1 week in *Mgp*^{-/-} mice.

Finally, we combined SEM and EDS to examine the structure and nature of the minerals. SEM images of calcified aortas from 10-month-old and 1-year-old *Mgp*^{-/-};*Eln*^{-/-};*ELN*^{+/+} mice show minerals in the form of compact material composed of smooth platelets (**Figure 7D**). Ca/P ratios determined by EDS vary from 1.3 to 1.8, thus confirming that *Mgp*^{-/-};*Eln*^{-/-};*ELN*^{+/+} samples contain several calcium phosphate phases, such as ACP, OCP, HA, and CHA [186] (**Figure 7D**).

2.4. Discussion

ECM mineralization is a physiologic process in the skeletal ‘hard’ tissues, and a pathologic condition, when occurs in the ‘soft’ tissues like the blood vessels [17]. Vascular calcification is commonly associated with a number of genetic and metabolic diseases and among the common causes of morbidity in these patients. A detailed understanding of the key determinants regulating vascular calcification with different etiology will be necessary to develop an effective treatment strategy, which is still missing.

Both physiologic and pathologic mineralization appear to involve two common determinants – systemic/extracellular levels of two mineral ions, Ca^{2+} and P_i , and a suitable ECM that can act as a scaffold for the nucleation of minerals. Additionally, the process is regulated by the extracellular levels of mineralization inhibitors [17, 161]. In the skeletal hard tissues, the hierarchical assembly of collagen triple helixes within the fibrils and the fibers create nanoscale intrafibrillar and interfibrillar gaps. These gaps provide a protected microenvironment, which are not accessible by large protein inhibitors, facilitating mineral nucleation [187]. Inorganic pyrophosphate (PP_i), a small ionic inhibitor of mineralization, may inhibit this process; however, it is cleaved by a promiscuous extracellular enzyme, alkaline phosphatase (ALPL). In fact, ALPL promotes skeletal ECM mineralization by cleaving PP_i , and at the same time, generating P_i through the same catalytic activity [54]. The nascent mineral crystals growing within and around the collagen fibrils at many different sites of the scaffold eventually coalesce together to form a continuous layer of mineralized bone.

An auxiliary mechanism involving several intracellular enzymes also initiates physiologic ECM mineralization in the skeletal tissues. SMPD3 has been identified as an important regulator of both cartilage and bone ECM mineralization [173, 181]. This enzyme together with a downstream phosphatase may work through the matrix vesicles (MVs), the nanoscale (20-200 nm) extracellular

bodies released by the cells, which provide a P_i rich microenvironment promoting the precipitation of apatitic crystals [17, 188].

The above determinants of skeletal tissue mineralization may also regulate different types of vascular calcification in humans and/or in the experimental models, if not always as the full array, but in isolation as independent regulators. For example, the reduction of mineralization inhibitor PP_i in the ECM is sufficient to cause generalized arterial calcification of infancy (GACI) [189]. Similarly, overexpression of ALPL in the VSMCs causes arterial calcification in a transgenic mouse model [16] and inhibition of SMPD3 in VSMC cultures inhibits the MV-mediated mineral deposition [174, 190].

Our current study investigates the determinants of medial calcification in *Mgp*^{-/-} mice, a model for human Keutel syndrome. Initially, it was reported that the Keutel syndrome patients do not show any deposition of minerals in their vascular tissues [3]. However, more recent studies have contradicted these reports showing calcified arteries in some Keutel syndrome patients [5, 6]. Despite these findings, it is generally agreed that the vascular calcification phenotype in the human patients is milder in comparison to that of the murine model.

In a previous study, we showed that chondrogenic/osteogenic transdifferentiation of the VSMCs was not a prerequisite for the initiation of vascular calcification in MGP-deficient mice [170]. In agreement with this finding, here we show that SMPD3, a chondrogenic/osteogenic marker, does not act as a regulatory enzyme for vascular calcification caused by MGP deficiency. This later finding suggests that MVs are less likely to be involved in medial calcification in *Mgp*^{-/-} mice. This result is not completely unexpected as we recently reported the presence of amorphous calcium phosphate without any presence of MVs in the calcified nasal septum of MGP-deficient mice [191].

Once the arterial wall in *Mgp*^{-/-} mice is heavily calcified, a partial phenotypic change of the VSMCs to chondrogenic cells have been noticed, which results in the deposition of a cartilaginous ECM [63, 170]. Since SMPD3 has been shown to be critical for cartilage ECM mineralization, we predicted that this enzyme might be involved in augmenting mineral deposition during the later stages (around 4 weeks after birth) of vascular calcification in MGP-deficient mice [173, 181]. However, our data presented in the current study ruled out this possibility. Nevertheless, this finding does not exclude the possible involvement of SMPD3 in other kind of vascular calcification e.g. heart valve and intimal calcification.

We earlier demonstrated that introducing *Phex* mutation (*Hyp*, causing hypophosphatemia) to *Mgp*^{-/-} mice, completely rescues the vascular calcification phenotype [16]. In addition to the known function of PHEX in the systemic regulation of P_i ; an intrinsic role of this membrane protein has been suggested recently. It has been shown that PHEX cleaves the mineralization inhibitor osteopontin, which is present in the skeletal ‘hard’ tissues [32]. This latter observation was particularly interesting for us, as Speer *et al.* showed that osteopontin expression was induced in the arteries of MGP-deficient mice and more importantly, there was a significant increase of vascular calcification in *Mgp*^{-/-};*Opn*^{-/-} double null mice [169]. Taken together, these findings raised a question regarding the role of FGF23-mediated reduction of P_i in the prevention of vascular calcification in *Mgp*^{-/-};*Hyp* mice. Our work presented here conclusively suggests that the increase of systemic FGF23 and the resultant hypophosphatemia is the primary cause of the rescue of the phenotype presented in our previous study. Unlike the heavily calcified *Mgp*^{-/-} aorta sections, the age-matched *Mgp*^{-/-};*ApoE-FGF23* sections did not stain blue upon Alcian blue treatment. This observation suggests that the late-stage transdifferentiation of the VSMCs to chondrocyte-like cells is secondary to the calcification event, but not directly due to the loss of MGP.

Circulating FGF23 has been associated with vascular dysfunction [192]. Additionally, FGF23 has been shown to be upregulated with the progression of coronary artery calcification in hemodialysis patients. However, whether FGF23 action is dependent or independent of its co-receptor Klotho, is still a matter of dispute. There are almost equal numbers of studies claiming the presence or absence of this receptor in the vascular tissues. It is well known that the circulating FGF23 level is high in CKD patients [193]. Numerous clinical and animal studies have identified a close relationship between FGF23 and the prevalence of cardiac events, including myocardial infarction, left ventricle hypertrophy and heart failure [194]. Although the mechanism is unknown, Klotho-independent pathologic cardiac remodelling by FGF23 has been reported [195]. On the contrary, anti-calcific effects were seen in human aortic VSMCs when FGF23 affinity was enhanced by Klotho overexpression [196].

Although we did not examine the full-spectrum vascular parameters in our *ApoE-Fgf23* mice, VKVG staining of the histological sections showed the absence of vascular calcification in these mice on a regular diet. Also, aging or feeding these mice a high phosphorus (2%) diet did not cause a vascular calcification phenotype. These observations suggest that systemic FGF23 level by itself may not cause vascular calcification, at least in mice. Considering the controversies over the expression of Klotho in the VSMCs, at this point it is difficult to predict a direct role of FGF23 in these cells to prevent vascular calcification caused by MGP-deficiency. However, our observation that feeding *Mgp^{-/-};ApoE-Fgf23* mice a high phosphorus diet only for 10 days can cause a severe vascular calcification suggests that in this model, systemic P_i but not any direct action of FGF23 on VSMCs, is the main determinant of the calcification phenotype.

Several mouse models are being currently used to study medial calcification. Diet-based methods are common; for instance, DBA/2 mice (genetically prone to develop ectopic calcification) fed a diet containing warfarin – a vitamin-k antagonist and vitamin K1 for 4 weeks develop medial calcification [197]. Additionally, combination an adenine-rich diet (known to cause renal failure) together with high phosphorus, causes medial calcification in mice [198]. Also, a combination of high phosphorus diet and partial nephrectomy in mice on the DBA/2 background has been used. Although studies on these models have significantly contributed to our understanding of vascular calcification, there are some shortcomings, such as dependency on the genetic background, mild and delayed appearance of the calcification phenotype, unexpected lethality and the technical complexities to generate the surgical models. On the contrary, the *Mgp*^{-/-};*ApoE-Fgf23* mice can be generated easily, maintained as a stock for a long time, and vascular calcification can be induced rapidly by simply feeding them a high phosphorus diet. While it is understandable that our model cannot be a replacement for all the existing models of medial calcification of different etiology, this model can be very useful to screen potential therapeutic agents designed to prevent the precipitation and growth of the deposited minerals.

Elastin provides unique mechanical properties to the connective tissues, which undergo cycles of stretching and contraction. Elastin fibers are responsible for the recoiling mechanism reinstating the stretched tissue to its original state. The similar pathological conditions associated with *ELN* mutations in humans and the genetically modified animals suggest that the functional properties of this protein are evolutionarily conserved [199]. This notion is further supported by the general pattern in the structure showing alternating hydrophobic and cross-linking domains in various elastin orthologs. Interestingly, despite the functional and structural conservation of elastin across the species, mouse and human elastin orthologs show only 64.1% identity at the amino acid level. This is much lower than the average

78.5% amino acid sequence identity between mouse and human proteins [199]. Despite this relatively low level of sequence identity, we found that the medial calcification in MGP-deficient mice, which were also heterozygotes for the mouse *Eln* gene and homozygotes for the human *ELN* transgene (*Mgp*^{-/-};*Eln*^{+/-};*ELN*^{+/+} mice), mineralize comparably to that of *Mgp*^{-/-} mice with two functional alleles of the mouse *Eln* gene. Considering that the particular elastin ortholog combinations and gene dosages in these two strains result in comparable amounts of total elastin in the arteries, this result suggests a similar mineralization promoting capacity of the human elastin to that of mouse elastin. It appears that as is the case with the elastic properties, the ability of elastin to promote mineral nucleation is also evolutionarily conserved.

Our data suggest that MGP has a critical role to protect the arterial elastic laminae from the P_i-induced mineral deposition. As mentioned above, the vascular calcification trait in Keutel syndrome patients is not as severe as in mice [5, 6]. This milder trait may not be attributed to the sequence differences between the mouse and human elastin orthologs, as our data presented here shows that the total elastin content, but not the ortholog type is a determinant of medial calcification. At this point, the cause of a milder vascular calcification phenotype in Keutel syndrome patients remains unknown. The basal P_i level in human blood is around 3.5 mg/dL as oppose to approximately 8 mg/dL in mice [65, 200]. It is possible that the lower amount of circulating P_i in humans prevents the massive buildup of minerals in the human arteries lacking MGP. However, the involvement of additional regulatory mechanisms to prevent vascular calcification in humans cannot be ruled out.

As in bones and teeth, the minerals deposited ectopically in the vascular tissues are CHA (Ca₁₀-p(PO₄)₆-p(OH)₂-p(CO₃)p) crystals [17]. However, whether there is ACP in bone is a matter of long-standing debate for the last 40 years [201]. On the other hand, the presence of ACP at the site of pathologic mineralization of the soft tissues is well documented [202-204]. We have recently reported

the presence of ACP at two sites of ectopic mineralization, i.e. the nasal septum and the aorta of *Mgp*^{-/-} mice [184, 191]. Our work shows that the mineral nucleation event in the arteries of *Mgp*^{-/-} mice is a multi-step process, starting from more rudimentary, precursor phases in the form of ACP and OCP, leading to an overall more crystalline deposit such as HA and CHA [204, 205]. Raman spectroscopy shows that mineral deposition in aged *Mgp*^{-/-};*Eln*^{-/-};*ELN*^{+/+} mice is much less severe than in *Mgp*^{-/-} mice at 5 weeks of age, when the arteries are severely calcified. Indeed, both the crystallinity and the amount of minerals found in *Mgp*^{-/-};*Eln*^{-/-};*ELN*^{+/+} mice after 10 months are similar to those of the minerals in 1-week-old *Mgp*^{-/-} mice. Both Raman and SEM/EDS data show that *Mgp*^{-/-};*Eln*^{-/-};*ELN*^{+/+} samples contain a significant amount of precursor phases, such as ACP and OCP, in addition to apatite phases. These results confirm that although the nature of the minerals is generally similar, a 40% reduction of medial content of elastin in *Mgp*^{-/-} mice significantly delays the initiation and progression of mineral deposition.

The presence of mineralization inhibitors PP_i and MGP protects the vascular tissues from spontaneous calcification. Interestingly, in GACI, reduced level of extracellular PP_i causes vascular calcification, despite the presence of MGP in the ECM [189]. Similarly, in MGP deficiency, elastic lamina calcification occurs although the PP_i transport and synthesis mechanisms in the arterial tissues are both functional [170]. While the ectopic ECM mineralization caused by the absence of either of these inhibitors can be rescued by the reduction of the systemic P_i levels [16], it remains to be seen whether they prevent the mineralization of different scaffolds in the arterial walls. Interestingly, despite an increase of the total collagen in the humanized arteries lacking MGP in *Mgp*^{-/-};*Eln*^{-/-};*ELN*^{+/+} mice, no early calcification was associated with the collagen scaffold. It is possible that while MGP prevents the calcification of the elastic laminae, the anti-mineralization function of PP_i is restricted to the collagen fibers present adjacent to the elastic laminae. Further work will be needed to examine the complementary role of MGP and PP_i in the prevention of vascular calcification.

Although vascular tissue mineralization in *Mgp*^{-/-} mice does not require the osteogenic or chondrogenic transdifferentiation of the VSMCs, it does rely on the common determinants of ECM mineralization. Indeed, except for the involvement of the MV-mediated auxiliary mechanism, the basic tenet of skeletal tissue mineralization identifying the mineral ions, mineral scaffolding ECM and the absence of mineralization inhibitor as the key determinants is also valid for vascular calcification in MGP-deficient mice. Like bone mineralization, the vascular calcification in MGP-deficiency is P_i dependent and for its initiation, an elastin-rich extracellular scaffold is required and a mineralization inhibitor, MGP, must be removed [17, 170].

Currently, we do not know how MGP protects the vascular tissues from P_i -induced calcification. It has been shown that this protein undergoes two post-translational events. There are 4 glutamic acid (Glu) residues in mouse MGP, which are γ -carboxylated by a vitamin K-dependent γ -carboxylase to be converted to Gla-residues. Additionally, there are 3 conserved serine residues at the N-terminal, which are post-translationally phosphorylated [9, 66]. However, until now, no genetic studies have been performed to investigate the role of these residues or the enzymes involved in their modifications in the vascular tissues. These genetic experiments will be essential to understand the role of the post-translational modifications on the anti-mineralization functions of MGP.

Our analyses of MGP-deficient mice have established that not all types of vascular calcification traits can be grouped together as ectopic bone formation. Further, the genetic experiments presented in the current study provide an in-depth understanding of how two determinants, P_i and elastin, regulate vascular calcification caused by MGP deficiency. As a proof of principle, we provide evidence that at least some types of vascular calcification can be effectively prevented by the modulation of these determinants. The yet unknown roles of these determinants in other forms of vascular calcification

must be elucidated to fully comprehend the scope of these findings to find the long-elusive cure for vascular calcification.

2.5. Materials and methods

2.5.1. Mouse models

The generation of *Mgp*^{-/-}, *ApoE-Fgf23* and *Eln*^{+/-}(*BAC_hELN*) mice (hereinafter referred to as *Eln*^{+/-}; *ELN*^{+/+}) have already been described [11, 35, 183]. *Hyp* mice were purchased from Jackson Laboratories. *ApoE-Fgf23* mice were generated by Dr. Karaplis' lab and the *Eln*^{+/-}; *ELN*^{+/+} mice were generated by Dr. Mecham's lab. The introduction of the *Mgp* mutation to the above mouse models was achieved through breeding. All the experiments were performed on mice with C57BL/6 background. Mice were maintained in a pathogen-free standard animal facility. All the strains were backcrossed to C57BL/6 inbred strain for at least six generations.

2.5.2. Genotyping PCR

Genotypes were determined by PCR on genomic DNAs isolated from tail biopsies. The sequences of the primers used for genotyping are provided upon request.

2.5.3. Micro-CT and mineral quantification

Micro-CT scanning of mouse aortas were performed with a SkyScan model 1272 instrument (SkyScan) set at a resolution of 8.0 μm and 0.25-mm Al filter. Image acquisition was performed at 40Kv and 250 μA with a 0.4-degree rotation between frames. Adaptive thresholding was applied to bone and aorta separately. Micro-CT image processing and analysis was performed with version 2.2f of the manufacturer's software (SkyScan). The 3D-reconstructions were done using the CtAn and CtVol software (SkyScan). Mineral quantification was calculated using CtAn software (SkyScan), considering the BV/mm^3 generated in the basic values.

2.5.4. Histology and tissue imaging

Mouse thoracic cages were fixed overnight in 10% formalin, embedded in methyl methacrylate, sectioned (7 μm), and stained by von Kossa and van Gieson (VKVG) to visualize calcified tissues and collagen, Hart's staining to visualize the elastic lamina; or Alcian blue and van Gieson (ABVG) to detect proteoglycans in the cartilaginous matrix. For SMPD3 (Santa Cruz, sc-67305) immunohistochemistry, 7- μm -thick paraffin sections of decalcified tissues were prepared. Images were taken using a light microscope (DM200; Leica Microsystems) with 20X (numerical aperture of 0.40) and 40X (numerical aperture of 0.65) objectives. All histological images were captured using a digital camera (DP72; Olympus Canada Inc), acquired with DP2-BSW software (XV3.0; Olympus Canada Inc) and processed using PhotoShop software (Adobe).

2.5.5. Gene expression analysis

Gene expression analyses were performed using a quantitative real-time PCR (qRT-PCR) system (Model 7500; Applied Biosystems, Mississauga, ON). Total RNA was extracted from different tissues with TRIZOL reagent (Invitrogen) and subjected to DNase I (Invitrogen) treatment. The first-strand cDNA synthesis and qRT-PCR were performed using a high-capacity cDNA reverse-transcription kit (Applied Biosystems) and Maxima SYBR green quantitative PCR master mix (Fermentas), respectively. Relative gene expression was analyzed using SDS software (Applied Biosystems) using comparative CT and hypoxanthine guanine phosphoribosyl transferase (*Hprt*, a housekeeping gene) expression as an endogenous control. In order to calculate the delta cycle threshold (DCT) value, the mean CT value of the expression of a gene in a sample was first normalized to the mean CT value of *Hprt* expression in that sample. The DCT value of the calibrator sample was subtracted from that of the sample-of-interest to obtain the DDCT value. The relative expression was reported as $2^{-\text{DDCT}}$.

2.5.6. Serum biochemistry

Serum Ca^{2+} and P_i levels were measured using commercially available kits (Sekisui Diagnostics P.E.I. Inc, Charlottetown, Canada). To measure tissue ALPL activity, aortic protein extracts were prepared with 1X Passive Lysis Buffer (Promega, WI, USA) and total proteins were measured by the Pierce Coomassie Plus Protein Assay (Thermo Scientific). ALPL activity was measured using para-nitrophenylphosphate (p-nitrophenyl phosphate) substrate (Sigma-Aldrich) and then normalized by the respective protein concentration in the extracts as described.

2.5.7. Tissue biochemistry

For collagen and elastin analysis, specimens were cut into small pieces and digested with high-purity bacterial collagenase (C0773; Sigma, Germany; 1 U/mL, 37°C, 12 hours). After centrifugation, the soluble fraction containing collagen was subjected to hydrolysis and amino acid analysis. The residual fraction was extracted by hot alkali (0.1 N NaOH, 95°C, 45 minutes). After centrifugation the supernatant containing noncollagenous/non-elastin proteins (NENCs) and the insoluble residue containing insoluble elastin were subjected to hydrolysis. Hydrolysis was performed in 6 N HCl at 110°C for 24 hours. Dried hydrolyzates were redissolved in sodium citrate loading buffer (pH 2.2) and amino acid analysis was performed by ion exchange chromatography with postcolumn derivatization with ninhydrin (Biochrom 30; Biochrom, United Kingdom). The amino acid profile of the supernatant after collagenase digestion showed a profile typical for collagen, whereas the supernatants after hot alkali treatment were free of hydroxyproline. The amino acid profile of the insoluble fraction after hot alkali extraction was typical for elastin. The content of collagen, elastin, and of non-elastin/noncollagenous protein was expressed per total protein ($\mu\text{g}/\mu\text{g}$).

2.5.8. Skeletal preparations

Skeletal tissues from adult mice were fixed overnight in 95% ethanol, stained in 0.015% Alcian Blue dye (Sigma-Aldrich) in a 1:4 solution of glacial acetic acid and absolute ethanol for 24 hours. Tissues were then treated with 2% potassium hydroxide for another 24 hours (or until the soft tissues were dissolved) and then stained by 0.005% Alizarin Red (Sigma-Aldrich) in a 1% potassium hydroxide solution. Finally, the stained skeletal tissues were clarified in 1% potassium hydroxide /20% glycerol for 2 days.

2.5.9. Raman spectroscopy

Aorta cross sections were analyzed by Raman spectroscopy using a Bruker Senterra confocal Raman spectrophotometer equipped with a 785nm diode laser coupled with an Olympus optical microscope, using a 40x objective. Spectra were collected at 100 mW laser power and spectral resolution of 3.5 cm^{-1} , between $400\text{ and }1800\text{ cm}^{-1}$, with an integration time of 40 seconds and 2 co-additions. In total, 10 points per sample were analyzed. The data was analyzed using OPUS software (OPUS 7.0.0, Bruker, Karlsruhe, Germany).

2.5.10. Scanning electron microscopy (SEM) and energy-dispersive X-ray spectroscopy (EDS)

Aorta cross sections were characterized using a combination of SEM and EDS. Samples were secured to an aluminum sample holder with carbon tape, and then coated with about 8 nm carbon (carbon sputter coater, EMS150R ES, Electron Microscopy Sciences (EMS)). The samples were then imaged using an Inspect-50 field emission SEM (FEI, Japan), at 10 kV operating voltage under high vacuum. EDS spectra were obtained in the regions of interest using an EDX spectrometer (EDX, Thermo Scientific, USA).

2.6. Data analysis

All results are shown as means \pm standard deviations. Statistical analyses were performed by Student's t test or analysis of variance (Tukey's multiple-comparison test) using GraphPad Prism software. Single asterisk indicates $p < 0.05$, two asterisks indicate $p < 0.01$ and three asterisks indicate $p < 0.001$.

2.7. Acknowledgements

We thank Mia Esser and Louise Marineau for animal husbandry Mark Lepik for the micro-CT images presented in Figure 6.

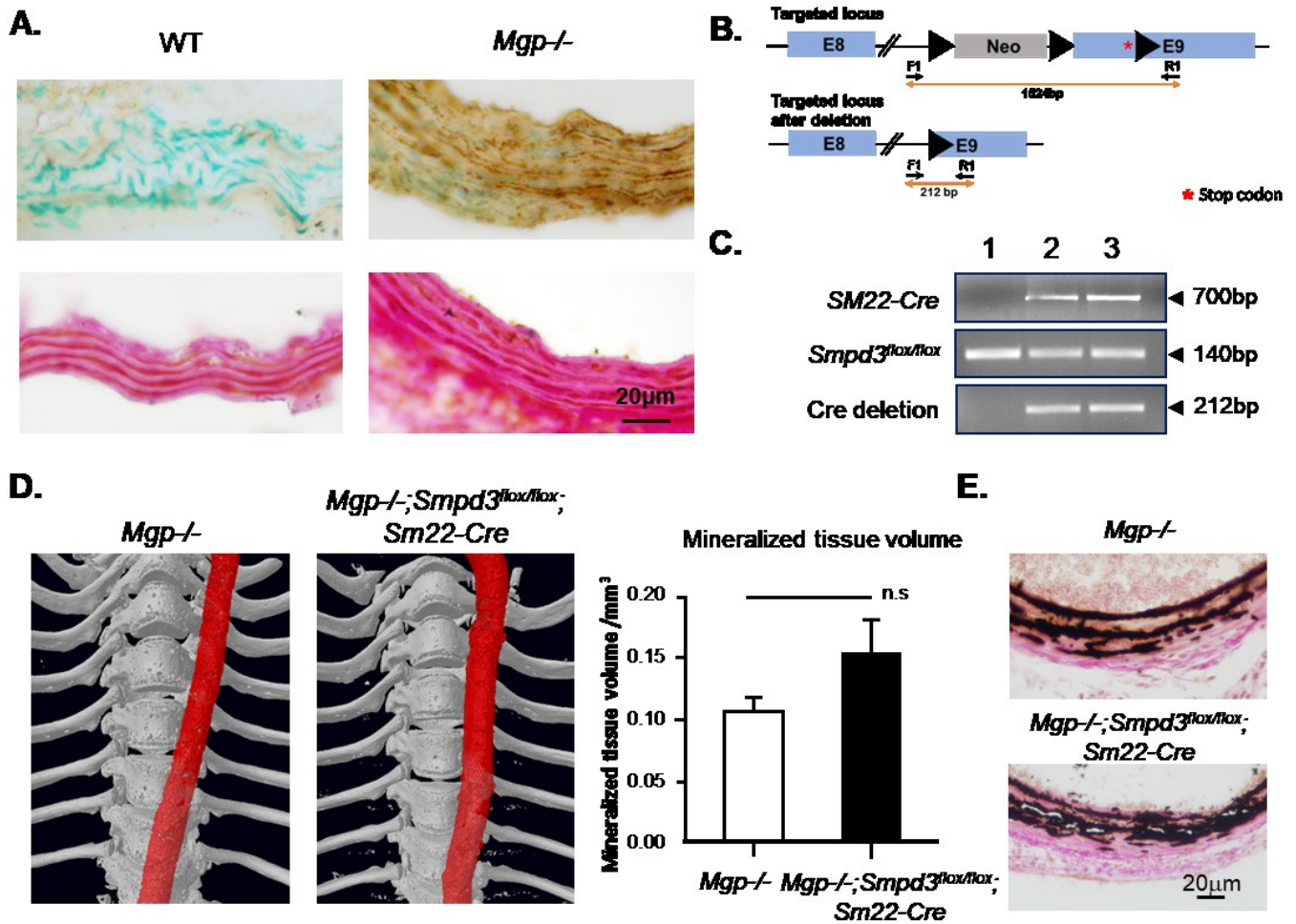


Figure 2.1. Ablation of *Smpd3* in *Mgp*^{-/-} VSMCs does not prevent vascular calcification in vivo.

A. Decalcified histological sections of 5-week-old WT and *Mgp*^{-/-} descending aortas immunostained using an anti-SMPD3 antibody (top panel) showing the presence of SMPD3 in the *Mgp*^{-/-}, but not in the WT aorta. The lower panels show the decalcified serial sections stained with VKVG showing the absence of minerals. **B.** Schematic representation of the targeted *Smpd3* locus before and after the deletion of the ‘floxed’ sequence in the presence of Cre recombinase in the *Smpd3*^{flx/flx}; *SM22-Cre* mice. The arrows represent the forward (F1) and reverse (R1) primers used for PCR to detect the *Smpd3* deletion in the arteries. *Stop codon. **C.** Top panel: PCR analysis to detect the *SM22-Cre* transgene; middle panel: PCR analysis to detect the *Smpd3*^{flx/flx} allele; bottom panel: PCR analysis to detect the Cre recombinase-mediated deletion of the targeted *Smpd3* locus. A 1524 bp fragment of the targeted locus has been shortened to 212 bp after the Cre recombinase activity. **D.** 3D reconstruction of the micro-CT scans of the 5-week-old *Mgp*^{-/-} control thoracic skeleton with the aorta and that of age-matched *Mgp*^{-/-}; *Smpd3*^{flx/flx}; *SM22-Cre* mice showing the comparable aortic calcification in both the models (left panel). Aortic mineral quantification of micro-CT scans confirmed the results above (right panel). Statistical test: Student’s *t* test, n.s: not significant. **E.** Histological sections stained with VKVG shows comparable mineral deposition in both the genotypes.

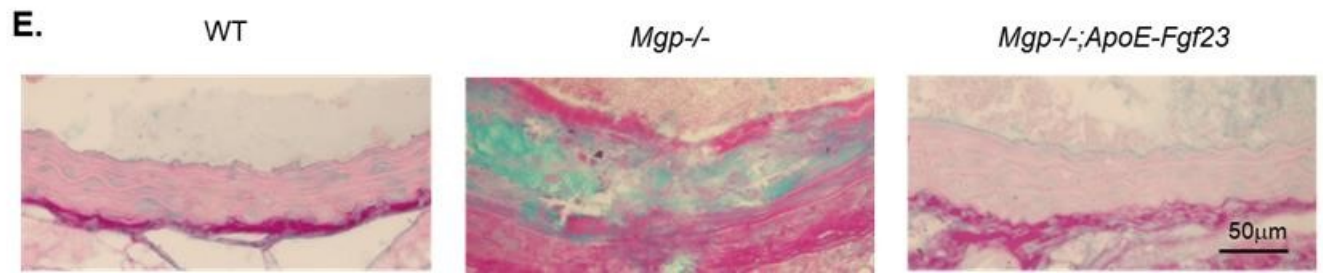
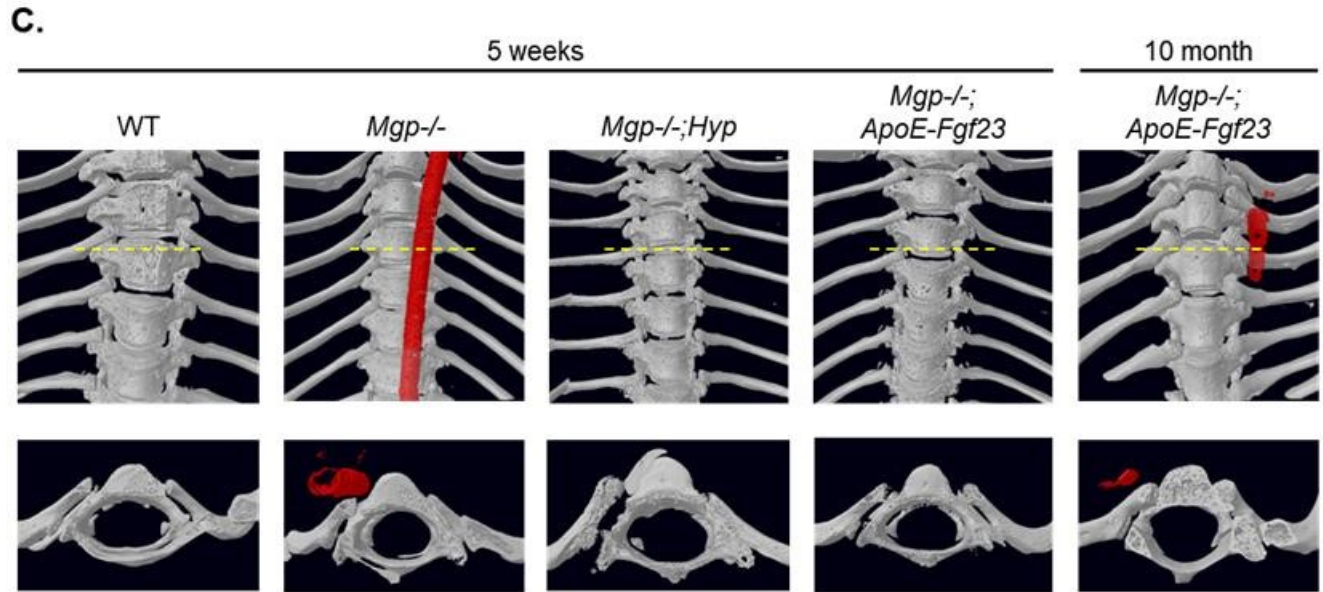
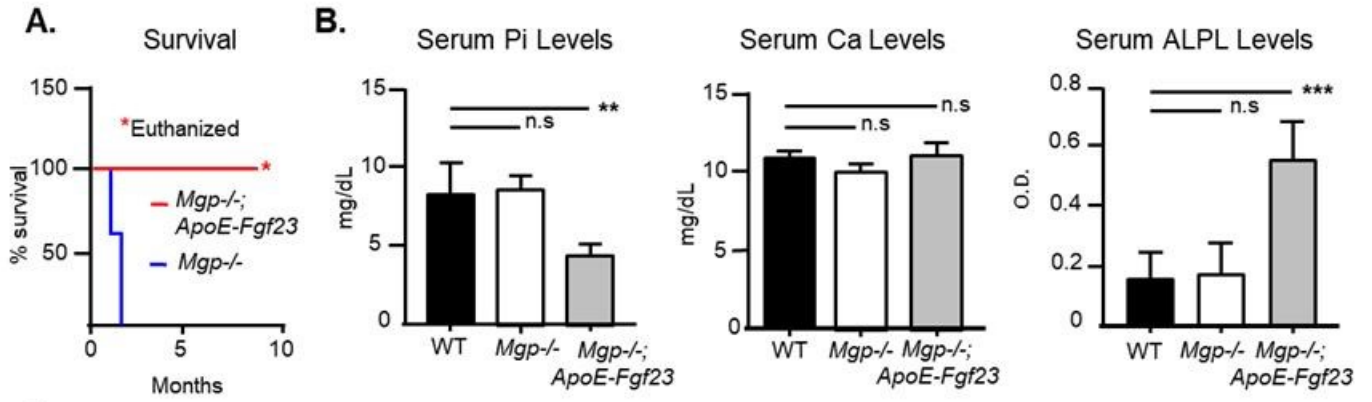


Figure 2.2. Increased circulating FGF23 corrects the vascular calcification phenotype in *Mgp*^{-/-} mice.

A. Kaplan-Meier survival curve showing the premature death of *Mgp*^{-/-} mice by 8 weeks. *Mgp*^{-/-}; *ApoE-Fgf23* mice survived at least up to 10 months (experimental end point), when they were euthanized for experimental purposes. **B.** Serum P_i, Ca²⁺ and alkaline phosphatase (ALPL) levels showing a significant reduction of P_i levels and a dramatic increase in ALPL in the transgenic *Mgp*^{-/-}; *ApoE-Fgf23* mice in comparison to WT and *Mgp*^{-/-} mice. **C.** 3D reconstructions of the micro-CT scans of 5-week-old WT, *Mgp*^{-/-}, *Mgp*^{-/-}-*Hyp* and *Mgp*^{-/-}; *ApoE-Fgf23* thoracic skeletons with the aorta, showing the presence of ectopic mineral deposition only in *Mgp*^{-/-} mice. Note that some mineral deposition was detected in the 10-month-old *Mgp*^{-/-}; *ApoE-Fgf23* thoracic aorta. The yellow line indicates the plane where cross section images presented in the lower panels were taken. The aortic minerals were artificially colored in red. **D.** VKVG staining of aortic histological plastic section of each genotype shown above, showing ectopic calcification only in the *Mgp*^{-/-} aortic section. **E.** ABVG staining of WT, *Mgp*^{-/-} and *Mgp*^{-/-}; *ApoE-Fgf23* aortic sections at 4 weeks of age, showing the presence of a cartilaginous ECM in the *Mgp*^{-/-} aortas as indicated by the blue staining. Statistical test: 1way ANOVA, n.s: not significant.

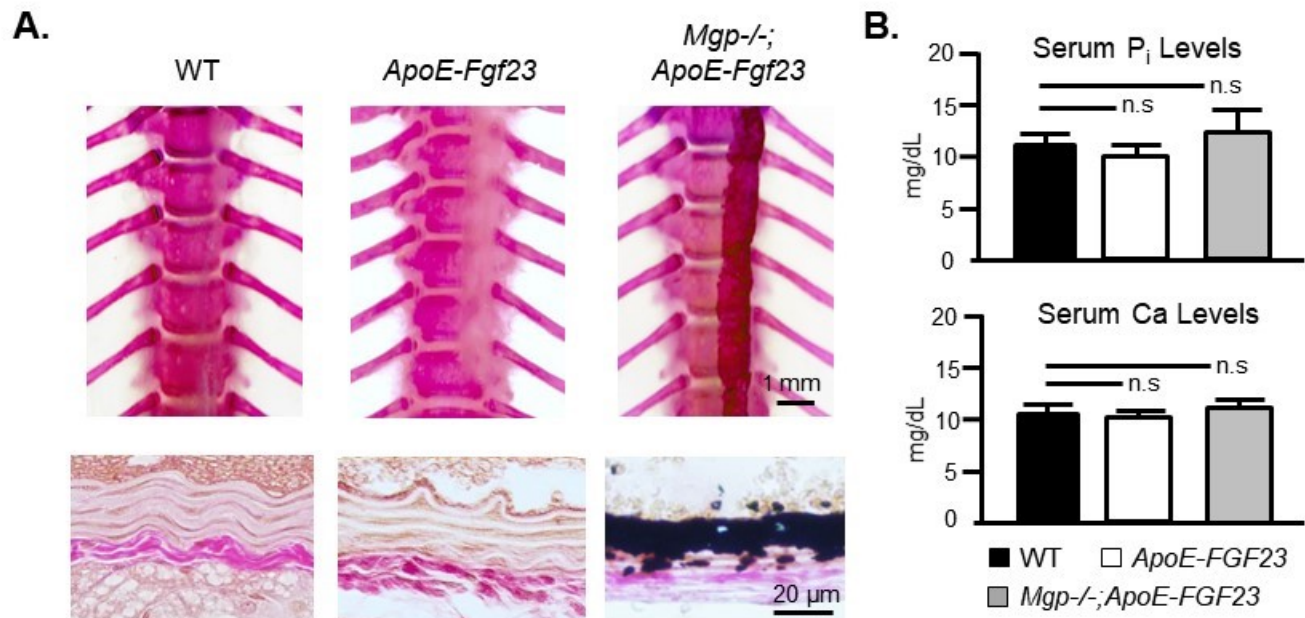


Figure 2.3. A high phosphorus diet induces rapid vascular calcification in *Mgp*^{-/-};*ApoE-Fgf23* mice. **A.** Alizarin red and Alcian blue staining of the thoracic aorta (top panel) of WT, *ApoE-Fgf23* and *Mgp*^{-/-};*ApoE-Fgf23* littermates after feeding a high phosphorus diet. Only *Mgp*^{-/-};*ApoE-Fgf23* mice developed rapid arterial calcification. Mice were switched to the high phosphorus diet at the age of 3 weeks for 10 days. VKVG stained histological sections (bottom panel) confirmed the presence of minerals in *Mgp*^{-/-};*ApoE-Fgf23* mice on the high phosphorus diet. **B.** Comparable serum P_i levels in the WT, *ApoE-Fgf23* and *Mgp*^{-/-};*ApoE-Fgf23* mice after the high phosphorus regimen. Serum Ca²⁺ levels remain unchanged. Statistical test: 1way ANOVA and Student *t* test, n.s: not significant.

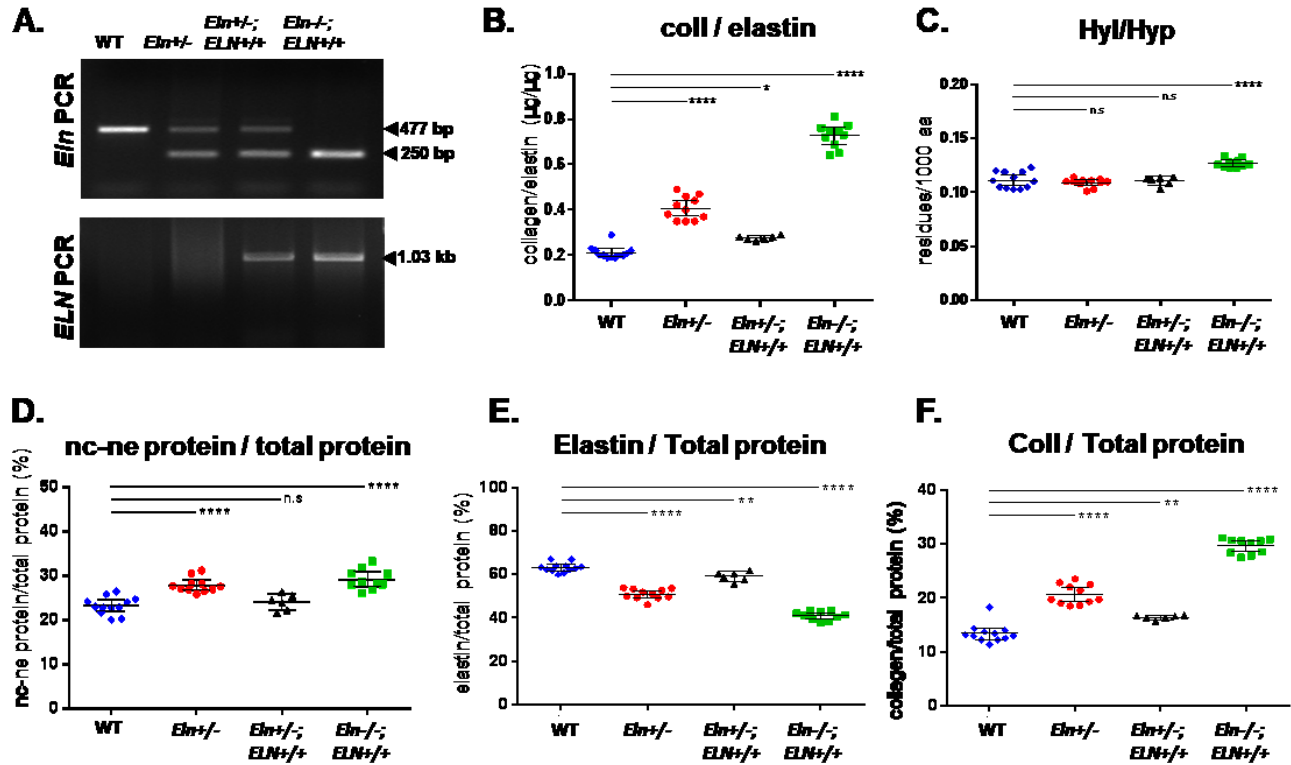


Figure 2.4. Comparative analyses of arterial elastin content in compound models expressing mouse and human elastin orthologs.

A. PCR performed on the genomic DNA confirms the genotype of WT, *Eln*^{+/-}, *Eln*^{+/-}; *ELN*^{+/+} and *Eln*^{-/-}; *ELN*^{+/+} mice. Mouse elastin (*Eln*) WT band is 477bp, ‘knockout’ band is 250bp (top panel) and the human elastin transgene band is 1.03 kbp (lower panel). Homozygosity of the human transgene was determined by the survival of the *Eln*^{-/-}; *ELN*^{+/+} mice, as all *Eln*^{-/-} and *Eln*^{-/-}; *ELN*^{+/+} die perinatally [183]. **B.** Collagen to elastin protein content (μg/μg) was increased in *Eln*^{+/-} and *Eln*^{-/-}; *ELN*^{+/+} aortic extracts in comparison to WT extracts. The latter showed the highest amount of collagen among all different genotypes. **C.** In agreement with the highest collagen content in the arteries, only *Eln*^{-/-}; *ELN*^{+/+} aortic extracts showed significant hydroxylysine to hydroxyproline ratio (per 1000aa) among all the genotypes. **D.** Amino acid analysis of non-collagenous/non-elastin proteins showed an increase in *Eln*^{+/-} and *Eln*^{-/-}; *ELN*^{+/+} arteries when compared to that of WT mice. **E.** The arterial elastin content in the *Eln*^{-/-}; *ELN*^{+/+} mice was the lowest. **F.** As is the case with the collagen to elastin ratio, there was an increase of collagen content over the total protein content.

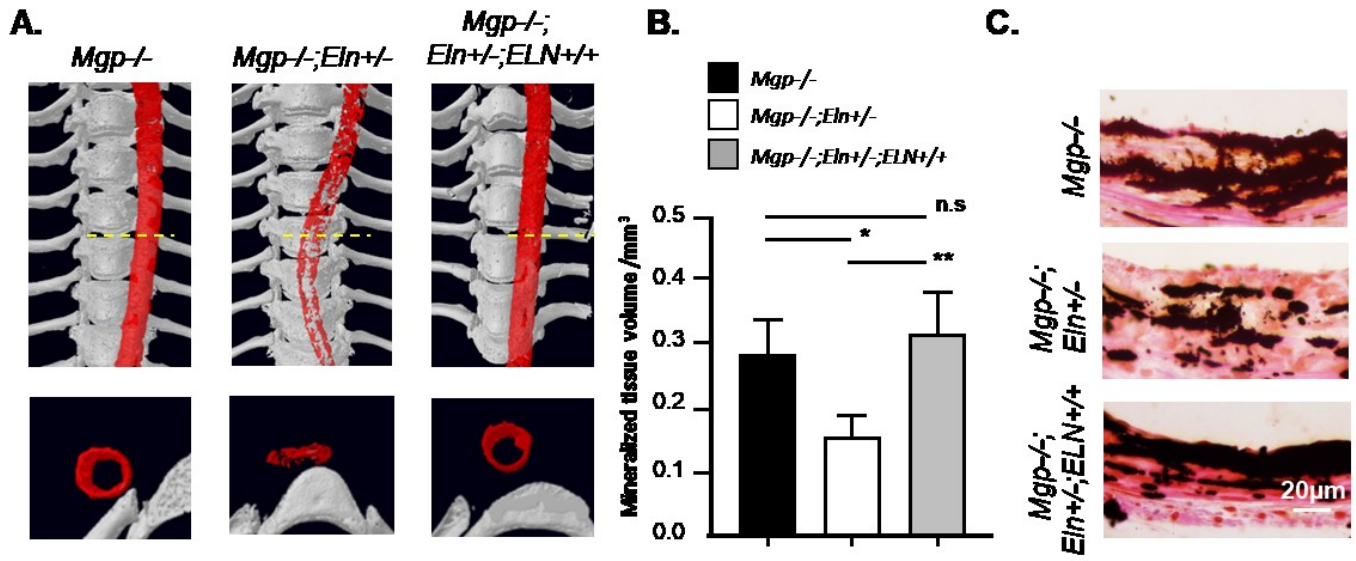


Figure 2.5. Arterial mineral deposition is affected by elastin content, but not by ortholog combination.

A. 3D reconstructions of micro-CT scans showing a severe thoracic aorta calcification in *Mgp*^{-/-} mice at 3-week-old and a reduced calcification in the littermate *Mgp*^{-/-};*Eln*^{+/-} mice. Of interest, the age-matched *Mgp*^{-/-};*Eln*^{+/-};*ELN*^{+/+} mice producing higher amount of elastin than the *Mgp*^{-/-};*Eln*^{+/-} mice show a more severe mineral accumulation (top panel). The lower panel shows the view of the cross-sectional plane at the yellow line. The aortic minerals were colored artificially in red. **B.** Aortic mineral quantification by micro-CT confirms the data presented above. **C.** VKVG staining of histological sections of the aorta reveals decreased mineral deposition in the *Mgp*^{-/-};*Eln*^{+/-} mice, while mineral deposition was comparable in the *Mgp*^{-/-} and *Mgp*^{-/-};*Eln*^{+/-};*ELN*^{+/+} aortas. Statistical test: 1way ANOVA, n.s: not significant.

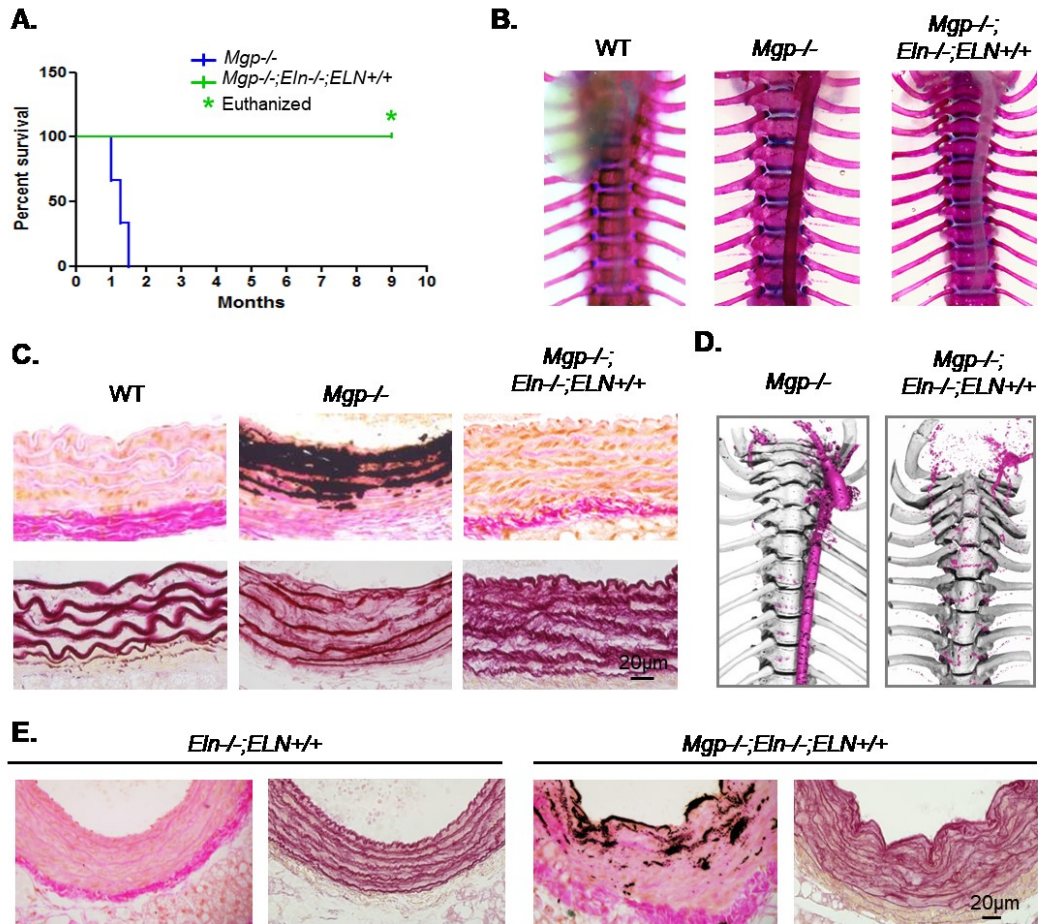


Figure 2.6. Prevention of vascular calcification in *Mgp*^{-/-};*Eln*^{-/-};*ELN*^{+/+} mice.

A. Kaplan-Meier survival curve showing the survival of the *Mgp*^{-/-};*Eln*^{-/-};*ELN*^{+/+} mice until the experimental end point (10 months), while all *Mgp*^{-/-} mice die by 8 weeks of age. The *Mgp*^{-/-};*Eln*^{-/-};*ELN*^{+/+} mice were euthanized at 10 months for experimental purposes. **B.** Alizarin red and Alcian blue staining of the thoracic aorta shows a severe vascular calcification phenotype in *Mgp*^{-/-} mice, but remarkably, no vascular calcification was detected in the *Mgp*^{-/-};*Eln*^{-/-};*ELN*^{+/+} mice. **C.** Histological analysis of undecalcified plastic sections stained with VKVG (top panel) showing medial calcification in 3-week-old *Mgp*^{-/-} thoracic aortas and a complete absence of minerals in the age-matched *Mgp*^{-/-};*Eln*^{-/-};*ELN*^{+/+} thoracic aortas. Note the augmented cell number (VSMCs stained orange) and collagen staining (pink) in this latter model. Hart's elastin staining of consecutive sections (lower panel) show the loss of the wavy architecture of the elastic lamina in *Mgp*^{-/-} aortas and an overall increased layering and decreased thickness of the elastic lamina in *Mgp*^{-/-};*Eln*^{-/-};*ELN*^{+/+} mice. **D.** 3D reconstructions of micro-CT scans of ribcages of *Mgp*^{-/-} mice at 5-weeks of age and *Mgp*^{-/-};*Eln*^{-/-};*ELN*^{+/+} mice at 1 year of age comparing the extent of aortic mineral accumulation. Note the severity of vascular calcification in the *Mgp*^{-/-} mice, and the minor ectopic calcification in the latter model, where the coronary and intercostal arteries seem to be most affected. **E.** Histological sections of 12-month-old *Eln*^{-/-};*ELN*^{+/+} (control) and *Mgp*^{-/-};*Eln*^{-/-};*ELN*^{+/+} thoracic aortas stained with VKVG showing a mild deposition of minerals along the elastic lamina in the latter genotype (left panels). The right panels show consecutive sections stained with Hart's elastin stain showing the overall reduction of elastic lamina in both models and the change in tissue architecture.

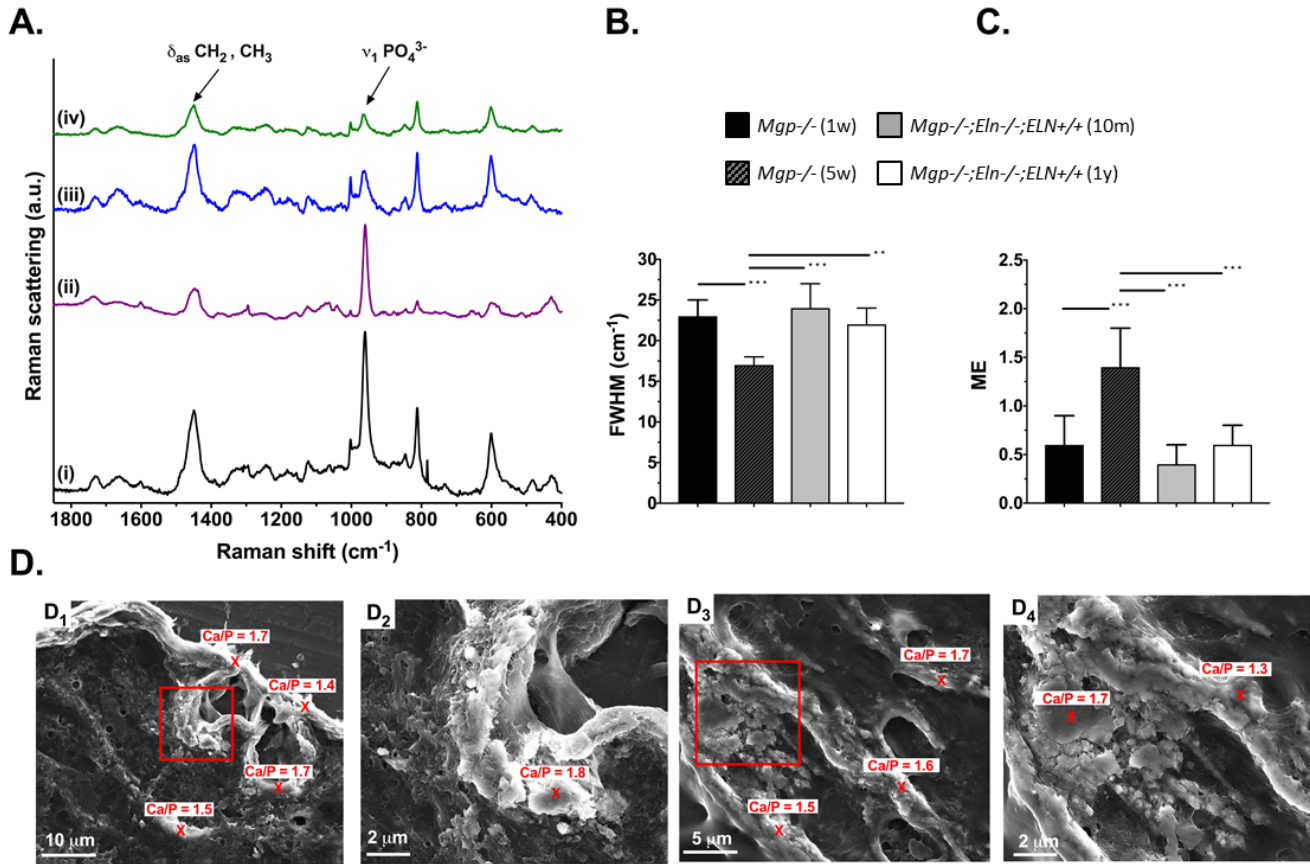


Figure 2.7. Mineral characterization in the aged *Mgp*^{-/-}; *Eln*^{-/-}; *ELN*^{+/+} mice

A. Representative Raman spectra of calcified aortas from (i) 1-week-old and (ii) 5-week-old *Mgp*^{-/-} mice, and from (iii) 10-month-old and (iv) 1-year-old *Mgp*^{-/-}; *Eln*^{-/-}; *ELN*^{+/+} mice. **B.** FWHM values measured on the Raman $\nu_1 \text{P}_1$ peak and **C.** Mineralization extend (ME) based on Raman spectra collected on aortas from 1-week-old and 5-week-old *Mgp*^{-/-} mice and from 10-month-old and 1-year-old *Mgp*^{-/-}; *Eln*^{-/-}; *ELN*^{+/+} mice. For each sample, 10 spectra were collected at different points. Statistical test: one-way ANOVA followed by Tukey's test correction. **D.** SEM images of calcified aortas from (D₁ and D₂) 10-month-old and (D₃ and D₄) 1-year-old *Mgp*^{-/-}; *Eln*^{-/-}; *ELN*^{+/+} mice. D₂ and D₄ are the magnified images of the regions highlighted by squares in D₁ and D₃, respectively. The Ca/P ratios indicates on the SEM images are based on the elemental atomic percentages obtained by EDS spectroscopy.

Chapter 3:

Prevention of Arterial Calcification Corrects the Low Bone Mass
Phenotype in MGP-Deficient Mice

**Prevention of Arterial Calcification Corrects the Low Bone Mass Phenotype in
MGP-Deficient Mice**

Juliana Marulanda^a, Chan Gao^{b,c}, Hassem Roman^d, Janet E Henderson^{c,d,e} and Monzur Murshed^{a,c}

^a Faculty of Dentistry, McGill University, Montreal, Quebec, Canada.

^b Bone Engineering Labs, Surgical Research, Research Institute-McGill University Health Centre.

^c Experimental Medicine, Department of Medicine, McGill University, Montreal, Quebec, Canada.

^d Department of Anatomy and Cell Biology, McGill University, Montreal, Quebec, Canada.

^e Experimental Surgery, Faculty of Medicine, McGill University, Montreal, Quebec, Canada.

***Bone*, 57(2013): 499-508**

3.1. Abstract

Matrix Gla protein (MGP), a potent inhibitor of extracellular matrix (ECM) mineralization, is primarily produced by vascular smooth muscle cells (VSMCs) and chondrocytes. Consistent with its expression profile, MGP deficiency in mice (*Mgp*^{-/-} mice) results in extensive mineralization of all arteries and cartilaginous ECMs. Interestingly, we observed a progressive loss of body weight in *Mgp*^{-/-} mice, which becomes apparent by the third week of age. Taken into account the new paradigm linking the metabolic regulators of energy metabolism and body mass to that of bone remodeling, we compared the bone volume in *Mgp*^{-/-} mice to that of their wild type littermates by micro-CT and bone histomorphometry. We found a decrease of bone volume over tissue volume in *Mgp*^{-/-} mice caused by an impaired osteoblast function. In culture, early differentiation of *Mgp*^{-/-} primary osteoblasts was not affected; however, there was a significant upregulation of the late osteogenic marker *Bglap* (osteocalcin). We examined whether the prevention of arterial calcification in *Mgp*^{-/-} mice could correct the low bone mass phenotype. The bones of two different genetic models: *Mgp*^{-/-};*SM22-Mgp* and *Mgp*^{-/-};*Eln*^{+/-} mice were analyzed. In the former strain, vascular calcification was fully rescued by transgenic overexpression of *Mgp* in the VSMCs, while in the latter, elastin haploinsufficiency significantly impeded the deposition of minerals in the arterial walls. In both models, the low mass phenotype seen in *Mgp*^{-/-} mice was rescued. Our data support the hypothesis that the arterial calcification, not MGP deficiency itself, causes the low bone mass phenotype in *Mgp*^{-/-} mice. Taken together, we provide evidence that arterial calcification affects bone remodeling and pave the way for further mechanistic studies to identify the pathway(s) regulating this process.

3.2. Introduction

Vascular calcification, a chronic degenerative condition often considered as a risk factor for many life-threatening cardiovascular diseases, has been associated with poor bone mineral density (BMD) in humans [206-208]. Pathologic mineral deposition in vascular tissues and physiologic mineralization of bone ECM are known to be regulated by several common determinants, as both appear to share common signaling pathways, transcription factors and ECM mediators [209, 210]. Despite this common link between the regulatory mechanisms of ECM mineralization in these two tissues, it is not known whether ectopic calcification in blood vessels may affect bone remodeling.

Vascular calcification can be categorized into two types — intimal and medial calcification. The former leads to atherosclerotic plaque erosion and rupture, while the latter increases arterial stiffness developing high systolic and pulse pressures [211, 212]. Patients suffering from osteoporosis, end-stage renal disease (ESRD) and diabetes mellitus type II have a high prevalence of atherosclerotic vascular calcification. The induction of chondro/osteogenic transdifferentiation of VSMCs and the loss of ECM mineralization inhibitors, such as inorganic pyrophosphate (PP_i), appear to be a common mechanism behind this process [48, 163, 213, 214].

Mice lacking matrix Gla protein (MGP), a potent inhibitor of ECM mineralization, show a low bone mass phenotype [11]. MGP, a 14 kDa mineral binding protein, is synthesized by chondrocytes in the cartilage and VSMCs in the arterial walls. All the members of the Gla protein family have their glutamic acid residues modified to gamma-carboxyglutamic acids by a vitamin K dependent reaction [167]. This post-translational modification leads to the active form of MGP, which is able to bind the hydroxyapatite crystals [215]. The level of circulating uncarboxylated MGP has been reported as a risk factor for vascular calcification [216-218].

Mutations in the gene encoding MGP in humans cause Keutel syndrome, a rare autosomal recessive condition, characterized by abnormal calcification of soft tissues [3]. Loss-of-function

mutations of MGP result in premature cartilage calcification, peripheral pulmonary stenosis and midface hypoplasia. Keutel syndrome patients also display brachytelephalangism, hearing loss, mild mental retardation, seizures, tracheobronchial stenosis and concentric calcification of pulmonary, coronary, hepatic, renal, meningeal and cerebral arteries [5, 166, 219].

The mouse model lacking MGP (*Mgp*^{-/-} mice) overtly mimics most of the Keutel syndrome pathophysiology including the abnormal calcification of the growth plate cartilage. However, the vascular calcification phenotype in *Mgp*^{-/-} mice is more severe to that seen in human patients. These mice die within two months of age because of the complications associated with the vascular phenotype [11, 220]. Transgenic overexpression of *Mgp* in the VSMCs of *Mgp*^{-/-};*SM22-Mgp* mice completely rescues the vascular calcification phenotype and the early lethality. There is no increase of serum Ca²⁺ and P_i levels in *Mgp*^{-/-} mice, however the reduction of serum P_i completely prevents the arterial mineral deposition in *Mgp*^{-/-};*Hyp* mice [16]. More recently, we observed that elastin, a major elastic lamina protein, acts as a key determinant of arterial calcification in MGP deficiency. Elastin haploinsufficiency significantly delays the progression of vascular calcification in *Mgp*^{-/-};*Eln*^{+/-} mice [170].

The original study reporting the MGP ‘knockout’ mice describes a short stature and a low bone mass phenotype [11]. However, the underlying cause of this latter phenotype is still unknown as no bone histomorphometry data is available till date. Also, it is not known whether ectopic calcification of arteries or cartilaginous tissues or both might cause the observed low bone mass phenotype in *Mgp*^{-/-} mice.

Another important question remains unanswered— is the low bone mass phenotype in *Mgp*^{-/-} mice caused by MGP deficiency per se, or is it a secondary effect of the ectopic calcification phenotype? In the current study, we performed bone histomorphometry of several ‘knockout’ and transgenic mouse models to provide answers to these important questions. Our work suggests that the

low bone mass phenotype in *Mgp*^{-/-} mice is caused by a functional defect in osteoblasts, as evident by their reduced mineral apposition rate (MAR) and bone formation rate (BFR/BS). We provide compelling evidence that vascular calcification is the primary cause of the low bone mass phenotype seen in *Mgp*^{-/-} mice.

3.3. Results

3.3.1. MGP deficiency leads to a low bone mass phenotype

At 5 weeks of age, the *Mgp*^{-/-} mice showed a severe vascular calcification phenotype and premature calcification of the growth plate cartilages in the long bones and vertebrae (Figure 1A and B). Also, these mice appeared smaller in size. We measured the body weights of *Mgp*^{-/-} males and females and compared to that of their gender-matched littermates and observed a markedly poor weight gain by all MGP-deficient mice during the post-weaning period (Figure 1C). Considering the association between body weight and bone mass, we performed micro-CT analyses of femur samples from 5-week-old *Mgp*^{-/-} mice and their control littermates. As evident by the micro-CT images in Figure 1D, *Mgp*^{-/-} mice showed a reduction of both trabecular and cortical bone mass. The measurements of static parameters affecting bone remodeling confirmed that BV/TV and trabecular numbers (Tb. No) are significantly reduced in MGP-deficient mice. Although not significant, we observed a reduced structural connectivity as shown by the Euler number (Eu No.) (Figure 1D). We next prepared histological sections of the lumbar vertebrae from 5-week-old mice and stained by von Kossa and van Gieson as described before [167]. In agreement with our micro-CT data, we found a significantly lower BV/TV in *Mgp*^{-/-} bones. The histomorphometric analysis revealed almost 25% decreased bone volume in *Mgp*^{-/-} mice when compared with their gender-matched littermates. Also, there was a significant reduction of trabecular thickness (Figure 1E).

3.3.2. Impaired osteoblast function in *Mgp*^{-/-} mice

In order to investigate the cause of the low bone mass phenotype in *Mgp*^{-/-} mice, we examined the dynamic parameters affecting bone remodeling by histomorphometry. The MAR and BFR/BS were measured using double calcein labeling in 5-week-old *Mgp*^{-/-} mice and their WT control littermates. There was a significant decrease in MAR and BFR/BS in *Mgp*^{-/-} mice (Figure 2A). We next examined

whether these reductions of bone formation parameters were due to a low osteoblast number. Toluidine blue (TB) stain of thin plastic sections showed that the osteoblast number in *Mgp*^{-/-} mice was not affected over the tissue area (Ob/T.Ar) or bone perimeter (Ob/B.Pm) (Figure 2B). As the bone mass is maintained through bone resorption by osteoclasts and new bone formation by osteoblasts, we counted the number of TRAP-positive osteoclasts on *Mgp*^{-/-} and control bone sections. The osteoclast numbers over tissue area (Oc/T.Ar) and over bone perimeter (Oc/B.Pm) in *Mgp*^{-/-} mice demonstrated a slight increase although it was not statistically significant (Figure 2C). We next examined the serum levels of osteocalcin, CTX and ALPL in WT and *Mgp*^{-/-} mice. There was a mild but significant upregulation of osteocalcin levels; however, no change in serum CTX and ALPL levels were detected (Figure 2D).

3.3.3. Abnormal vasculature in *Mgp*^{-/-} bones

Abnormalities in blood vessel structure and branching have been reported in the soft tissues of *Mgp*^{-/-} mice [221]. In order to investigate whether this is also the case in bone, we performed micro-CT analyses of the vertebral bones of barium sulfate perfused 4-week-old WT and *Mgp*^{-/-} mice. Our data showed enlarged, heavily branched arteries in the latter strain (Figure 3).

3.3.4. Early differentiation markers are normal in *Mgp*^{-/-} osteoblasts

We isolated calvarial osteoblasts from newborn WT and *Mgp*^{-/-} mice, cultured them in the differentiation medium for 7 days and prepared RNA for the expression analysis of several osteogenic markers. We detected *Mgp* expression in WT osteoblasts, but not in *Mgp*^{-/-} osteoblasts. MGP deficiency however did not affect early differentiation of osteoblasts as we did not observe any significant change of *Runx2*, *Osx* (*Sp7*) and *Colla1* expression in *Mgp*^{-/-} cultures in comparison to WT cultures. Interestingly, *Bglap* (Osteocalcin) expression was significantly upregulated in the knockout cells (Figure 4A). As shown in Figure 4B, there was no significant alteration of ALPL activity in *Mgp*^{-/-}

-/- cultures. The treatment of WT and *Mgp*^{-/-} osteoblasts with Alamar Blue showed comparable cell viability/metabolic activity in these two cultures (Figure 4C). We observed almost 2-fold increase of deposited minerals in *Mgp*^{-/-} cultures, when stained with Alizarin Red (Figure 4D).

3.3.5. Restoration of *Mgp* expression in VSMCs normalizes bone mass in *Mgp*^{-/-};*SM22-Mgp* mice

We reported earlier that smooth muscle actin promoter (*SM22*)-driven expression of *Mgp* in VSMCs fully rescued the arterial calcification phenotype in *Mgp*^{-/-};*SM22-Mgp* mice [167]. In order to examine the bone phenotype of these compound mutants, we first regenerated the *SM22-Mgp* mice. As evident by sqRT-PCR analysis, only 20 amplification cycles were sufficient to detect the specific transgene expression in the arterial tissues (Figure 5A). After confirming the transgene expression, we crossed these mice with *Mgp*^{+/-} mice. The resultant *Mgp*^{+/-};*SM22-Mgp* mice were then backcrossed with *Mgp*^{+/-} mice to generate *Mgp*^{-/-};*SM22-Mgp* mice. We examined the growth plates of the latter strain by histology. In agreement with our sqRT-PCR data showing the absence of transgene expression in the cartilage, we observed a severe calcification of the growth plate in the 5-week-old *Mgp*^{-/-};*SM22-Mgp* mice (Figure 5B).

We next examined the BV/TV in the lumbar vertebrae of WT, *Mgp*^{-/-}, *Mgp*^{-/-};*SM22-Mgp* and *SM22-Mgp* mice at 5-week-of-age and found a rescue of the bone phenotype in the *Mgp*^{-/-};*SM22-Mgp* mice (Figure 5C and D). To investigate the bone remodeling process in the rescued strain, we performed analysis of the dynamic parameters as described above. We found that in *Mgp*^{-/-};*SM22-Mgp* mice, MAR and BFR/BS were similar to that of the WT and *SM22-Mgp* control mice (Figure 5E and F). Accordingly, the osteoblast as well as the osteoclast counts were normal in the rescued model when compared with their WT littermates and *SM22-Mgp* controls, with no statistical differences (Figure 5G - J). However, as described before, *Mgp*^{-/-} mice showed a significantly lower bone mass, MAR and

BFR/BS with no difference in osteoblast and osteoclast numbers in comparison to the WT mice. Our micro-CT analyses showed a correction of both trabecular and cortical bone mass in the rescued model (Supplemental Figure 1). Taken together, these data suggest that along with the prevention of arterial calcification, there is a normalization of the bone mass in *Mgp*^{-/-};*SM22-Mgp* mice.

3.3.6. Prevention of arterial calcification independent of *Mgp* expression corrects the low bone mass phenotype in *Mgp*^{-/-};*Eln*^{+/-} mice

The analysis of *Mgp*^{-/-};*SM22-Mgp* mice does not reveal whether the restoration of *Mgp* expression in the VSMCs or the ensuing prevention of arterial calcification independently rescues the low bone mass phenotype. In order to investigate this, we analyzed the bones of *Mgp*^{-/-};*Eln*^{+/-} mice. In these MGP-deficient compound mutants *Eln* haploinsufficiency significantly impedes the progression of arterial calcification (Figure 6A) [170]. The histology of vertebral sections of the WT and *Mgp*^{-/-};*Eln*^{+/-} littermates confirmed that the growth plates were abnormally calcified in the latter model (Figure 6B). Despite the presence of abnormally calcified growth plates, our histomorphometric analyses showed a normalization of the bone volume in 5-week-old *Mgp*^{-/-};*Eln*^{+/-} mice, while a significant low bone mass persisted in the *Mgp*^{-/-} mice (Figure 6C and D).

We observed a normal MAR and BFR/BS in the *Mgp*^{-/-};*Eln*^{+/-} mice (Figure 6E and F). Consistent with our previous findings, the osteoblast counts (Ob/T.Ar, Ob/B.Pm) and osteoclast counts (Oc/T.Ar, Oc/B.Pm) remained unchanged (Figure 6G - J). Additionally, a correction of both trabecular and cortical bone mass in the rescued model was observed by micro-CT analyses (Supplemental Figure 1). Collectively, these data suggest that the bone phenotype was rescued by delaying the progression of arterial calcification in the *Mgp*^{-/-};*Eln*^{+/-} mice.

3.4. Discussion

MGP deficiency leads to ectopic calcification of cartilaginous and vascular tissues in Keutel syndrome patients [3, 219]. These abnormalities are also present in *Mgp*^{-/-} mice, albeit these mice show a more severe vascular calcification phenotype than seen in the human patients [11, 220]. In the current study, we analyzed various bone remodeling parameters in *Mgp*^{-/-} mice and investigated how the rescue of the vascular calcification phenotype affects them.

Our micro-CT and histomorphometric analyses showed that the mineralized tissue mass is reduced in the long bones as well as in the vertebrae of *Mgp*^{-/-} mice affecting both cortical and trabecular bones. Although osteoblast numbers are not significantly decreased in these mice, there was a reduction in MAR and BFR/BS indicative of poor bone formation by the mutant osteoblasts. Additionally, *Mgp*^{-/-} bones showed decreased trabecular numbers and thickness. There was no alteration of osteoclast numbers and serum CTX levels in *Mgp*^{-/-} mice. Taken together, we conclude that the low bone mass phenotype in *Mgp*^{-/-} mice is primarily due to the poor bone formation by osteoblasts.

The reduced bone mass in *Mgp*^{-/-} mice could be caused by an intrinsic defect in osteoblast differentiation. However, our gene expression analysis rules out this possibility as none of the early osteogenic markers e.g. *Runx2*, *Osx* and *Coll1a1* were altered in cultured MGP-deficient osteoblasts. Also, there was no significant alteration of cell membrane-bound ALPL activity. Our data shows that *Mgp* is expressed by differentiated WT osteoblasts but not by *Mgp*^{-/-} osteoblasts. A total absence of MGP, a potent mineralization inhibitor, may explain why the *Mgp*^{-/-} osteoblast cultures deposit more minerals than the WT cultures. Interestingly, we found that osteocalcin expression was significantly upregulated in MGP-deficient osteoblasts. This finding was further confirmed by our observation that despite a reduced bone mass, there was a

mild but significant increase of serum osteocalcin levels in *Mgp*^{-/-} mice. Osteocalcin, a late osteogenic marker, has been shown to regulate energy metabolism and testicular functions through its pleiotropic endocrine actions [222, 223]. It is possible that *Mgp* deficiency in osteoblasts through an unknown mechanism, upregulates the expression of a related Gla protein osteocalcin and thereby modulates its proposed endocrine actions in *Mgp*^{-/-} mice.

In mice, *Mgp* is primarily expressed by two cell types, the VSMCs and the chondrocytes [11, 224]. A key focus of our ongoing study has been to determine whether the loss of *Mgp* expression in one or both of these cell types causes the observed low bone mass phenotype. Previously, we reported the generation of *Mgp*^{-/-};*SM22-Mgp* mice, in which VSMC-specific expression of *Mgp* corrected all the vascular abnormalities seen in *Mgp*^{-/-} mice [167]. We used the same transgene construct for the pronuclear injections to regenerate *SM22-Mgp* transgenic mice. As reported earlier, we observed transgene expression in the arterial tissues of the regenerated line; no expression was detected in the cartilage. This latter observation was further supported by the histology of *Mgp*^{-/-};*SM22-Mgp* growth plates, expectedly showing a severe calcification of this cartilaginous tissue. As shown before, there was no mineral accumulation in the arteries of *Mgp*^{-/-};*SM22-Mgp* mice [167]. Despite the excessive mineralization of the growth plates, prevention of arterial calcification in *Mgp*^{-/-};*SM22-Mgp* mice alone was sufficient to fully rescue the low bone mass phenotype. In agreement with this finding, all the bone remodeling parameters affected by MGP-deficiency were corrected in this rescued model.

While the bone phenotype was corrected in *Mgp*^{-/-};*SM22-Mgp* mice, these data do not conclusively establish whether it is the rescue of *Mgp* expression by VSMCs per se, or the prevention of vascular calcification by the local synthesis of MGP in the arteries that corrected the bone phenotype. We reasoned that this issue could be addressed in a mouse model that lacks

MGP globally, but the arterial calcification is significantly delayed or prevented without the restoration of *Mgp* expression [225-227]. We recently observed that the *Mgp*^{-/-};*Eln*^{+/-} mice accumulate a significantly lesser amount of minerals in the arterial walls [170]. Our histomorphometric analysis of the bones of these mice showed that there was a normalization of the bone mass accrual. This later finding further strengthens the notion that vascular calcification is the cause of the low bone mass phenotype in *Mgp*^{-/-} mice.

It is not precisely known how arterial calcification may affect osteoblast function. One possible cause of this phenotype might be vascular abnormalities hampering the nutrient supply to the active osteoblasts. Indeed, in a recent study, arteriovenous malformations (AVMs) have been reported in multiple organs in *Mgp*^{-/-} mice [221]. In agreement with these findings, we observed that calcified arteries in *Mgp*^{-/-} bones become thickened and unusually branched which may affect the local nutrient transport. At this stage, however, a generalized effect of vascular calcification on the overall growth cannot be fully ruled out.

Apart from vascular calcification, increased serum levels of osteocalcin in *Mgp*^{-/-} mice may also contribute to the low bone mass phenotype. This possibility is raised by the findings that bone formation is increased in osteocalcin-deficient mice, while increased serum undercarboxylated osteocalcin results in low bone mineral density in humans [228, 229]. However, considering the observation that the low bone mass phenotype is fully rescued in *Mgp*^{-/-};*Eln*^{+/-} mice, the upregulation of osteocalcin does not appear to be a major cause of the reduced bone mass in *Mgp*^{-/-} mice. Further work is needed to examine how various interplays among multiple factors like vascular calcification, abnormal vascular morphology and the altered osteocalcin expression by osteoblasts may affect bone formation in *Mgp*^{-/-} mice.

Our data presented in the current study, raise an interesting question, whether a similar effect on bone mass is seen in other mouse models with arterial calcification. Currently, we have limited *in vivo* data to provide an answer to this question. At least one line of *Opg*^{-/-} mice show arterial calcification and a low bone mass phenotype [75]. However, this low bone mass phenotype does not appear to depend on the ectopic calcification of blood vessels, as a different *Opg*^{-/-} line shows the low bone mass phenotype despite the complete absence of vascular calcification [76]. Also, the mechanism behind the low bone mass phenotype in *Opg*^{-/-} mice is different than that of *Mgp*^{-/-} mice; unlike the latter, *Opg*^{-/-} mice show increased bone resorption.

Several studies showed an association between arterial calcification and low bone mass in human patients [208, 230]. However, the exact nature of this association and its significance is still unresolved. Our current study conclusively shows that the prevention of arterial calcification through overexpression of *Mgp* in the arterial walls or reduction of *Eln* gene dosage is sufficient to rescue the low bone mass phenotype seen in *Mgp*^{-/-} mice. These findings may help understanding the association between the pathophysiology of some forms of vascular calcification and the loss of bone mass in humans.

3.5. Materials and methods

3.5.1. Mice

Generation of *Mgp*^{-/-} and *Eln*^{+/-} mice were described previously [11, 225]. *SM22-Mgp* mice were regenerated as described before [167]. All mice were maintained in a pathogen-free standard animal facility and the experimental procedures were performed following an animal use protocol approved by the Animal Care Committee of McGill University. Genotypes were determined by PCR on genomic DNAs isolated from the tail biopsies. The nucleotide sequences of the primers used for genotyping are available upon request.

3.5.2. Primary osteoblast culture

Primary osteoblasts were isolated from the calvaria of newborn WT and *Mgp*^{-/-} mice as described [231] and cultured in α -MEM (Invitrogen) supplemented with 10% FBS (Hyclone) and 100 U/ml penicillin–streptomycin (Invitrogen) at 37 °C under 5% CO₂ in a humidified incubator.

3.5.3. Alkaline phosphatase and Alamar blue reduction assay

To measure tissue ALPL activity, cell extracts were prepared with 1x Passive Lysis Buffer (Promega) and total proteins were measured by the Pierce Micro BCA Protein Assay (Thermo Scientific). ALPL activity was measured using *p*-nitrophenyl phosphate substrate (Sigma-Aldrich) and then normalized by the respective protein concentration in the extracts as described previously [232]. In order to examine cellular viability/metabolic activity in each culture well, Alamar Blue solution was directly added to the medium to 100 μ M final concentration. The

reduction of Alamar Blue was measured at 560nm (reference wavelength 610nm) after 4 hours incubation at 37°C using a microplate reader (Infinite 200, Tecan).

3.5.4. *Quantification of in vitro mineralization*

Osteoblasts differentiation was induced by addition of ascorbic acid (100µg/ml), β-glycerol phosphate (5mM) and dexamethasone (10mM) to the culture medium. For quantification of deposited minerals, mineralized cultures were stained with 40 mM Alizarin Red solution (pH 4.0) for 5 min and thoroughly washed in deionized water. Bound dye was dissolved in 10% glacial acetic acid and measured at 405 nm using a microplate reader (Infinite 200, Tecan). The values were normalized by the relative levels of Alamar Blue reduction for each well.

3.5.5. *Gene expression analysis*

Gene expression analyses were performed using a quantitative Real Time-PCR (qRT-PCR) system (model 7500, Applied Biosystems). Total RNA was extracted with TRIZOL reagent (Invitrogen) and subjected to DNase I (Invitrogen) treatment. The first-strand cDNA synthesis and qRT-PCR were performed using a high-capacity cDNA reverse transcription kit (Applied Biosystems) and Maxima SYBR green quantitative PCR master mix (Fermentas), respectively. Relative gene expression was analyzed by SDS software (Applied Biosystems) using comparative C_T and hypoxanthine guanine phosphoribosyl transferase (*Hprt*; a housekeeping gene) expression as an endogenous control. In order to calculate the ΔC_T value, the mean C_T value of the expression of a gene in a sample was first normalized to the mean C_T value of *Hprt* expression in that sample. The ΔC_T value of the calibrator sample was subtracted from that of the sample of interest to obtain the $\Delta\Delta C_T$ value. The relative expression was reported as $2^{-\Delta\Delta C_T}$. Transgene expression was analyzed using semi-quantitative reverse transcription PCR (sqRT-

PCR). DNA was amplified using Taq polymerase purified in our lab. The nucleotide sequences of the primers used for gene expression analysis are available upon request.

3.5.6. Micro-CT analysis

Micro-CT analyses of the skeletal samples were performed at the Bone Engineering Labs, at the Research Institute-McGill University Health Centre. Bone samples were imaged with a Skyscan1172 micro-CT instrument (Skyscan, Kontich, Belgium) using an Al0.5 filter with a spatial resolution of 5.5 microns at a voltage of 50KV and power of 10W. Skyscan softwares were used for cross sectional reconstructions with NRecon, 3D reconstruction with CTAn and CTVol. Mineral content of bone was defined by setting the segmentation threshold between 50 and 255 in the binary mode of CTAn. The region of interest (ROI) was defined for both as a cubic area measured 1.2 mm (length) x 0.8mm (height) x 0.3mm (thickness) located at the center of the growth plate and the whole upper portion of the tibia/femur. 3D reconstruction has been performed in the ROIs as defined on 3 biological replicates in each group.

For the micro-CT imaging of arteries, barium sulfate (BaSO_4) compound solution (50% v/w BaSO_4) was prepared as reported previously [233]. The mouse was anesthetized, and the thoracic cage was dissected to expose the heart. An aperture was made in the heart and the left ventricle was catheterized by a 20G plastic catheter. The catheter was fixed to the heart by arterial clamp and perfused with 5ml of PBS, 4% paraformaldehyde and BaSO_4 compound solution. The spine was harvested 5 minutes after perfusion, fixed with 4% paraformaldehyde solution overnight and kept in PBS at 4°C. The spines harvested were imaged by micro-CT scanner (Skyscan 1172) with Al 1.0 mm filter, 60KV, 10W and 8 μm spatial resolution. The vertebrae were segmented from blood vessels in CTAn software based on different X ray attenuation of bone and BaSO_4 . 3D reconstruction was done in CTVol software.

3.5.7. Histomorphometric analysis

For calcein double labeling, 4-week-old mice were injected intraperitoneally with 10 μ l/g body weight of calcein solution (0.25% calcein and 2% NaHCO₃ dissolved in 0.15M NaCl) twice at a 3-day interval. Mice were euthanized 2 days after the second injection and skeletal tissues were processed for histomorphometric analyses. For plastic sectioning, vertebrae were fixed overnight in 4% PFA/PBS, embedded in methyl methacrylate, and sectioned (5- μ m thickness). Von Kossa and van Gieson (VKVG), Toluidine Blue (TB) or Tartrate Resistant Acid Phosphatase (TRAP) staining were applied. Stained bone sections were analyzed for bone volume/tissue volume (BV/TV), osteoblast count, osteoclast count, MAR and BFR/BS analyses using the Osteomeasure software (Osteometrics, Inc.). The region of interest (ROI) was selected in the lumbar vertebrae (L3 and L4) sections avoiding the areas adjacent to the cortical bones and hypertrophic chondrocytes of the growth plates. Images were taken at room temperature using a light microscope (DM200; Leica) with a 2.5 x (numerical aperture of 0.07), 20 \times (numerical aperture of 0.40) or 40 \times (numerical aperture of 0.65) objective. All histological images were captured using a camera (DP72; Olympus), acquired with DP2-BSW software (XV3.0; Olympus), and processed using Photoshop (Adobe).

3.5.8. Serum analysis

Serum osteocalcin and the C terminal telopeptides of type I collagen (CTX) levels were measured using Mouse Osteocalcin ELISA (Immutopics) and RatLaps EIA (IDS) kits.

3.6. Data analysis

All results are shown as means of the standard deviation. Statistical analyses were performed by ANOVA and Student's *t* test as applicable, with $P < 0.05$ considered significant as indicated by a single asterisk, $P < 0.005$ by double asterisks and $P < 0.0005$ as triple asterisks.

3.7. Acknowledgments

We thank Dr. Florent Elefteriou and Dalida Wilson for critical reading of the manuscript. This work was supported by operating grants from Canadian Institutes of Health Research (CIHR; Funding Reference Number 123310) and Réseau de Recherche en Santé Buccodentaire et Osseuse (RSBO) / Fonds de la Recherche en Santé du Québec (FRQS) to M. Murshed. J. Marulanda receives a stipend from Colfuturo (Colombia) and McGill University Health Center, and M. Murshed receives salary support from the FRQS. Authors are thankful to Seemun Ray and Aarti Angrula for technical assistance and Mia Esser for the maintenance of the mouse colonies.

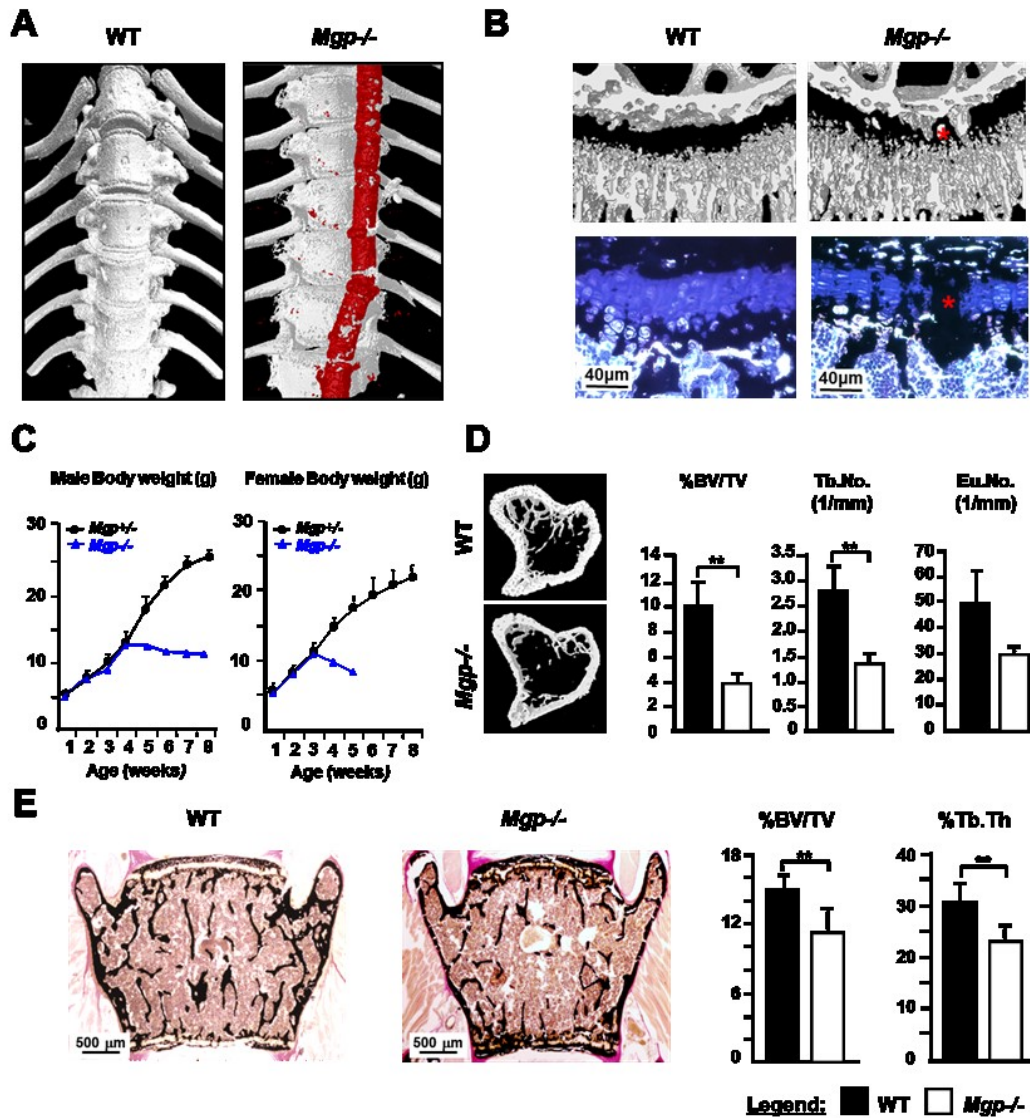


Figure 3.1. MGP deficiency leads to a low bone mass phenotype

A. Micro-CT analysis of the thoracic skeleton from a 5-week-old WT and *Mgp*^{-/-} mouse showing the calcified aorta (in red) in the latter. **B.** Micro-CT images of the proximal tibia (top) and von Kossa and Toluidine blue stained histology sections of lumbar vertebrae (bottom) from a 5-week-old WT and *Mgp*^{-/-} mice showing deposition of minerals in the mutant growth plate (asterisks). **C.** Body weight measurements of wild type and *Mgp*^{-/-} male and female mice from birth onwards. *Mgp*^{-/-} mice exhibit poor weight gain during the post-weaning period. **D.** Micro-CT analysis of 5-week-old WT and age-matched *Mgp*^{-/-} femur. Cross sectional views show low bone mass in the trabecular and cortical bones. The comparative analysis of the trabecular bones confirms a reduction of bone volume over tissue volume (BV/TV), trabecular number (Tb.No) and Euler number (Eu.No.) in the *Mgp*^{-/-} mice. **E.** Von Kossa and van Giesson (VKVG) staining of lumbar vertebrae sections show a significant decrease of BV/TV in the *Mgp*^{-/-} mice when compared with WT mice. The trabecular thickness (Tb.Th) is also significantly reduced. Error bars represent standard deviations; n ≥ 6 male mice for each group.

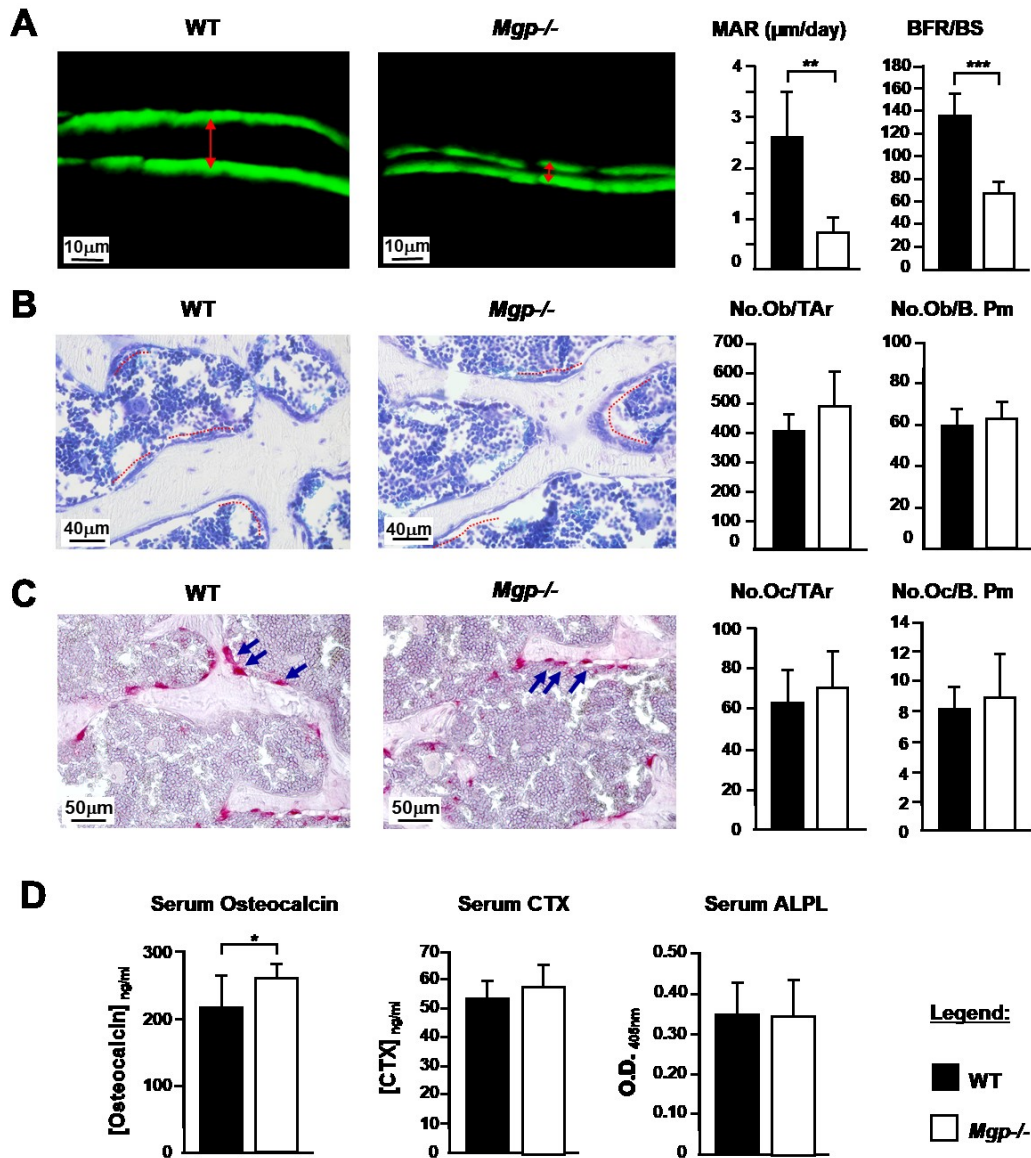


Figure 3.2. Osteoblast function is affected in *Mgp*^{-/-} mice

A. Calcein double labeling shows a significantly reduced MAR and BFR/BS in *Mgp*^{-/-} mice compared to the WT controls. The red arrows show the distance between calcein double labels. **B.** Toluidine blue-stained undecalcified plastic sections show an unaltered number of osteoblasts per tissue area (No.Ob/T.Ar) and per bone perimeter (No.Ob/B.Pm) in *Mgp*^{-/-} trabecular bones in comparison to WT control bones. Osteoblast clusters are highlighted by the dotted red lines. No significant difference was detected among the two groups. **C.** No significant differences in osteoclast numbers were evident in the tartrate resistant acid phosphatase (TRAP) stained *Mgp*^{-/-} bone sections when compared with WT sections. Two parameters No.Oc/T.Ar and No.Oc/B.Pm were shown. Osteoclasts are indicated with arrows. **D.** Serum osteocalcin levels were upregulated in *Mgp*^{-/-} mice, while CTX and ALPL levels remained unchanged. Error bars represent standard deviations; n \geq 6 mice for each group.

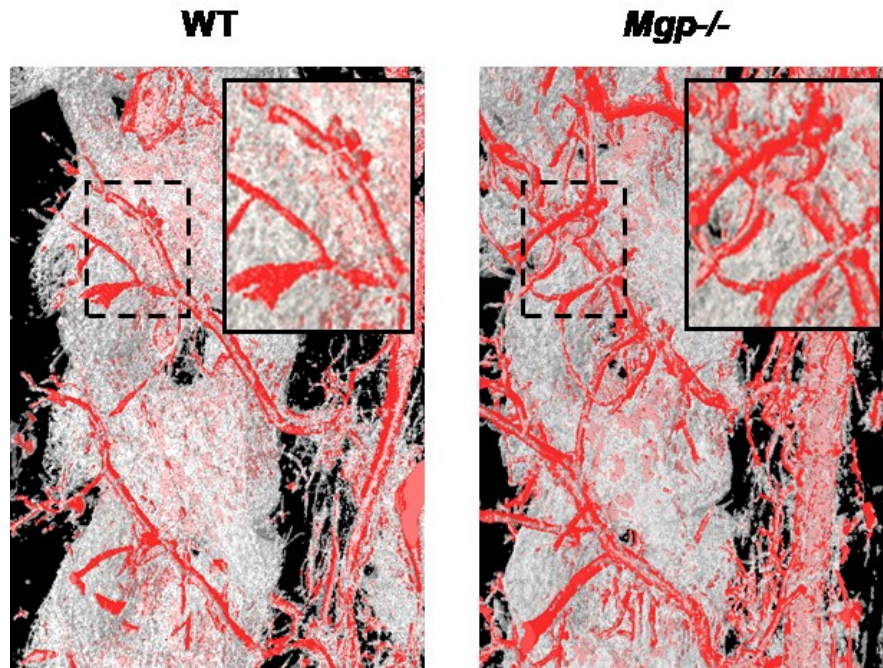


Figure 3.3. Abnormal vasculature in Mgp^{-/-} bones

Micro-CT analysis of BaSO₄-perfused arteries shows abnormal thickening and excessive branching of arteries in the lumbar vertebrae of *Mgp^{-/-}* mice.

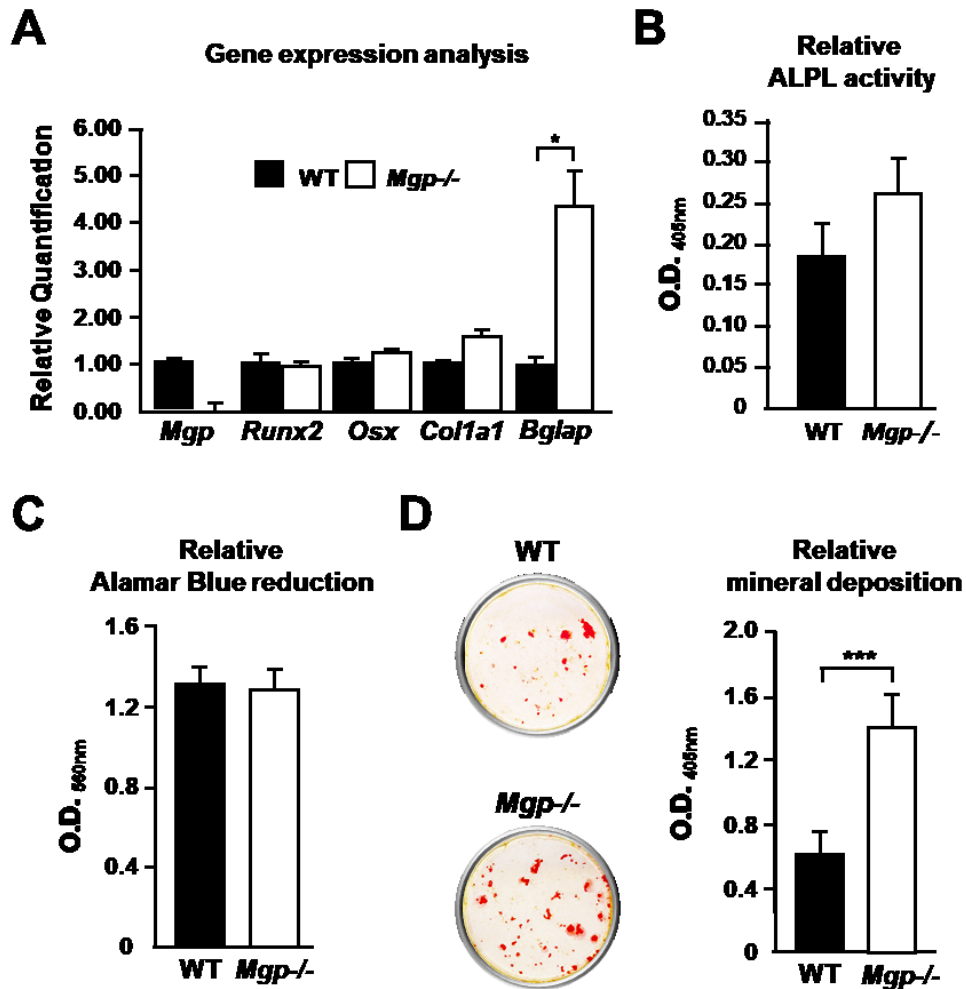


Figure 3.4. Early differentiation markers are normal in *Mgp*^{-/-} osteoblasts

A. qRT-PCR analysis shows no expression of *Mgp* in *Mgp*^{-/-} osteoblasts, while comparable *Runx2*, *Osx* and *Colla1* expression were seen in WT and *Mgp*^{-/-} cultures. Osteocalcin (*Bglap*) expression was upregulated in *Mgp*^{-/-} osteoblasts in comparison to WT osteoblasts. **B.** There was a mild but non-significant increase of cell membrane-bound Alkaline phosphatase activity in *Mgp*^{-/-} primary osteoblast cultures when compared with the controls. **C.** Alamar Blue absorbance (560nm) shows no significant difference in the cell viability/metabolic activity between WT and *Mgp*^{-/-} primary osteoblasts. **D.** Alizarin Red staining of WT and *Mgp*^{-/-} primary osteoblast cultures after 14 days of induction of mineralization shows a significant increase of deposited minerals in *Mgp*^{-/-} cultures. Error bars represent standard deviations.

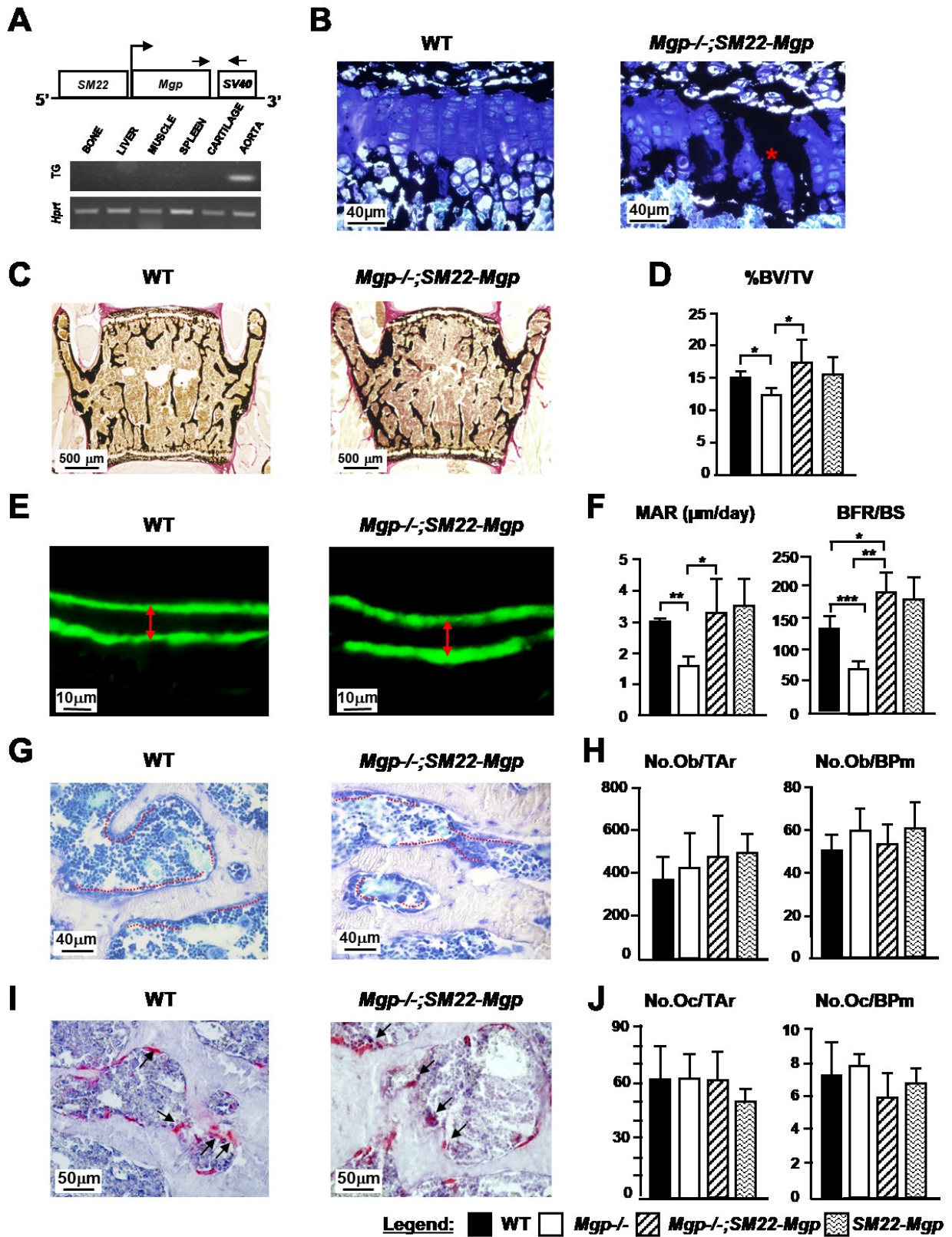


Figure 3.5. Restoration of *Mgp* expression in the arteries of *Mgp*^{-/-};*SM22-Mgp* mice rescues the low bone mass phenotype

A. Schematic representation of *Mgp*^{-/-};*SM22-Mgp* transgene construct (upper panel). Semi-quantitative PCR analysis (20 cycles) shows transgene expression only in arterial tissues. **B.** Histology images stained with von Kossa and Toluidine blue display the growth plate (lumbar vertebrae) from a 5-week-old WT and gender-matched *Mgp*^{-/-};*SM22-Mgp* mice. Note the severe growth plate calcification (shown by the asterisk) in the latter strain, confirming that the *Mgp* transgene was not expressed in the chondrocytes (n=3). **C.** VKVG stained undecalcified sections of WT and *Mgp*^{-/-};*SM22-Mgp* vertebrae show no apparent differences in bone mass. **D.** BV/TV analysis of 5-week-old WT, *Mgp*^{-/-}, *Mgp*^{-/-};*SM22-Mgp* and *SM22-Mgp* lumbar vertebrae show a correction of the bone mass in the *Mgp*^{-/-};*SM22-Mgp* mice when compared with their WT littermates; whereas the low bone mass persists in the *Mgp*^{-/-} littermates. Note that the *SM22-Mgp* control mice show no difference in bone mass when compared with WT mice. **E** and **F.** Calcein double labeling shows a comparable MAR in *Mgp*^{-/-};*SM22-Mgp* and WT mice. The red arrows show the distance between calcein double labels. While *Mgp*^{-/-} mice show a significantly reduced MAR and BFR/BS in comparison to their gender-matched WT littermates, there was not significant difference in the MAR and BFR/BS between WT, *Mgp*^{-/-};*SM22-Mgp* and *SM22-Mgp* controls. **G – J.** TB and TRAP – stained slides show normal osteoblast (dotted red lines) and osteoclast (arrows) numbers in all the groups analyzed. Error bars represent standard deviations; n ≥ 6 male mice for each group.

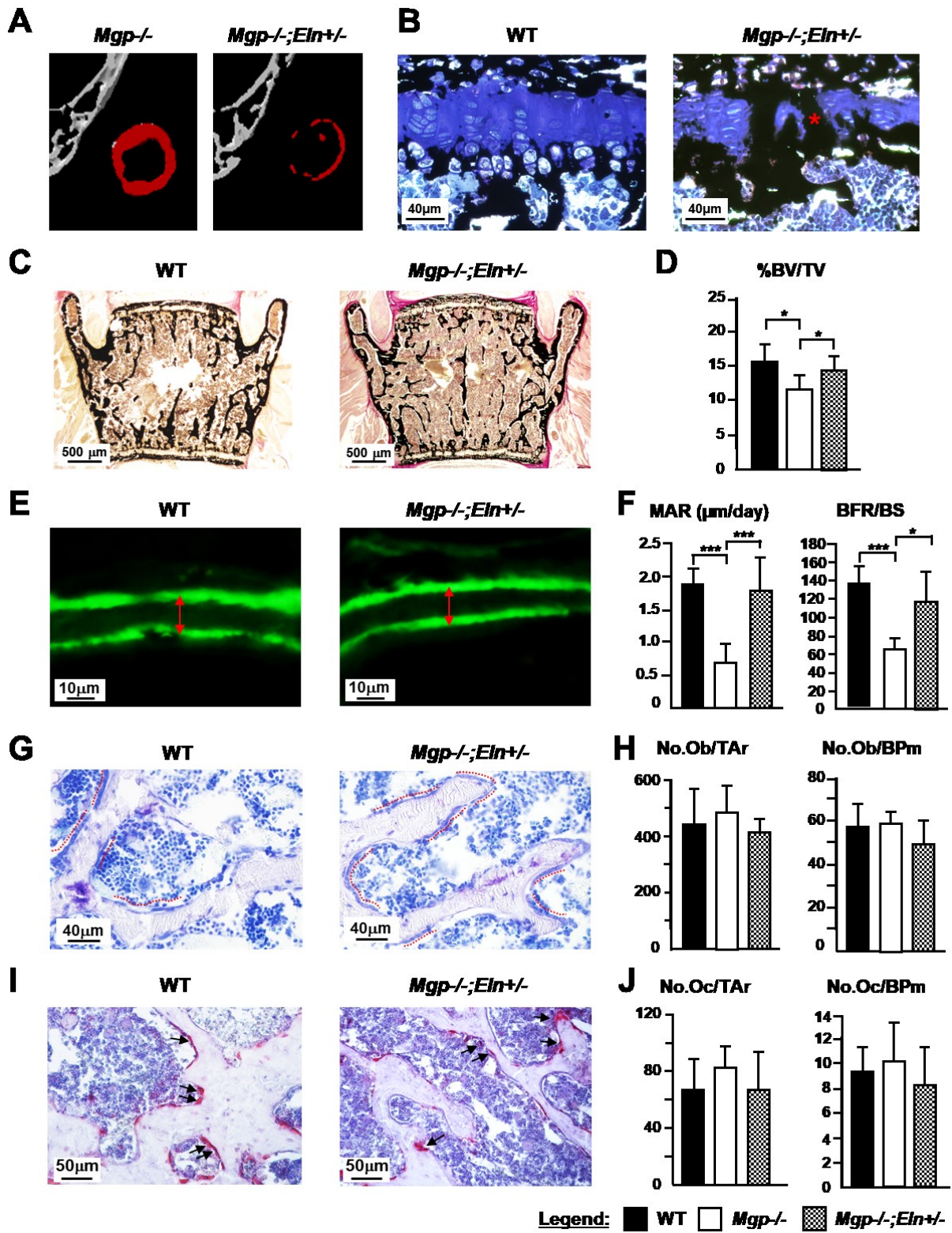


Figure 3.6. *Eln* haploinsufficiency delaying arterial calcification significantly improves bone mass in *Mgp*^{-/-};*Eln*^{+/-} mice

A. Micro-CT images of the thoracic aorta in *Mgp*^{-/-} and *Mgp*^{-/-};*Eln*^{+/-} mice show a significantly reduced mineral deposition in the latter genotype. **B.** Histology of 5-week-old lumbar vertebrae from WT and *Mgp*^{-/-};*Eln*^{+/-} mice stained with von Kossa and Toluidine blue showing the presence of the ectopic calcification in the growth plates of the latter model. **C.** and **D.** Histomorphometric analysis of lumbar vertebrae sections stained with VKVG, revealed a normal bone mass in the *Mgp*^{-/-};*Eln*^{+/-} transgenic mice when compared with WT controls, demonstrating that as a consequence of the reduction of arterial calcification, the bone phenotype is corrected in the *Mgp*^{-/-};*Eln*^{+/-} mice. In contrast, the low bone mass phenotype persists in the *Mgp*^{-/-} littermates. **E** and **F.** The quantification of the calcein double labeling shows a significant reduction of the MAR and BFR/BS in the *Mgp*^{-/-} mice and a correction in the *Mgp*^{-/-};*Eln*^{+/-} mice when compared with the WT controls. The red arrows show the distance between calcein double labels. **G** and **H.** Toluidine blue-stained vertebral sections show no change in the osteoblast (dotted red lines) counts in the mutant mice compared to WT and *Mgp*^{-/-} controls. **I** and **J.** The TRAP stained sections reveal comparable osteoclast (arrows) numbers in *Mgp*^{-/-};*Eln*^{+/-} mice. Error bars represent standard deviations; n ≥ 6 male mice for each group.

Chapter 4:

Matrix Gla Protein Deficiency Impairs Nasal Septum Growth,
Causing Midface Hypoplasia

Matrix Gla Protein Deficiency Impairs Nasal Septum Growth Causing Midface Hypoplasia

Juliana Marulanda¹, Hazem Eimar¹, Marc D. McKee^{1,2}, Michelle Berkvens¹, Valentin Nelea¹, Hassem Roman³, Teresa Borrás⁴, Faleh Tamimi¹, Mathieu Ferron⁵ and Monzur Murshed^{1,3,6}

¹Faculty of Dentistry, McGill University, Montreal, H3A1G1, Canada

²Department of Anatomy and Cell Biology, Faculty of Medicine, McGill University, Montreal, H3A0C7, Canada

³Division of Experimental Medicine, Department of Medicine, McGill University, Montreal, H4A3J1, Canada

⁴Department of Ophthalmology, School of Medicine, University of North Carolina, Chapel Hill, NC 27516, U.S.A

⁵Institut de Recherches Cliniques de Montréal, Montréal, H2W1R7, Canada

⁶Shriners Hospital for Children, Montreal, H4A0A9, Canada

J Biol. Chem., 2017;292(27): 11400-11412

4.1. Abstract

Genetic and environmental factors may lead to abnormal growth of the orofacial skeleton affecting the overall structure of the face. In the current study, we investigated the craniofacial abnormalities in a mouse model for Keutel syndrome, a rare genetic disease caused by loss-of-function mutations in the matrix Gla protein (*MGP*) gene. Keutel syndrome patients show diffuse ectopic calcification of cartilaginous tissues and impaired midface development. Our comparative cephalometric analyses of micro-CT images revealed a severe midface hypoplasia in *Mgp*^{-/-} mice. *In vivo* reporter studies demonstrated that the *Mgp* promoter is highly active at the cranial sutures, cranial base synchondroses and nasal septum. Interestingly, the cranial sutures of the mutant mice showed normal anatomical features. Although we observed a mild increase of mineralization of the spheno-occipital synchondrosis, it did not reduce the relative length of the cranial base in comparison to the total skull length. Contrary to this, we found the nasal septum to be abnormally mineralized and shortened in *Mgp*^{-/-} mice. Transgenic restoration of *Mgp* expression in chondrocytes fully corrected the craniofacial anomalies caused by MGP deficiency, suggesting a local role for MGP in the developing nasal septum. Although there was no upregulation of markers for hypertrophic chondrocytes, TUNEL assay showed a marked increase of apoptotic chondrocytes in the calcified nasal septum. Transmission electron microscopy confirmed unusual mineral deposits in the septal extracellular matrix (ECM) of the mutant mice. Of note, systemic reduction of inorganic P_i level was sufficient to prevent abnormal mineralization of the nasal septum in *Mgp*^{-/-};*Hyp* compound mutants. Our work provides evidence that modulation of local and systemic factors regulating ECM mineralization can be possible therapeutic strategies to prevent ectopic cartilage calcification and some forms of congenital craniofacial anomalies in humans.

4.2. Introduction

Congenital anomalies or birth defects are a major cause of perinatal lethality, affecting 2-3% of all newborns [234]. A significant number of these infants show abnormal craniofacial development that often disrupts the overall body functions and may lead to long-term disabilities [234]. Both genetic and epigenetic factors regulating the concerted morphogenesis of two craniofacial tissues, bone and cartilage, may affect the craniofacial growth and patterning. Although the primary causes are genetic, maternal exposure to toxic substances and nutritional status during pregnancy may also lead to these inborn deformities [3, 132, 133, 235, 236].

Midface hypoplasia is a developmental anomaly in which the nasal, maxillary and zygomatic bones in the cheek grow slower than other facial structures [144]. Genetic mutations, epigenetic factors or traumatic injuries during the early stage of life may lead to midface hypoplasia [150, 237-239]. A mild form of this disorder is usually considered as a harmless developmental anomaly of the face, while a severe form may seriously affect health and well-being. Clinical complications associated with this disease may include sleep apnea, misalignment of the jaws and eyelids, dental malocclusion, chewing and swallowing difficulties, impaired speech and overall disfigurement of the face [145, 147, 240].

Multiple genetic mutations have been associated with craniofacial malformations with severely impaired midface development. For instance, autosomal dominant mutations affecting fibroblast growth factor signaling cause midface hypoplasia in several diseases including Pfeiffer syndrome, Crouzon syndrome and Apert syndrome [237, 241, 242]. In these diseases, the primary cause of midface abnormalities is the early fusion of the cranial sutures (craniosynostosis), which is generally associated with the premature closure of the cranial base synchondroses [160, 243].

Although the above developmental anomalies are commonly associated with midface hypoplasia, some rare forms of this disease may have a different etiology that is not yet elucidated. For example, children born to mothers treated with warfarin during pregnancy develop Warfarin embryopathy, a disease characterized mainly by brain haemorrhages and severe midface hypoplasia [236, 238, 244]. Warfarin is a commonly prescribed anti-coagulant that inhibits vitamin K epoxide-reductase (VKORC1), which converts the oxidized form of vitamin K₁ to its reduced form. The reduced vitamin K₁ acts as a co-factor for γ -glutamyl carboxylase (GGCX) that is essential for the post-translational gamma-carboxylation of specific glutamic acid residues (Gla) in proteins, collectively known as ‘Gla proteins’ [245]. Similarly, patients with mutations in matrix Gla protein (*MGP*) develop Keutel syndrome, a rare genetic disorder primarily characterized by abnormal mineralization (calcification) of all cartilaginous tissues, short stature, stocky distal phalanges, arterial calcification and severe midface hypoplasia [3, 246].

MGP and a related protein, osteocalcin (bone Gla protein, encoded by *Bglap*), are known as skeletal Gla proteins [65]. While *Bglap* is expressed specifically by bone-forming osteoblasts, *Mgp* is expressed at high levels by chondrocytes in cartilaginous tissues, vascular smooth muscle cells (VSMCs) in the cardiovascular system and by the endothelial-like cells of the trabecular meshwork (TM) of the eye [247, 248]. Although initially, both of these proteins were proposed to be potent inhibitors of extracellular matrix (ECM) mineralization, our previous work demonstrated that only *MGP* possesses these anti-mineralization functions [65].

MGP-deficient mice (*Mgp*^{-/-} mice) recapitulate most of the phenotypic abnormalities of Keutel syndrome patients, including as recently reported, ectopic arterial calcification [249]. However, this latter phenotype is more severe in the mouse model and represents its primary

cause of death [11]. Although MGP-deficient mice have been well-characterized for their vascular calcification phenotype, their craniofacial anomalies are still understudied.

In the current study, we show that the midface hypoplasia in MGP-deficient mice is primarily caused by the impaired growth of the maxillary and palatine bones associated with abnormal mineralization and shortening of the nasal septum. For the first time, we show the activity of the *Mgp* promoter in the craniofacial complex using an *in vivo* reporter model, and we demonstrate that septal chondrocytes undergo apoptosis in the absence of MGP. Additionally, we show a novel mechanism of cartilage mineralization that, unlike the endochondral bones, does not require differentiated hypertrophic chondrocytes. Also of importance, we demonstrate that the extent of ectopic nasal septum mineralization in MGP-deficiency is P_i -dependant, where reduction of systemic P_i levels impedes nasal septum mineralization, preventing craniofacial malformations. Considering their phenotypic similarities to human patients, MGP-deficient mice may be a useful tool to understand the pathology and underlying cause of Keutel syndrome.

4.3. Results

4.3.1. *Mgp* deficiency causes midface hypoplasia

In order to investigate the effects of MGP and osteocalcin (BGLAP) deficiency in craniofacial development, the images of lateral and frontal heads of 5-week-old male wild type (WT), *Mgp*^{-/-} and *Bglap*^{-/-} mice were visually examined for gross craniofacial abnormalities. *Mgp*^{-/-} mice showed a severe blunting of the snout and a more rounded and wider face, whereas the *Bglap*^{-/-} mice were indistinguishable from WT mice, as demonstrated by the superimposition of the facial profiles presented in the lateral and frontal images. (**Figure 1A-C**).

Lateral cephalic X-rays of age- and gender-matched WT, *Mgp*^{-/-} and *Bglap*^{-/-} mice revealed a severe dental malocclusion characterized by an anterior crossbite only in *Mgp*^{-/-} mice; this phenotype was consistent in all the *Mgp*-null mice analyzed. Additionally, we detected an intense radiopaque area above the upper incisors in *Mgp*^{-/-} mice, which was not present in *Bglap*^{-/-} or WT mice (**Figure 1D, asterisk and arrow, respectively**). 3D reconstruction of micro-CT scans of the craniofacial complex of WT and *Mgp*^{-/-} mice confirmed the presence of a severe class III malocclusion (overbite) in the mutant mice (**Figure 1E**). Considering the absence of any craniofacial phenotype in *Bglap*^{-/-} mice, we conclude that of these two skeletal Gla proteins, only MGP is essential for normal craniofacial development.

We then performed a detailed cephalometric analysis and found that the maxillary and palatine lengths were more severely affected than other craniofacial structures in the *Mgp*^{-/-} mice. In contrast, the skull height, anterior cranial height and inter-molar maxillary distance were not affected, while only modest decreases were observed in the mandibular measurements (**Figure 2A and B** and Supplemental Table S1). Taken together, these data identify midface hypoplasia as the major craniofacial phenotype in MGP-deficient mice.

4.3.2. Ectopic calcification of the cartilaginous nasal septum in MGP-deficient mice

The aforementioned phenotype called for an understanding of the mechanism by which MGP could affect craniofacial development. As a first step in addressing this question, we studied *Mgp* expression in the craniofacial complex. To that end, we used a ‘knock in’ model (*Mgp-Cre*) in which a Cre recombinase gene has been inserted at the *Mgp* locus after the stop codon [248]. These mice were crossed with a reporter transgenic line, *Gtrosa6tm1Sor*, carrying a ubiquitous *Rosa* promoter followed by a ‘floxed’ insulator sequence and the bacterial β -galactosidase gene. In the resultant compound mutants *Mgp-Cre;Gtrosa6tm1Sor* (referred to hereafter as *Mgp-Cre;LacZ*), the β -galactosidase gene is expressed in tissues where the *Mgp* promoter is active [248]. The whole-mount and dissected heads from 2-week-old WT and *Mgp-Cre;LacZ* mice were stained with X-gal for β -galactosidase activity. Intense blue staining revealed *Mgp* promoter expression in all the cranial sutures, more strongly in the lambdoidal and frontonasal sutures (**Figure 3A**). Also, intense β -galactosidase activity was detected in the spheno-occipital synchondrosis (SOS), intersphenoidal synchondrosis (ISS) and in the cartilaginous nasal septum (NS) of the *Mgp-Cre;LacZ* mice (**Figure 3B**).

The lambdoidal, coronal, frontonasal and palatomaxillary sutures were analyzed using 2D micro-CT images, which failed to detect any sign of craniosynostosis or other anomalies in the sutures of *Mgp*^{-/-} mice (**Figure 3C**). Similarly, 2D-imaging of micro-CT scans of the SOS and ISS (top panel, sagittal view; lower panel, frontal view) did not detect premature closure of the ISS in these mice. However, at 5 weeks of age, the SOS appeared to be disorganized with an aberrant pattern of mineralization (**Figure 3D**).

Considering our X-ray analysis showing increased radiopacity in the region corresponding to the nasal septum and the very high expression of *Mgp* promoter in this tissue,

we examined its mineralization status in 5-week-old MGP-deficient mice by micro-CT. As presented in Figure 3E, frontal sections detected a striking ectopic mineralization of the nasal septum, which normally remains unmineralized throughout life [250].

Von Kossa and van Gieson (VKVG) staining of histological sections showed that although not calcified at birth, by the first week of life, mineral deposition is already detectable in the septal cartilage of MGP-deficient mice. Mineral accumulation then progressively increases as shown by the analyses of septal cartilage of 2- and 5-week-old mutant mice, whereas it remains unmineralized in the WT littermates (**Figure 4**).

4.3.3. Local expression of MGP in the cartilage corrects midface hypoplasia in MGP-deficient mice

We next investigated whether the local expression of *Mgp* in chondrocytes is sufficient to correct the midface hypoplasia in *Mgp*^{-/-} mice. For this purpose, we generated two transgenic lines that expressed *Mgp* under the *Col2a1* promoter (**Figure 5A, top panel**). Semi-quantitative PCR analyses showed higher level of transgene expression in the rib cartilage of one of these founders, although a weak expression of the transgene was also detected in the aorta (**Figure 5A, lower panel**). This observation was further confirmed by quantitative real time PCR (qRT-PCR) (**Figure 5B**). We mated the *Col2a1-Mgp* mice with *Mgp*^{+/-} mice to eventually generate *Mgp*^{-/-}, *Col2a1-Mgp* mice in the F2 generation. These mice showed approximately a 6-fold increase of *Mgp* expression in the nasal septum when compared to the WT littermates (**Figure 5C**).

In order to examine whether the relative weak expression of MGP transgene in the aorta could prevent arterial calcification, we performed alizarin red staining of the thoracic skeleton and vascular tissues of 5-week-old WT, *Mgp*^{-/-} and *Mgp*^{-/-}; *Col2a1-Mgp* littermates. We

confirmed that the weak expression of the transgene in *Mgp*^{-/-};*Col2a1-Mgp* mice was not sufficient to correct the vascular calcification phenotype, suggesting that this is a valid model for our experiments (**Figure 5D**).

We next studied the mineralization status of the nasal septum in *Mgp*^{-/-};*Col2a1-Mgp* mice. Histological analyses revealed a complete absence of ectopic mineralization in the septal cartilage. In contrast, the nasal septum of the *Mgp*^{-/-} littermates were severely mineralized (**Figure 5E**). Cephalic X-ray imaging of the *Mgp*^{-/-};*Col2a1-Mgp* mice were comparable to that of the WT littermates, confirming a complete correction of the dental and skeletal malocclusion (**Figure 5F**). Similarly, the cranial, maxillary and palatine lengths that were affected in *Mgp*^{-/-} mice, were normalized in the *Mgp*^{-/-};*Col2a1-Mgp* mice (**Figure 5G**). Taken together, these data suggest that local expression of MGP by chondrocytes can correct the midface hypoplasia in *Mgp*^{-/-} mice.

4.3.4. MGP-deficient mice have a shorter nasal septum with apoptotic chondrocytes

We next examined the effects of *Mgp* ablation on the growth of the nasal septum. The exposed septal cartilages of WT and *Mgp*^{-/-} littermates were stained with Safranin O, and the longitudinal lengths were measured. There was a significant reduction in the length of the nasal septum of *Mgp*^{-/-} mice (**Figure 6A**). We then analyzed 2D micro-CT images to measure the rostral, basicranial and total skull lengths in WT and *Mgp*^{-/-} mice following previously determined landmarks [251] (**Figure 6B, left panel and Supplemental Table S2**). The rostral (point 1-2) and basicranial (point 2-3, 3-4 and 4-5) lengths were measured and individually normalized by the total cranial length (point 1-5). We found that the rostral segment, but none of the basicranial lengths measured, were shorter in *Mgp*^{-/-} mice (**Figure 6B, right panel**). This result further

suggests that the shortening of the nasal septum is the cause of the hypoplastic maxilla in *Mgp*^{-/-} mice.

In order to understand the cause of nasal septum shortening in *Mgp*^{-/-} mice, we first assessed the cell size by calculating the average chondrocyte area. We did not observe any difference between WT and *Mgp*^{-/-} septal chondrocytes (**Figure 7A**). Then, we evaluated chondrocyte proliferation and apoptosis. Anti-Ki67 immunostaining showed a comparable cell proliferation rate between WT and *Mgp*^{-/-} nasal septum chondrocytes (**Figure 7B**). However, we observed an increase of TUNEL positive immature chondrocytes in the calcified nasal septum of *Mgp*^{-/-} mice (**Figure 7C**).

4.3.5. Chondrocyte hypertrophy is not a prerequisite for nasal septum calcification in MGP-deficient mice

We afterwards interrogated whether ectopic nasal septum calcification in *Mgp*^{-/-} mice is analogous to growth plate cartilage mineralization, a physiologic event that occurs during endochondral bone development. First, we compared the expression of a general chondrogenic marker *Col2a1* (encodes type II collagen) in the nasal septum of 1-week-old WT and *Mgp*^{-/-} mice; there was no detectable difference in mRNA levels (**Figure 8A**). Similarly, there was a comparable deposition of type II collagen as evident by immunostaining of the histological sections of the septal cartilage from 2-week-old WT and *Mgp*^{-/-} mice (**Figure 8B**). Interestingly, although the cartilaginous ECM was mineralized, there was no upregulation of the hypertrophic chondrocyte marker *Col10a1* by qRT-PCR analysis, nor was there any alteration of the encoded protein type X collagen when analyzed by immunostaining (**Figure 8C and 8D**). Also, we did not detect any increase of alkaline phosphatase activity, a hallmark of chondrocyte hypertrophy,

in the tissue extracts or histological sections prepared from *Mgp*^{-/-} septal cartilage in comparison to that of WT cartilage (**Figure 8E and 8F**).

4.3.6. Amorphous calcium phosphate as a main mineral species in MGP-deficient nasal septum

Ultrastructural analysis of *Mgp*^{-/-} calcified nasal septa by transmission electron microscopy showed globular structures in the ECM, in the vicinity of the chondrocytes. We observed incremental growth lines at the peripheral regions of the deposited mineral (**Figure 9A**). Detailed characterization of the mineral deposits by energy-dispersive X-ray spectroscopy identified them to contain abundant Ca²⁺ and phosphorus (**Figure 9B**). X-ray diffraction (**Figure 9C**) and electron diffraction (**inset in Figure 9C**) revealed that the inorganic mineral present in the MGP-deficient nasal septa was primarily an amorphous calcium phosphate phase, with a slight degree of crystallization towards an apatitic mineral phase as demonstrated by diffraction rings/spectra labelled 1 and 2 (**Figure 9C**). It was also noted that matrix vesicles which are normally present in the mineralizing growth plates, were generally not observed in the calcified nasal septum.

4.3.7. Prevention of nasal septum mineralization in *Mgp*^{-/-};*Hyp* mice

In order to understand whether ectopic mineralization in the nasal septum is regulated by global mechanisms that control bone and cartilage mineralization, we generated *Mgp*^{-/-};*Hyp* compound mutants. *Hyp* mice show an approximately 50% reduction of P_i levels in the serum, with poor bone and tooth mineralization, largely being attributable to this low level of circulating P_i, otherwise required for appropriate mineralization of the skeleton and dentition [26]. As we reported previously, the systemic reduction of P_i level persists in *Mgp*^{-/-};*Hyp* mice, while the serum Ca²⁺ level was not affected [16] (**Figure 10A**). We performed 3D micro-CT on 5-week-old WT, *Mgp*^{-/-} and *Mgp*^{-/-};*Hyp* heads, which revealed a complete absence of cartilaginous

nasal septum mineralization in the double mutants (**Figure 10B**). These findings were further confirmed by histology of nasal septum sections demonstrating a complete absence of mineralized ECM in *Mgp*^{-/-};*Hyp* mice (**Figure 10C**). Interestingly, there was no TUNEL-positive nuclei detected on the septal sections of *Mgp*^{-/-};*Hyp* mice (**Figure 10D**). Cephalometric analyses of micro-CT images showed a correction of the class III malocclusion, together with a normal maxillary and palatine lengths (**Figure 10E**). Although there was a significant increase of the cranial length in *Mgp*^{-/-};*Hyp* mice in comparison to *Mgp*^{-/-} mice, it remained shorter in comparison to that of WT mice (**Figure 10F**).

4.4. Discussion

Cephalometric analyses of *Mgp*^{-/-} heads at 5-week-old revealed severe midface abnormalities. Until now, these abnormalities were not fully characterized, and the underlying cause of this phenotype was unknown. Interestingly, the facial morphology of this mouse model closely resembles that of Keutel syndrome and Warfarin embryopathy patients, which justifies a thorough mechanistic study of this pathology.

Our micro-CT analyses clearly identified the key features of the facial phenotype in MGP-deficient mice. These measurements suggest that overall; the craniofacial bones are undersized in the mutant mice, which is expected considering their stunted growth. However, the maxilla and palatine bones are disproportionately smaller affecting the overall anteroposterior length. Taken together, the cephalometric analyses confirm that midface hypoplasia is the major cause of craniofacial defects in MGP-deficient mice.

As evident in the published literature, the two major causes of midface hypoplasia are premature cranial base synchondroses fusion, and craniosynostosis – premature closure of the cranial vault sutures [160]. It is now believed that the sutures play a passive role during the growth of the craniofacial complex, whereas the synchondroses act as growth centers, providing sites for rapid bone growth until fusion. Particularly, the spheno-occipital synchondrosis has been shown to play a major role as its late ossification and the closure timing correlates with the severity of the midface hypoplasia seen in syndromic patients [160, 251-253].

Impaired vitamin K metabolism has also been associated with midface hypoplasia. For instance, inactivating mutations in the gene for VKORC1, which generates the reduced form of vitamin K₁, and GGCX, which uses it as a co-factor, both lead to Vitamin K-dependent clotting

factor deficiency and midface hypoplasia [254, 255]. Similarly, babies born to mothers under anticoagulation therapy with warfarin suffer from Warfarin embryopathy, which also show midface abnormalities [236]. Considering that GGCX/VKORC1 mutations or fetal exposure to warfarin both affect gamma-carboxylation of Gla proteins, it is expected that these conditions would lead to the inactivation of the skeletal Gla proteins, *e.g.* MGP and osteocalcin. However, our experimental data presented here show that only MGP, but not osteocalcin deficiency, causes midface hypoplasia in mice.

The role of the nasal septum in midface development has been a matter of controversy for over half a century. Scott, in 1951, proposed that the nasal septum, as all other primary cartilages, acts as a growth center, separating the facial structures allowing the sagittal growth of the face [256]. This observation was supported by the findings that the nasal septum responds to hormones and growth factors and has an intrinsic ability to grow. Additionally, extirpation of the nasal septum has been shown to impair midface development in rats and rabbits [149, 150]. However, such experimental approaches were criticized as facial development is slower in humans than in the animal models used; thus, the observed midface malformations were attributed to the surgical trauma.

In 1968, Moss proposed the nasal septum as a passive structure that serves a supportive role for the other craniofacial structures [151]. This notion was challenged by *in vitro* and *in vivo* studies showing that the intrinsic growth capacity of the nasal septum is comparable to that of epiphyseal cartilages [152, 153]. Furthermore, the early corrections of nasal septum deformities in infants with cleft lip and palate or other facial defects show a greater effect on the correction of the overall craniofacial irregularities [154]. In agreement with these findings, we provide evidence that during the early phases of facial development, ectopic nasal septum mineralization

affects the growth of the midface. We report here that the prevention of nasal septum mineralization by transgenic expression of *Mgp* or by systemic reduction of P_i levels both corrected the midface abnormalities in MGP-deficient mice. These data support the original theory proposed by Scott that nasal septum acts as a critical growth element during facial development.

We performed an *in vivo* reporter assay to determine *Mgp* promoter activity in the developing craniofacial complex. For this purpose, we used a *Cre* transgenic line in which the gene encoding *Cre* recombinase was ‘knocked in’ at the *Mgp* locus by placing it directly under the control of the endogenous *Mgp* promoter and its regulatory elements. Crossing this model with the *R26R-lacZ* reporter line enabled us to faithfully establish endogenous *Mgp* expression by following β -galactosidase activity in the resultant offspring [248]. The ‘knock in’ strategy we used is superior to the conventional transgenic approach as the reporter gene expression is not driven by a truncated promoter at a random location in the genome, but by the single copy-endogenous promoter with all its proximal and distal regulatory elements. We found strong *Mgp* promoter activity in the cranial vault sutures, cranial base synchondroses and in the nasal septum. However, our reporter assay only suggests that the promoter is/was active in the β -galactosidase-positive tissues, but does not precisely indicate its time of activity during development. Considering that the cartilaginous part of the nasal septum remains unmineralized throughout adulthood [250], it is likely that *Mgp* is constitutively expressed in this tissue. Collectively, our data from the *in vivo* reporter assay and qRT-PCR gene expression analyses performed at two different time points (2 and 3 weeks of age, respectively) suggest that this is indeed the case.

It is interesting to note that despite the high level of *Mgp* expression in both SOS and ISS, only the SOS growth plates in *Mgp*^{-/-} mice showed mild mineralization irregularities, while the

ISS growth plates remained unaffected. In addition, the cranial sutures were also not abnormally mineralized in these mice. The absence of ectopic mineralization at some of these sites could be explained by the action of other mineralization inhibitor(s) [161], which may have differential distributions in various connective tissues. In fact, inorganic pyrophosphate, a potent mineralization inhibitor, may provide complementary anti-mineralization functions in some cartilaginous tissues. This notion is supported by the observation that the severe articular cartilage mineralization caused by impaired pyrophosphate metabolism is absent in MGP-deficient mice [49, 51]

Despite the presence of ectopic mineralization at the SOS, the proportional length of the cranial base was not smaller in *Mgp*^{-/-} skulls. Considering this observation, it is unlikely that the mild ectopic mineralization of the SOS significantly contributed to the disproportionate shortening of the midface. On the other hand, the relative length of the nasal septum as well as the viscerocranium were significantly smaller, suggesting that ectopic mineralization of the septal cartilage is the major cause of midface hypoplasia in MGP-deficient mice.

In order to investigate whether MGP acts locally to prevent abnormal nasal septum mineralization, we generated *Mgp*^{-/-};*Col2a1-Mgp* mice. Unexpectedly, the *Col2a1-Mgp* transgene showed a weak expression in the aorta. This can be explained by the positional effects of the transgene integration site in the chromosome alone, or combined effects of both integration site and copy number of the transgene. However, this weak ‘leaky’ expression of the transgene was not sufficient to prevent ectopic mineralization of the arteries in *Mgp*^{-/-};*Col2a1-Mgp* mice. Our observation that abnormal nasal septum mineralization was fully prevented despite the presence of mineralized arteries, has two important implications: firstly, it rules out the possibility that the calcified blood vessels adjacent to the nasal septum perichondrium serve

as nidi for the observed septal cartilage calcification; and secondly, in agreement with our previous findings, it establishes that MGP acts locally to prevent ectopic calcification [65].

During endochondral bone development, growth plate cartilage mineralization is a normal process that requires chondrocyte hypertrophy, hallmarked by type X collagen expression, and the release of matrix vesicles. Interestingly, chondrocyte hypertrophy and matrix vesicles appear not to be a prerequisite for ectopic mineralization of the cartilaginous ECM in the nasal septum of MGP-deficient mice. This observation suggests that mineral accumulation in the septal cartilage is likely not analogous to growth plate cartilage mineralization, where terminally differentiated chondrocytes undergo hypertrophy, and matrix vesicles seem to participate in the initiation of mineralization [37, 257]. We reported a similar nonchondrogenic ectopic mineralization event in the arteries of MGP-deficient mice [258]. Based on our observation, we conclude that the initiation of ECM mineralization in the MGP-deficient nasal septum does not require cellular differentiation (nor release of abundant matrix vesicles), but happens spontaneously by calcium phosphate precipitation. As is the case in blood vessels, whether any particular ECM protein promotes this mineral precipitation in the absence of MGP is yet to be determined.

Our analyses of the deposited mineral in the calcified nasal septum of MGP-deficient mice indicate that the mineral is primarily amorphous (noncrystalline) calcium phosphate. This finding indicates that MGP normally influences the early stages of calcium phosphate precipitation. Although at this point it is not known what structural features in MGP are essential for this function, it may not be solely attributable to the post-translational gamma-carboxylation of its glutamic acid residues. Our earlier work showed that osteocalcin, a closely related structural Gla protein, does not possess any significant anti-mineralization function [65]. In

agreement with this, we did not observe nasal septum mineralization or craniofacial abnormalities in osteocalcin-deficient mice. Recent published *in vitro* data indicate that N-terminal serine residues in MGP undergo phosphorylation and may facilitate the interaction between MGP and hydroxyapatite minerals [66]. The *in vivo* significance of these findings is yet to be determined. Identification of the functional residues in MGP is essential to understand the mechanism underlying MGP's anti-mineralization function.

Vascular smooth muscle cells produce large amounts of MGP, which prevents mineralization of the elastic lamina in arterial tissues [258]. The vascular mineralization phenotype in MGP-deficient mice is fully penetrant and appears at the same time as the initiation of nasal septum mineralization. This raises the question as to whether mineral deposition in the nasal septum is actually within the blood vessels present in the tissue. However, this possibility can be ruled out by our observation that although the blood vessels are extensively mineralized in *Mgp*^{-/-};*Col2a1*-*Mgp* mice, as is the case in *Mgp*^{-/-} mice, there was no detectable presence of mineral deposits in the septal cartilage of *Mgp*^{-/-};*Col2a1*-*Mgp* mice. Furthermore, although vascular calcification is not reported in most of the Keutel syndrome patients, midface hypoplasia has always been associated with this disease, suggesting that these two phenotypic traits may not be interrelated.

Our experimental data revealed an increase in apoptosis in the MGP-deficient septal chondrocytes, which may explain, at least in part, the observed shortening of the nasal septum in these mice. Hayano *et al* found that augmented BMP-SMAD signalling leads to apoptosis in the developing nasal cartilage through p53 upregulation [259]. Additionally, other laboratories have reported that MGP inhibits BMP signalling in vascular smooth muscle cells [88]. Therefore, it is possible that MGP-deficiency in the nasal septum may induce BMP signalling and cause

chondrocyte apoptosis. However, this data needs to be confirmed experimentally. A second hypothesis that can explain the increased apoptosis in the nasal septum of *Mgp*^{-/-} mice is the local increase of P_i in the cartilaginous ECM. Inorganic phosphate has been shown to be a major regulator of apoptosis of hypertrophic chondrocytes in the developing endochondral bones [260]. As reported here, we found the presence of amorphous calcium phosphate precipitates in the calcified nasal septum. The unstable nature of this transient phase may allow the minerals to be readily dissolved, increasing the local P_i levels inducing apoptosis of the neighbouring cells. In addition to chondrocytes apoptosis, another possible mechanism that may affect the anteroposterior growth of the nasal septum is the stiffening of its ECM caused by ectopic mineral deposition. Future studies on the mechanical properties of the mineralized septal cartilage will reveal whether this is indeed the case.

Lastly, we found that systemic regulation of P_i levels in the serum is sufficient to prevent nasal septum mineralization in *Mgp*^{-/-};*Hyp* double mutant mice. Mutations in the *Phex* gene lead to X-linked hypophosphatemia (*Hyp mice*) characterized by phosphaturia and increased osteoid volume. Interestingly, lowering serum P_i levels in the *Mgp*^{-/-} mice also completely prevents the vascular calcification phenotype, as we reported previously [16]. This finding has a substantial clinical implication in that it demonstrates that nasal septum mineralization and craniofacial malformations can be modulated by systemic factors. Future preventive interventions can be developed based on this finding.

4.5. Materials and methods

4.5.1. Mice

The generation of *Mgp*^{-/-}, *Bglap*^{-/-} (*Ocn*^{-/-}) and *Mgp*-*Cre*;*Gtrosa6tm1Sor* mice have already been described [11, 228, 248]. All the experiments were performed on mice with C57BL/6 background. *Col2a1-Mgp* transgenic mice were generated by pronuclear injection at the Transgenic Core Facility at the Goodman Cancer Center of McGill University following standard techniques. *Hyp* mice were purchased from Jackson Laboratories. *Mgp*^{-/-};*Hyp* double mutants were generated through breeding, and only male mice were used for our analyses. Mice were maintained in a pathogen-free standard animal facility.

Genotypes were determined by PCR on genomic DNAs isolated from tail biopsies. The sequences of the primers used for genotyping are provided upon request.

4.5.2. Skeletal preparation

Skeletal tissues from adult mice were fixed overnight in 95% ethanol, stained in 0.015% Alcian Blue dye (Sigma - Aldrich) in a 1:4 solution of glacial acetic acid and absolute ethanol for 24 hours. Tissues were then treated with 2% potassium hydroxide for another 24 hours (or until the soft tissues were dissolved) and then stained by 0.005% Alizarin Red (Sigma - Aldrich) in a 1% potassium hydroxide solution. Finally, the stained skeletal tissues were clarified in 1% potassium hydroxide /20% glycerol for 2 days.

4.5.3. Radiography and X-ray micro-computer tomography (micro-CT)

Radiographic analyses of the mouse heads were performed at the Centre for Bone and Periodontal Research core facility at McGill University, with an XPERT X-ray imaging system (Kubtec). Micro-CT scanning of mouse skulls was performed with a SkyScan model 1072 instrument (SkyScan) set at a resolution of 8.0 μm and 0.5-mm Al filter. Micro-CT image processing and analysis was performed with version 2.2f of the manufacturer's software (SkyScan). Cephalometric measurements, sutures and cranial base analyses were done using the software Data Viewer (SkyScan). The 3D-reconstructions of head scans were done using the CtAn and CtVol software (SkyScan).

4.5.4. Cephalometric analysis

Cephalometric analyses of micro-CT scans of whole heads were done following the method reported by Eimar, *et al* [261]. Cephalometric analysis of the basicranium was done according to the modified method reported by Laurita, *et al* [251]. Only male mice were used for the cephalometric and basicranial studies.

4.5.5. Histology and tissue imaging

Mouse skulls were fixed overnight in 10% formalin, embedded in methyl methacrylate, sectioned (7 μm), and stained by von Kossa and van Gieson (VKVG) or Hematoxylin and eosin for cell size assessment. For type II (ab21291, Abcam Inc) and type X collagen (a generous gift from Dr. Pierre Moffatt, Shriners Hospital for Children, Montreal [262]) and Ki-67 (ab66155, Abcam Inc) immunohistochemistry, 7- μm -thick paraffin sections of decalcified tissues were prepared. Hematoxylin (Fisher Diagnostics) was used for visualization of cell nuclei. Images

were taken using a light microscope (DM200; Leica Microsystems) with 20X (numerical aperture of 0.40) and 40X (numerical aperture of 0.65) objectives. Exposed cartilaginous nasal septa were stained with Safranin-O (BioShop) and scanned using an Epson V700 PHOTO scanner. Cell area (μm^2) was measured using PhotoShop (Adobe). All histological images were captured using a digital camera (DP72; Olympus Canada Inc), acquired with DP2-BSW software (XV3.0; Olympus Canada Inc) and processed using PhotoShop software (Adobe).

4.5.6. TUNEL assay

Terminal deoxynucleotidyltransferase-mediated dUTP nick end labeling (TUNEL) assay was performed using a colorimetric (Trevigen) or a fluorometric (Promega) kit following the manufacturer's instructions. Samples from 2- and 3-week-old mice were decalcified in 25% EDTA (Sigma - Aldrich) in PBS and embedded in paraffin to cut 7-micron sections. Upon labeling, sections were counterstained with 1% methyl green or H33258 (Sigma - Aldrich). TUNEL-positive cells were visualized using light (DM200; Leica Microsystems Inc) and fluorescence (EVOS FL Cell Imaging System, ThermoFisher Scientific) microscopes and quantified using Image-J software from NIH.

4.5.7. Alkaline phosphatase activity

Tissue extracts were prepared with 1x Passive Lysis Buffer (Promega) and total proteins were measured by the Micro BCA protein assay (Thermo Scientific). Alkaline phosphatase activity was measured using p -nitrophenyl phosphate substrate (Sigma-Aldrich) and then normalized by the respective protein concentration in the extracts.

4.5.8. X-gal staining

For 5-Bromo-4-Chloro-3-Indolyl- β -D-Galactopyranoside (X-gal) (BioShop) staining; mouse heads were dissected and fixed for 5 min in 2% formalin and 0.2% glutaraldehyde in PBS containing 5mM EGTA and 2mM MgCl₂. Fixed tissues were rinsed with PBS containing 2mM MgCl₂ and 0.2% IGEPAL® CA 630 and left 4 hours in the same buffer supplemented with 5mM of K₃Fe(CN)₆ and 5mM of K₄Fe(CN)_{6,3}H₂O. Later, the whole mount heads were stained for 4 hours at 37°C in 25 mg/mL X-gal diluted in the same buffer.

4.5.9. Gene expression analysis

Gene expression analyses were performed using a quantitative real-time PCR (qRT-PCR) system (Model 7500; Applied Biosystems, Mississauga, ON). Total RNA was extracted from different tissues with TRIZOL reagent (Invitrogen) and subjected to DNase I (Invitrogen) treatment. The first-strand cDNA synthesis and qRT-PCR were performed using a high-capacity cDNA reverse-transcription kit (Applied Biosystems) and Maxima SYBR green quantitative PCR master mix (Fermentas), respectively. Relative gene expression was analyzed using SDS software (Applied Biosystems) using comparative CT and hypoxanthine guanine phosphoribosyl transferase (*Hprt*, a housekeeping gene) expression as an endogenous control. In order to calculate the delta cycle threshold (DCT) value, the mean CT value of the expression of a gene in a sample was first normalized to the mean CT value of *Hprt* expression in that sample. The DCT value of the calibrator sample was subtracted from that of the sample-of-interest to obtain the DDCT value. The relative expression was reported as 2-DDCT.

4.5.10. Electron microscopy

Ultrastructural characterization was performed by transmission electron microscopy (TEM). Tissues were fixed with 2% glutaraldehyde (Electron Microscopy Sciences) in 0.1 M sodium cacodylate buffer at pH 7.2, followed by dehydration through a series of graded ethanol dilutions. Samples were embedded in LR White acrylic resin (Electron Microscopy Sciences). Ultrathin sections (80-nm-thick) were cut using a Leica EM UC6 ultramicrotome (Leica Microsystems Inc), and were placed on formvar-coated nickel grids (Electron Microscopy Sciences) and stained conventionally with uranyl acetate and lead citrate (Electron Microscopy Sciences) for viewing by TEM. A field-emission FEI Tecnai 12 BioTwin TEM (FEI) was used to image the stained sections at 120 kV.

4.5.11. Electron diffraction

Electron diffraction in the selected-area configuration (SAED) and energy-dispersive X-ray spectroscopy (EDS) were performed at 200 kV with a FEI Tecnai G² F20 200 cryo-scanning transmission electron microscope equipped with a Gatan Ultrascan 4000 4k x 4k CCD camera system model 895, and an EDAX Octane T Ultra W /Apollo XLT2 SDD and TEAM EDS analysis system (FEI). Samples were as those used for electron microscopy imaging, but sections were left unstained.

4.5.12. X-ray diffraction

X-ray diffraction (XRD) analysis was performed using a D8 Discover diffractometer (Bruker-AXS Inc) equipped with a copper X-ray tube (wavelength, 1.54056 Å) and a HI-STAR general area detector diffraction system mounted on a vertical θ - θ goniometer (Bruker-AXS Inc).

Measurements were run in coupled θ - θ scan in microbeam analysis mode (50 μm X-ray beam spot size). Samples examined were the same as those used for electron microscopy, where here the microtomed LR White plastic block face (from which TEM sections were obtained) was analyzed directly in the X-ray beam spot mode.

4.6. Data analysis

All results are shown as means \pm standard deviations. Statistical analyses were performed by Student's *t* test or analysis of variance (Tukey's multiple-comparison test) using GraphPad Prism software. Single asterisk indicates $p < 0.05$, two asterisks indicate $p < 0.01$ and three asterisks indicate $p < 0.001$.

4.7. Acknowledgements

We thank Dr. Gerard Karsenty for critical reading of the manuscript. We also thank Mia Esser, Louise Marineau and Maude Danis Ladouceur for animal husbandry. The core facility for skeletal phenotyping was supported by Le Réseau de Recherche en Santé Buccodentaire et Osseuse (RSBO). This work was supported by operating grants from the Canadian Institutes of Health Research (CIHR) Fund (number 123310 to M.M.). M.M. is an FRQS chercheur-boursier and J.M. received a studentship from RSBO.

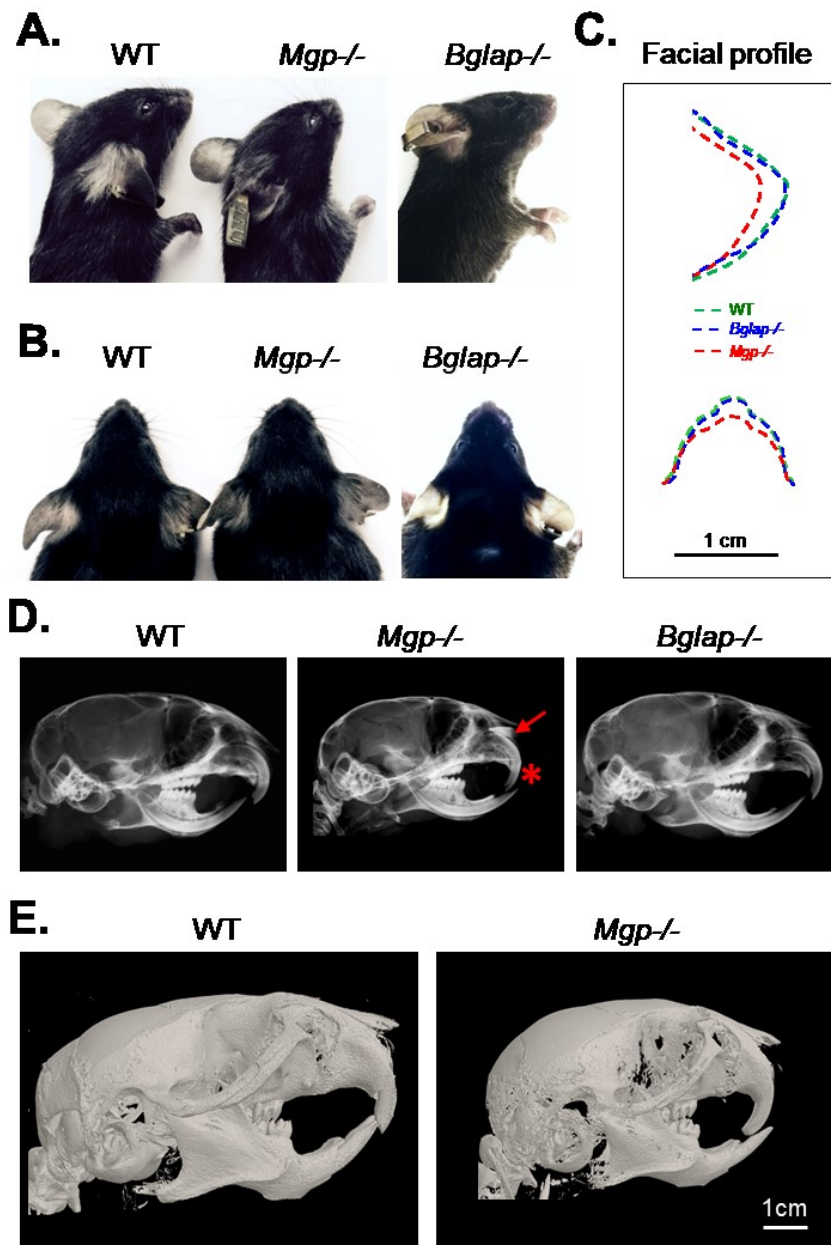
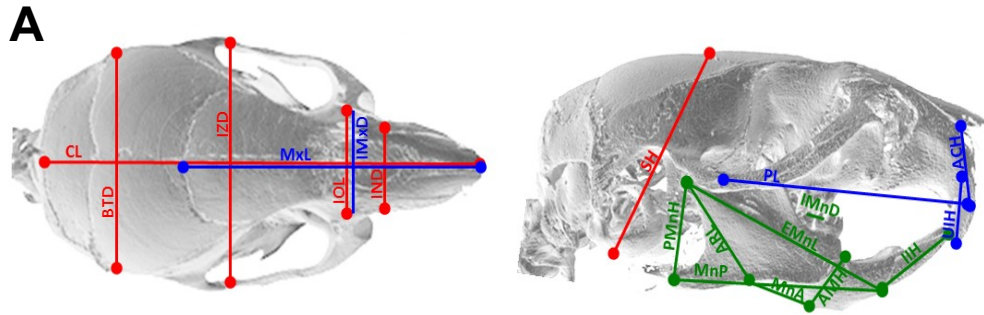


Figure 4.1. Ablation of *Mgp*, but not *Bglap* causes craniofacial malformations

A. Lateral cephalic photographs of WT, *Mgp*^{-/-} and *Bglap*^{-/-} mice showing a blunt and shorter snout in *Mgp*^{-/-} mice. **B.** Frontal cephalic photographs confirming the abnormal craniofacial phenotype in *Mgp*^{-/-} mice. **C.** Superimposition of the lateral and frontal cephalic photographs showing a comparable facial profile between WT and *Bglap*^{-/-} mice and a blunt and wider profile in *Mgp*^{-/-} mice. **D.** Lateral cephalic X-ray of WT, *Mgp*^{-/-} and *Bglap*^{-/-} mice. *Mgp*^{-/-} mice show a severe anterior crossbite with a radiopaque nasal structure (red asterisk and arrow, respectively). **E.** 3D reconstruction of micro-CT scans of WT and *Mgp*^{-/-} mice confirming the dental malocclusion and craniofacial deformities in the latter genotype.



B. Cephalometric

Measurement (mm)	WT	SD	<i>Mgp</i> ^{-/-}	SD	p
Craniofacial					
Cranial length (CL)	21.94	0.21	19.19	0.23	***
Skull height (SH)	9.01	0.07	8.84	0.06	NS
Inter-nasal distance (IND)	3.45	0.05	3.19	0.08	*
Inter-orbitary length (IOL)	4.2	0.13	4.29	0.11	NS
Inter-zygomatic distance (IZD)	11.96	0.11	11.58	0.1	*
Bi-temporal distance (BTD)	10.13	0.09	9.57	0.11	**
Maxillary					
Maxillary length (MXL)	11.15	0.16	9.2	0.2	***
Palatine length (PL)	12.96	0.14	10.98	0.35	***
Anterior cranial height (ACH)	2.72	0.08	2.68	0.11	NS
Upper incisor height (UIH)	3.2	0.07	3.2	0.1	NS
Inter-molar maxillary distance (IMMD)	3.72	0.03	3.8	0.07	NS
Mandibular					
Effective mandibular length (EML)	10.87	0.12	10.24	0.1	**
Mandibular plane (MNP)	7.14	0.09	6.3	0.07	***
Mandibular axis (MNA)	3.43	0.07	3.14	0.06	*
Inferior incisor height (IIH)	3.83	0.04	3.5	0.08	**
Ascending ramus length (ARL)	5.43	0.1	5.06	0.07	**
Posterior mandibular height (PMNH)	4.91	0.07	4.33	0.07	***
Inter-molar mandibular distance (IMND)	3.9	0.03	3.88	0.07	NS

Figure 4.2. *MGP* deficiency causes midface hypoplasia

A. Depiction of the selected landmarks for cephalometric analyses of WT and *Mgp*^{-/-} mice. Red, blue and green lines represent the overall craniofacial, maxillary and mandibular measurements, respectively. Description of each landmark's anatomical location is presented in Supplemental Table S1. **B.** Craniofacial, maxillary and mandibular measurements in millimetres. Each value represents the mean of 6 mice analyzed for each genotype at 5-week-old. Statistical analysis: Student's *t* test, SD (Standard deviation).

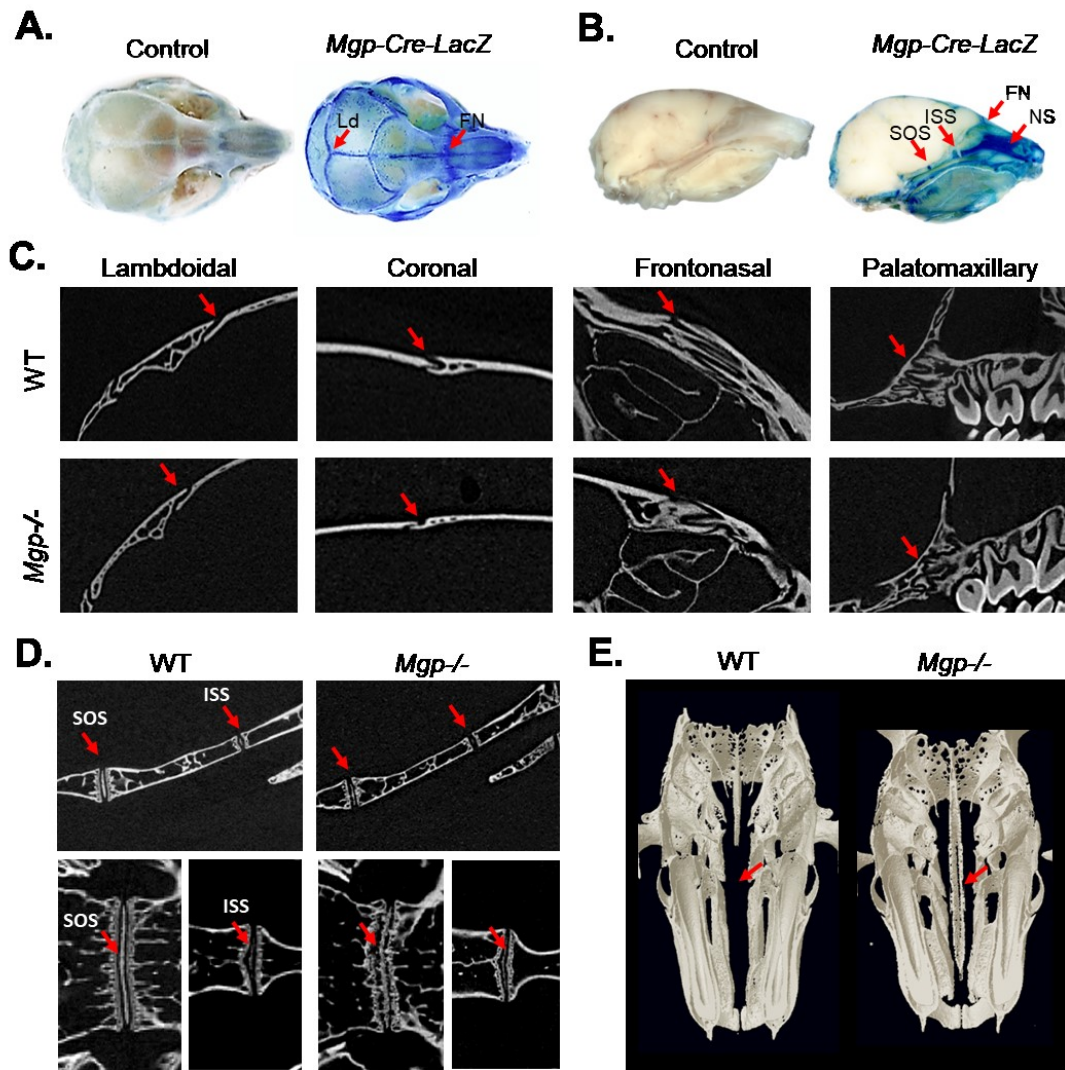


Figure 4.3. Ectopic calcification of the cartilaginous nasal septum in MGP-deficient mice

A. and **B.** Whole-mount heads of 2-week-old *Mgp-Cre;LacZ* and control mice were stained with X-gal for bacterial β -galactosidase detection. Intense blue staining revealed *Mgp*-promoter activity in all the craniofacial sutures, more intensely in the lambdoidal (Ld) and frontonasal (FN) sutures. The spheno-occipital synchondrosis (SOS), intersphenoidal synchondrosis (ISS) in the basicranial region and nasal septum (NS) were also strongly stained (red arrows; n=3 mice for each group). **C.** 2D images of micro-CT scans of WT and *Mgp*^{-/-} mice showing the absence of craniosynostosis in the mutant mouse in the lambdoidal, coronal, frontonasal and palatomaxillary sutures (red arrows, n=6 in each group). **D.** 2D micro-CT scans (top panels: sagittal view; lower panels: frontal view) of the basicranium of WT and *Mgp*^{-/-} mice showing the normal anatomy of the ISS in the mutant mouse. However, the SOS appeared to be disorganized with an aberrant pattern of mineralization (n=3 mice in each group) **E.** 3D reconstruction of WT and *Mgp*^{-/-} heads in the frontal plane showing a severe nasal septum mineralization in the *Mgp*^{-/-} mice (red arrow, n=6 mice in each group). All the analyses were done on 5-week-old mice unless indicated otherwise.

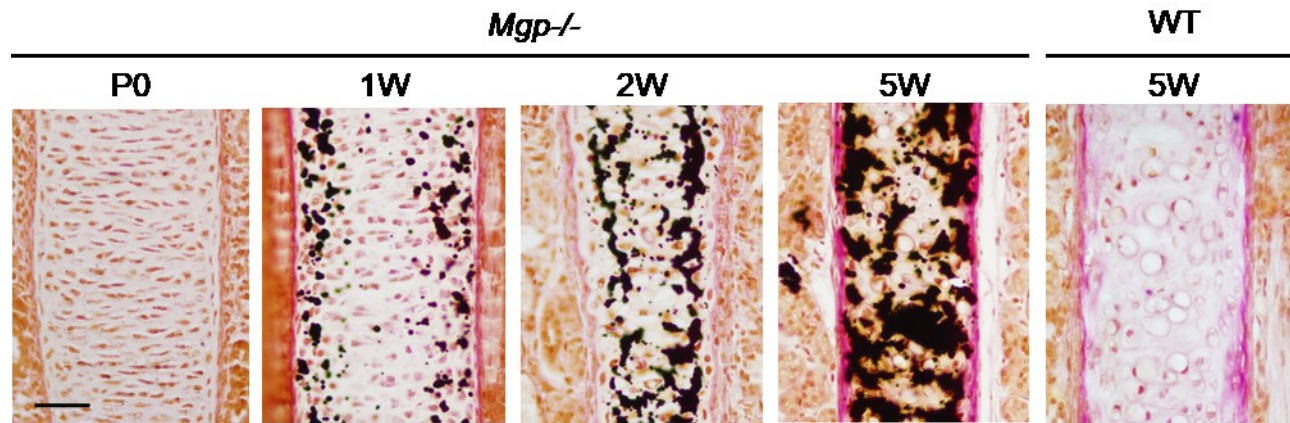


Figure 4.4. Progressive ectopic mineralization of MGP-deficient nasal septum

Histological analysis of *Mgp*^{-/-} nasal septa by VKVG staining of 7 μ m-thick plastic sections showing the initiation of pathologic cartilage mineralization at 1 week of age and its progression until 5 weeks of age (n=3 mice for each time point). The last panel represents an unmineralized WT nasal septum at 5 weeks of age stained with VKVG. Scale bar represents 40 μ m.

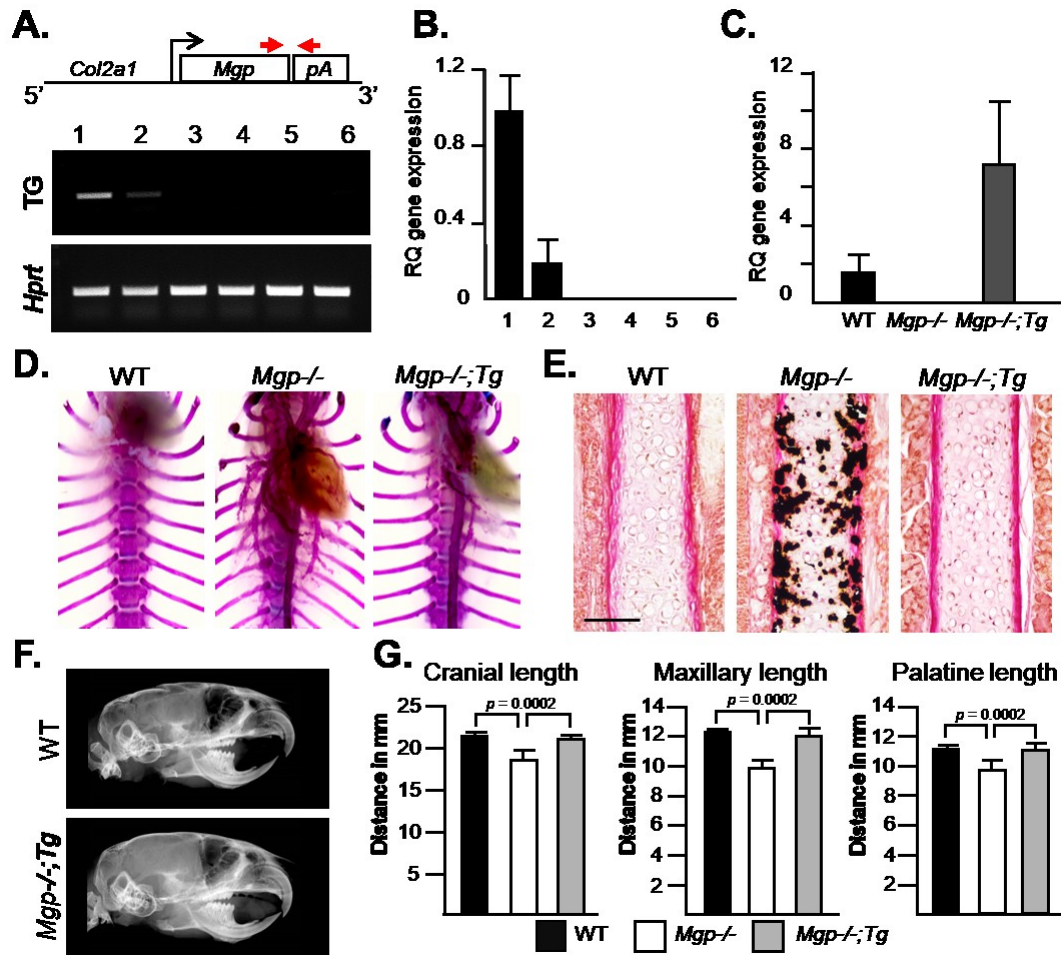


Figure 4.5. Local expression of *Mgp* in the cartilage corrects the midface hypoplasia in MGP-deficient mice

A. Schematic representation of genetic construct used to generate *Col2a1-Mgp* transgenic mice expressing *Mgp* under the cartilage-specific *Col2a1* promoter (top panel). The red arrows represent the primers used to detect the transgene by PCR. Semi-quantitative PCR showing the tissue-specific expression of the transgene in 2-week-old *Col2a1-Mgp* mice (middle panel, 1: Cartilage, 2: Aorta, 3: Calvaria 4: Muscle, 5: Brain, and 6: Long bone) showing a strong *Mgp* expression in cartilage and minor expression in aorta. **B.** qRT-PCR analysis of transgene expression in the same tissues described in Panel A. **C.** qRT-PCR showing approximately 6-fold increased *Mgp* expression in the nasal septum cartilage of *Mgp*^{-/-};*Col2a1-Mgp* (*Mgp*^{-/-};*Tg*) mice when compared with the WT littermates. Note the absence of *Mgp* expression in the nasal septum of *Mgp*^{-/-} mice. **D.** Ribcage skeletal preparations of 5-week-old mice stained with alizarin red and alcian blue showing the vascular mineralization in *Mgp*^{-/-} mice and in *Mgp*^{-/-};*Tg* mice. **E.** VKVG staining showing a complete absence of mineralization in the nasal septum of *Mgp*^{-/-};*Tg* mice. Scale bar represents 100μm. **F.** Lateral cephalic X-ray of WT and *Mgp*^{-/-};*Tg* littermates showing the correction of the craniofacial and dental phenotypes in the latter model. **G.** Craniofacial measurements showing the normalization of the cranial, maxillary and palatine lengths in *Mgp*^{-/-};*Tg* mice. Statistical analysis: ANOVA (Tukey's multiple-comparison test). All the analyses were done with 5-week-old mice (n=3 in each group for each experiment).

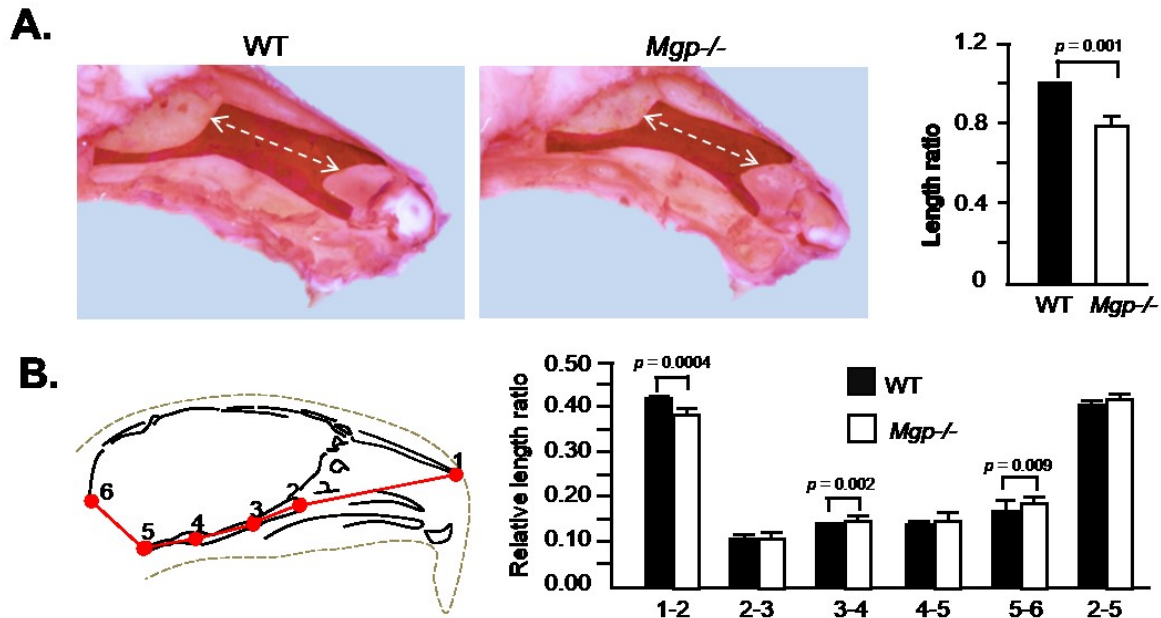


Figure 4.6. MGP-deficient mice have a shorter nasal septum

A. Exposed cartilaginous nasal septa of 5-week-old WT and *Mgp*^{-/-} mice stained with Safranin O. Measurement of the lengths presented as relative length ratio shows a significantly smaller nasal septum in *Mgp*^{-/-} mice. **B.** 2D cephalometric analysis of the viscerocranium and basicranium of 5-week-old WT and *Mgp*^{-/-} mice. The viscerocranium (1-2) in *Mgp*^{-/-} mice is significantly smaller when compared to WT mice, whereas the total basicranial length (2-5) is not affected. Values represent the ratio of the linear distance between points over the total cranial length (1-5). Description of the landmark's anatomical locations is presented in supplemental material Table S2, (n=5 in both groups). Statistical analysis: Student's *t* test in all cases.

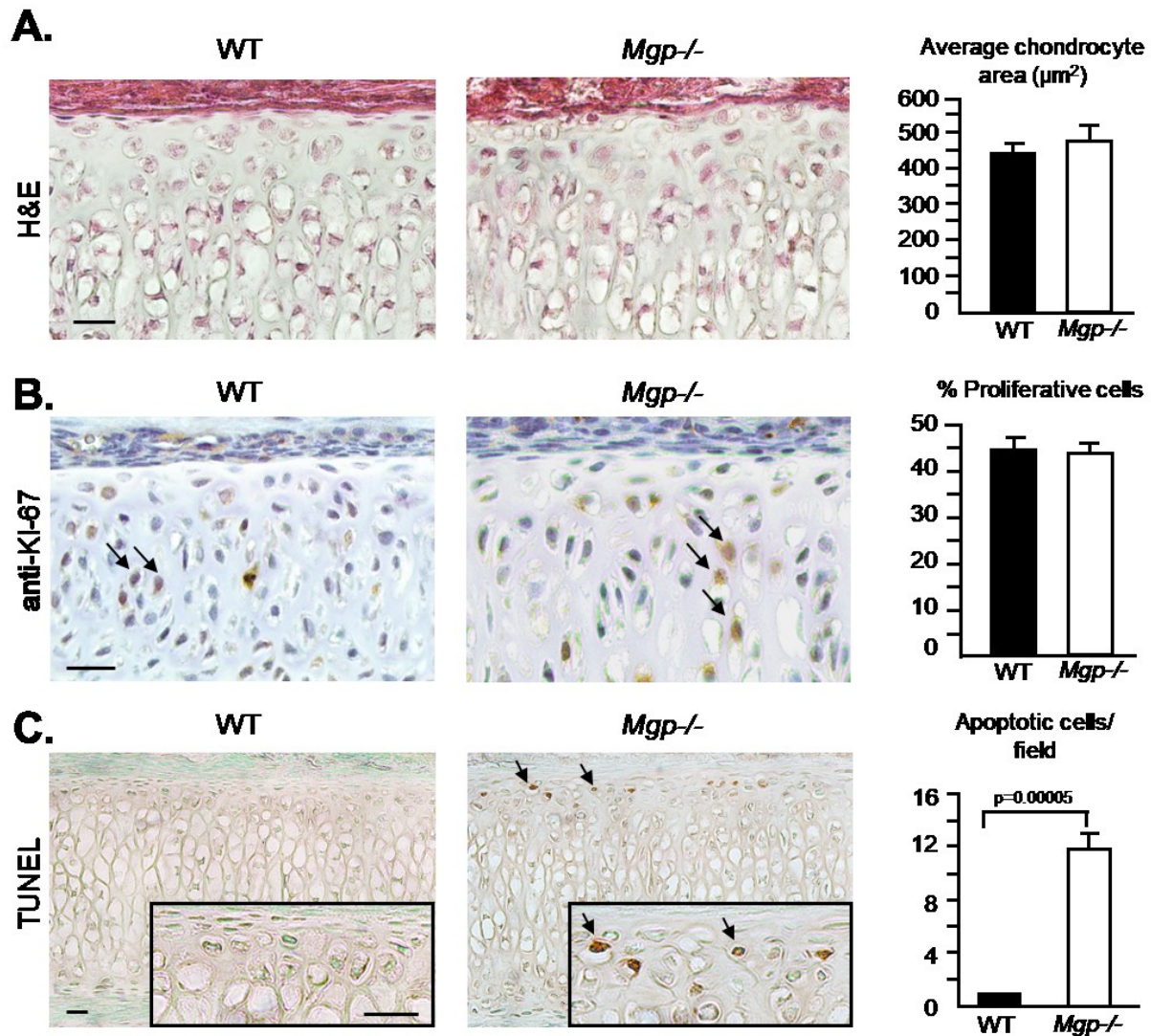


Figure 4.7. MGP-deficient septal chondrocytes undergo apoptosis

A. Quantification of cell area on histological sections of WT and *Mgp*^{-/-} nasal septa stained with hematoxylin and eosin (H&E) shows no difference in chondrocyte size between the genotypes. Three fields were quantified per sample (n=3 in both groups). Scale bar represents 20 μm . **B.** Anti-Ki67 antibody and hematoxylin staining of septal sections showing the proliferating chondrocytes (arrows). Quantification of proliferative cells/total cell count shows no difference between WT and *Mgp*^{-/-} mice (n=6 in both groups). Scale bar represents 20 μm . **C.** Colorimetric apoptosis detection assay (TUNEL) performed on WT and *Mgp*^{-/-} septal sections shows the presence of apoptotic cells (arrow) in the MGP-deficient nasal septum but not in the WT nasal septum sections. The sections were counter-stained by methyl green (n=3 in both groups). Scale bars represent 20 μm . All analyses were performed on 2-week-old mice; statistical analysis: Student's *t* test in all cases.

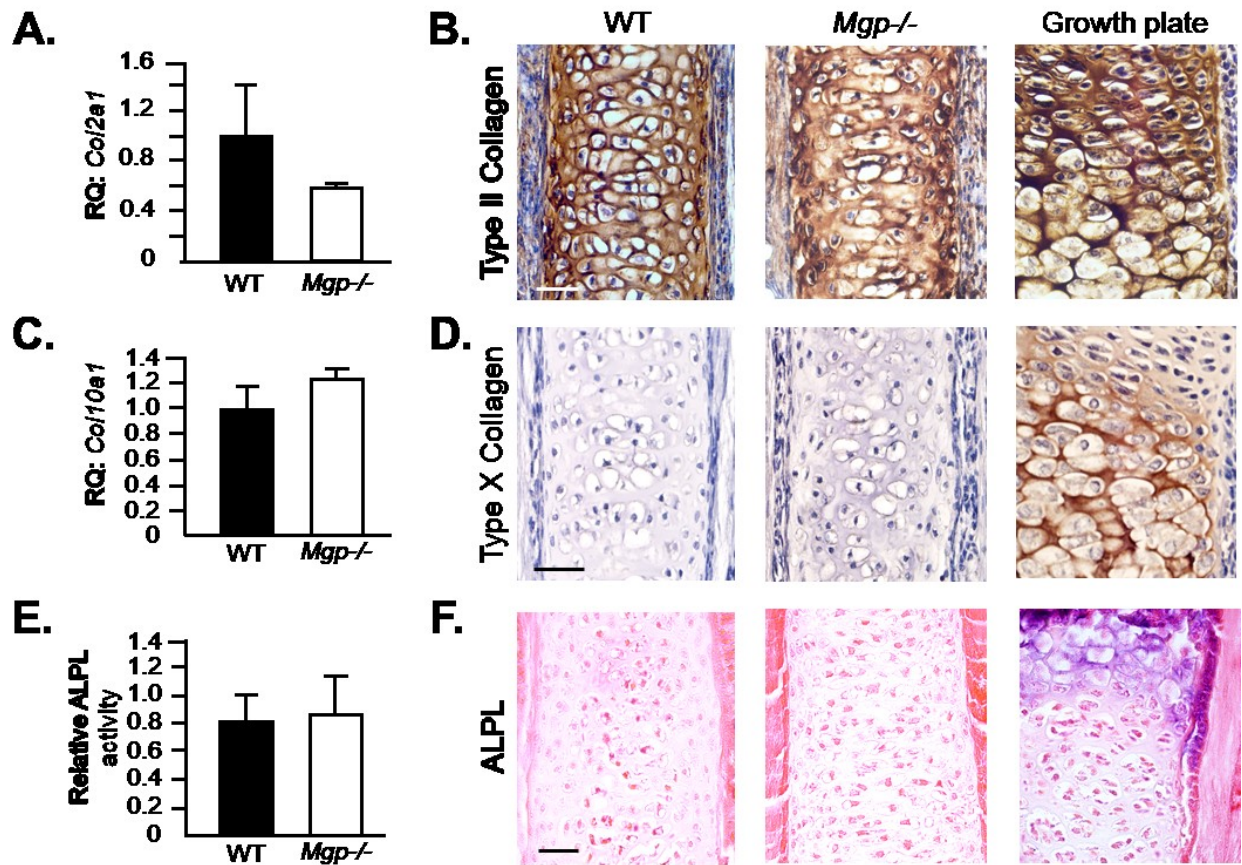


Figure 4.8. Chondrocyte hypertrophy is not a prerequisite for ectopic mineralization of the nasal septum in MGP-deficient mice

A. Gene expression analysis of *Col2a1* in 1-week-old WT and *Mgp*^{-/-} nasal septa showing comparable expression in both groups. **B.** Immunohistochemistry showing similar expression pattern of type II collagen in 2-week-old WT and *Mgp*^{-/-} nasal septa. Embryonic humerus growth plate staining was used as a positive control. **C.** *Col10a1* gene expression in 1-week-old WT and *Mgp*^{-/-} mice showing no induction in the ‘knockout’ tissue. **D.** Absence of anti-Type X collagen staining in the WT and *Mgp*^{-/-} 2-week-old nasal septum. Embryonic humerus growth plate staining was used as a positive control. **E.** The alkaline phosphatase (ALPL) basal activity in *Mgp*^{-/-} nasal septum extracts from 2-week-old mice is comparable to that of WT littermates. **F.** ALPL staining confirms the absence of ALPL activity in the septal cartilage of *Mgp*^{-/-} mice. Staining of septal growth plate sections from 2-week-old WT mice was used as a positive control. Scale bars for histological sections represent 40µm. Statistical analysis: Student’s *t* test in all cases.

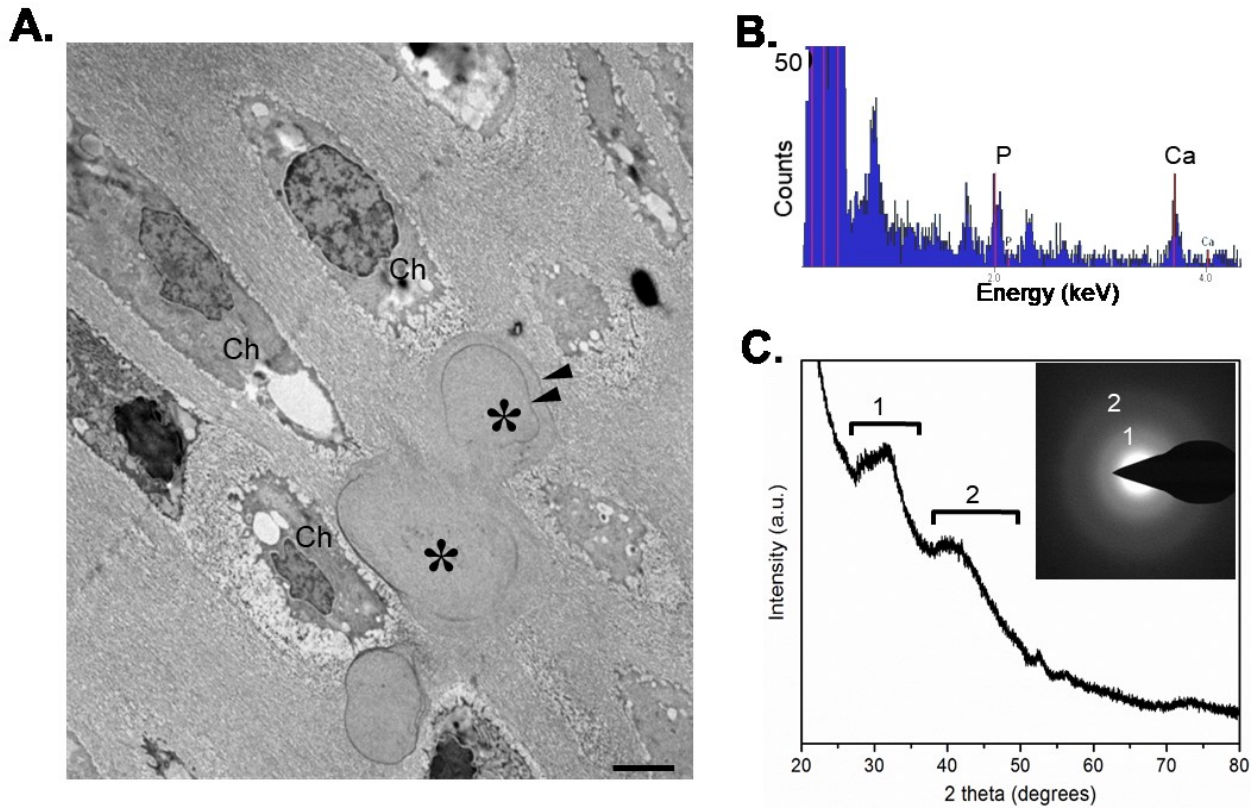


Figure 4.9. Amorphous calcium phosphate as main mineral species in MGP-deficient nasal septum

A. Transmission electron microscopy of 1-week-old *Mgp*^{-/-} nasal septum showing the presence of chondrocytes (Ch), and mineral deposits (asterisks) having an unusual globular shape. Note the incremental lines (suggesting periodic mineral deposition) within the mineral deposits (arrowheads). **B.** Energy-dispersive X-ray spectroscopy showing the presence of phosphorus and Ca^{2+} within the mineral deposits. **C.** X-ray diffraction showing that the mineral phase is largely amorphous calcium phosphate. Minor spectral peaks labelled 1 and 2 indicate tendencies toward crystallization (initiation) of an apatitic phase. Inset in C: Electron diffraction pattern confirming the presence of mostly amorphous mineral showing only diffuse (rather than sharp) electron diffraction rings labelled as 1 and 2 (n=3 mice for each group and each experiment).

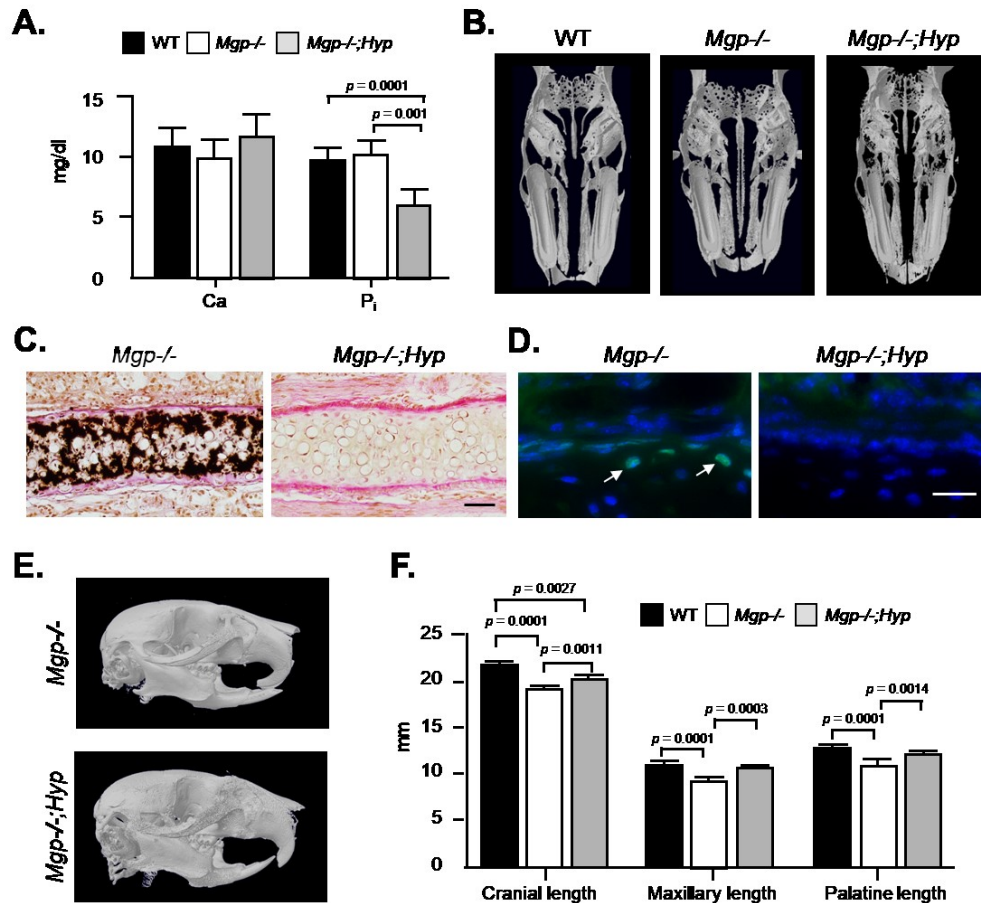


Figure 4.10. Prevention of nasal septum mineralization in *Mgp*^{-/-};*Hyp* mice

A. Serum Ca²⁺ and P_i levels in the WT, *Mgp*^{-/-} and *Mgp*^{-/-};*Hyp* mice show similar Ca²⁺ levels in all the genotypes and confirms the presence of hypophosphatemia in the *Mgp*^{-/-};*Hyp* mice. Values are shown in mg/dl. (n=4). **B.** 3D reconstruction of micro-CT scans of gender- and age-matched WT, *Mgp*^{-/-} and *Mgp*^{-/-};*Hyp* mice showing the correction of nasal septum mineralization in the double mutant. **C.** Histology of nasal septum of *Mgp*^{-/-} and *Mgp*^{-/-};*Hyp* mice stained with VKVG confirming the absence of apatitic minerals in the latter phenotype. Scale bar represents 50µm. **D.** Fluorometric TUNEL assay shows the presence of apoptotic immature chondrocytes in 3-week-old *Mgp*^{-/-} (arrows), but not in *Mgp*^{-/-};*Hyp* nasal septa. Images of the same field showing fluorescein-12-dUTP (labels fragmented DNA ends) and H33258 (nuclear stain) fluorescence were overlaid to create the combined images. Scale bar represents 25µm. **E.** 3D reconstruction of micro-CT scans of *Mgp*^{-/-} and *Mgp*^{-/-};*Hyp* mice. Note the correction of the midface hypoplasia and class III malocclusion in the compound mutant. **F.** Cephalometric analysis of WT, *Mgp*^{-/-} and age- and gender-matched *Mgp*^{-/-};*Hyp* mice showing a complete correction of the palatine and maxillary lengths in the *Mgp*^{-/-};*Hyp* mice. Although the cranial length is corrected in the *Mgp*^{-/-};*Hyp* mice when compared to *Mgp*^{-/-} mice, it remains shorter than the WT controls. All the analyses were performed in 5-week-old mice unless indicated otherwise (n=3 male mice in each group for each experiment) Statistical analysis: ANOVA (Tukey's multiple-comparison test).

Chapter 5:

General Discussion

5.1. General discussion

ECM mineralization is a physiologic process in the skeletal hard tissues, and a pathologic condition, when occurs in the soft tissues like cartilage and blood vessels [17]. The current understanding of ectopic calcification has been greatly benefited by our understanding of bone mineralization. A recurring theme explaining the spatial restriction of physiologic mineralization in bone suggests that the mineralization of bone ECM can be explained, in part, by the unique co-expression of tissue-nonspecific genes in bone forming osteoblasts [16]. Based on our understanding of bone mineralization and the identification of the common regulators of the ECM mineralization in general, several theories, not necessary mutually exclusive, have been proposed to explain the possible mechanisms for ectopic calcification of cartilage and blood vessels.

Keutel syndrome is a rare autosomal disorder caused by mutations in the *MGP* gene, hall marked by ectopic cartilage calcification, midface hypoplasia, peripheral pulmonary stenosis and vascular calcification [3, 6, 61]. MGP-null mice (*Mgp*^{-/-} mice) recapitulate most of the phenotypic abnormalities of the Keutel syndrome patients, albeit with a more severe vascular calcification phenotype. The first traces of vascular calcification in the thoracic aorta appear around day 8 and shortly thereafter, the homozygous mutant mice start growing slower, developing short stature [11, 62-64]. All *Mgp*^{-/-} mice die within two months of age due cardiovascular complications. As in Keutel syndrome patients, *Mgp*^{-/-} mice show a distinct craniofacial phenotype characterized by blunting of the midface and nasal bridge.

In the current thesis, I characterized the phenotype of the *Mgp*^{-/-} mice as a model to study the mechanisms of ectopic calcification in vascular tissues and cartilage, and thus, gaining insights into the pathophysiology of Keutel syndrome.

In the first paper (in the process of submission), I investigate the determinants of medial calcification in *Mgp*^{-/-} mice, in the light of skeletal tissue mineralization. The determinants that regulate bone and tooth mineralization also regulate different types of vascular calcification in humans and/or in the experimental models, if not always as the full array, but in isolation as independent regulators.

Indeed, an auxiliary mechanism involving several intracellular enzymes initiates physiologic ECM mineralization in the skeletal tissues. SMPD3 has been identified as an important regulator of both cartilage and bone ECM mineralization [173, 181]. This enzyme together with a downstream phosphatase may work through the MVs, the nanoscale (20-200 nm) extracellular bodies released by the cells, which provide a P_i rich microenvironment promoting the precipitation of apatitic crystals [17, 188].

A previous study showed that the initiation of vascular calcification in MGP-deficient mice does not involve chondrogenic/osteogenic transdifferentiation of the VSMCs [170]. In agreement with this finding, here I show that SMPD3, a chondrogenic/osteogenic marker, does not act as a regulatory enzyme for vascular calcification caused by MGP deficiency. This later finding suggests that MVs are less likely to be involved in medial calcification in *Mgp*^{-/-} mice. This result is not completely unexpected as I also report the presence of amorphous calcium phosphate without any presence of MVs in the calcified nasal septum of MGP-deficient mice [191].

However, once the arterial wall in *Mgp*^{-/-} mice is heavily calcified, a partial phenotypic change of the VSMCs to chondrogenic cells has been noticed, which results in the deposition of a cartilaginous ECM [63, 170]. Since SMPD3 has been shown to be critical for cartilage ECM

mineralization, we predicted that this enzyme might be involved in augmenting mineral deposition during the later stages (around 4 weeks after birth) of vascular calcification in MGP-deficient mice [173, 181]. However, the data presented in the first study ruled out this possibility. Nevertheless, this finding does not exclude the possible involvement of SMPD3 in other kind of vascular calcification e.g. heart valve and intimal calcification.

PHEX, an osteocyte-/osteoblast-specific protein acts as a systemic regulator of P_i ; and it has been shown that introducing *Phex* mutation (*Hyp*, causing hypophosphatemia) to *Mgp*^{-/-} mice, completely rescues the vascular calcification phenotype [16]. However, an intrinsic role of this membrane protein has been suggested recently. It has been shown that PHEX cleaves the mineralization inhibitor osteopontin, which is present in the skeletal hard tissues [32]. This latter observation was particularly interesting, as Speer *et al.* showed that osteopontin expression was induced in the arteries of MGP-deficient mice and more importantly, there was a significant increase of vascular calcification in *Mgp*^{-/-};*Opn*^{-/-} double null mice [169]. Thus, these findings raised a question regarding the role of FGF23-mediated reduction of P_i in the prevention of vascular calcification in *Mgp*^{-/-};*Hyp* mice. Here, I show that on a normal diet *Mgp*^{-/-};*ApoE*-*Fgf23* mice do not develop vascular calcification. This data conclusively show that the increase of systemic FGF23 and the resultant hypophosphatemia is the primary cause of the rescue of the phenotype in *Mgp*^{-/-};*Hyp* mice.

Additionally, my observation that feeding *Mgp*^{-/-};*ApoE*-*Fgf23* mice a high phosphorus diet only for 10 days can cause severe vascular calcification, provides an excellent model to study medial calcification. The strategies that have been commonly used to generate the models of vascular calcification are the DBA/2 mice, genetically prone to develop ectopic calcification,

fed a diet containing warfarin for 4 weeks [197]. Also, an adenine-rich diet together with high phosphorus, causes medial calcification in mice [198]. Additionally, a combination of high phosphorus diet and partial nephrectomy in mice on the DBA/2 background has been used. Although studies on these models have significantly contributed to our understanding of vascular calcification, there are some shortcomings, such as dependency on the genetic background, mild and delayed appearance of the calcification phenotype, unexpected lethality and the technical complexities to generate the surgical models.

Lastly, in the first paper I show that the total elastin content, but not the ortholog type is a determinant of medial calcification. Despite the functional and structural conservation of elastin across the species, mouse and human elastin orthologs show only 64.1% identity at the amino acid level. This is much lower than the average 78.5% amino acid sequence identity between mouse and human proteins [199]. This relatively low level of sequence identity, together with the fact that vascular calcification in Keutel syndrome patients is not as severe as in mice, [5, 6] raised the question whether mouse and human elastin have a comparable capacity to nucleate minerals.

I found that the medial calcification in MGP-deficient mice, which were also heterozygotes for the mouse *Eln* gene and homozygotes for the human *ELN* transgene (*Mgp*^{-/-}; *Eln*^{+/-}; *ELN*^{+/+} mice), mineralize comparably to that of *Mgp*^{-/-} mice with two functional alleles of the mouse *Eln* gene. Considering that the particular elastin ortholog combinations and gene dosages in these two strains result in comparable amounts of total elastin in the arteries, this result suggests a similar mineralization promoting capacity of the human elastin to that of mouse elastin. It appears that as is the case with the elastic properties, the ability of elastin to promote

mineral nucleation is also evolutionarily conserved. At this point, the cause of a milder vascular calcification phenotype in Keutel syndrome patients remains unknown. However, the much lower serum P_i levels in humans when compared to mice, may prevent the massive buildup of minerals in the human arteries lacking MGP. At this point, the involvement of additional regulatory mechanisms to prevent vascular calcification in humans cannot be ruled out.

The current analyses of MGP-deficient mice have established that not all types of vascular calcification traits can be grouped together as ectopic bone formation. Further, the genetic experiments presented here, provide an in-depth understanding of how two determinants, P_i and elastin, regulate vascular calcification caused by MGP deficiency. As a proof of principle, I provide evidence that at least some types of vascular calcification can be effectively prevented by the modulation of these determinants.

In the second paper, I analyzed various bone remodeling parameters in *Mgp*^{-/-} mice and investigated how the rescue of the vascular calcification phenotype affects them. Micro-CT and histomorphometric analyses showed that the mineralized tissue mass is reduced in the long bones as well as in the vertebrae of *Mgp*^{-/-} mice affecting both cortical and trabecular bones. Although osteoblast numbers were not significantly decreased in these mice, there was a reduction in MAR and BFR/BS indicative of poor bone formation by the mutant osteoblasts, which led me to conclude that the low bone mass phenotype in *Mgp*^{-/-} mice is primarily due to the poor bone formation by osteoblasts.

As *Mgp* is primarily expressed by VSMCs and chondrocytes [11, 224], a key focus of this study was to determine whether the loss of *Mgp* expression in one or both of these cell types caused the observed low bone mass phenotype. Previously, Murshed *et al* reported the

generation of *Mgp*^{-/-};*SM22-Mgp* mice, in which VSMC-specific expression of *Mgp* corrected all the vascular abnormalities seen in *Mgp*^{-/-} mice [167]. We generated the same transgenic line, and observed that despite the excessive mineralization of the growth plates, prevention of arterial calcification in *Mgp*^{-/-};*SM22-Mgp* mice alone was sufficient to fully rescue the low bone mass phenotype. Also, all the bone remodeling parameters affected by MGP-deficiency were corrected in this rescued model.

While the bone phenotype was corrected in *Mgp*^{-/-};*SM22-Mgp* mice, these data did not conclusively establish whether it is the rescue of *Mgp* expression by VSMCs per se, or the prevention of vascular calcification by the local synthesis of MGP in the arteries that corrected the bone phenotype. I reasoned that this issue could be addressed in a mouse model that lacks MGP globally, but the arterial calcification is significantly delayed or prevented without the restoration of *Mgp* expression [225-227]. For this purpose, I used the *Mgp*^{-/-};*Eln*^{+/-} mice, which accumulate a significantly lesser amount of minerals in the arterial walls [170]. Histomorphometric analysis of the bones of these mice showed that there was a normalization of the bone mass accrual. This later finding further strengthens the notion that vascular calcification is the cause of the low bone mass phenotype in *Mgp*^{-/-} mice.

It is not precisely known how arterial calcification may affect osteoblast function. One possible cause of this phenotype might be vascular abnormalities hampering the nutrient supply to the active osteoblasts. Indeed, arteriovenous malformations (AVMs) had been reported in multiple organs in *Mgp*^{-/-} mice [221]. In agreement with these findings, we observed that calcified arteries in *Mgp*^{-/-} bones become thickened and unusually branched which may affect the local nutrient transport. At this stage, however, a generalized effect of vascular calcification on the overall growth cannot be fully ruled out.

Several studies have shown an association between arterial calcification and low bone mass in human patients [208, 230]. However, the exact nature of this association and its significance is still unresolved. This study conclusively shows that the prevention of arterial calcification through overexpression of *Mgp* in the arterial walls or reduction of *Eln* gene dosage is sufficient to rescue the low bone mass phenotype seen in *Mgp*^{-/-} mice. These findings may help understanding the association between the pathophysiology of some forms of vascular calcification and the loss of bone mass in humans.

Despite the craniofacial phenotype of the Keutel syndrome patients and the analogous mouse model, the *Mgp*^{-/-} mice, the role of MGP in craniofacial development was unknown. In the third paper, I performed cephalometric analyses of *Mgp*^{-/-} heads at 5-week-old, which revealed severe midface abnormalities. Until now, these abnormalities were not fully characterized, and the underlying cause of this phenotype was unknown. These results suggested that overall; the craniofacial bones were undersized in the *Mgp*^{-/-} mice, which is expected considering their stunted growth. However, the maxilla and palatine bones were disproportionately smaller affecting the overall anteroposterior length.

Impaired vitamin K metabolism has also been associated with midface hypoplasia. For instance, inactivating mutations in the gene for VKORC1, which generates the reduced form of vitamin K₁, and GGCX, which uses it as a co-factor, both lead to Vitamin K-dependent clotting factor deficiency and midface hypoplasia [254, 255]. Similarly, babies born with Warfarin embryopathy also show midface abnormalities [236]. Considering that GGCX/VKORC1 mutations or fetal exposure to warfarin both affect gamma-carboxylation of Gla proteins, it is expected that these conditions would lead to the inactivation of the skeletal Gla proteins, e.g.

MGP and osteocalcin. However, I demonstrate that only MGP, but not osteocalcin deficiency, causes midface hypoplasia in mice.

The role of the nasal septum in midface development has been a matter of controversy for over half a century. Scott, in 1951, proposed that the nasal septum, as all other primary cartilages, acts as a growth center, separating the facial structures allowing the sagittal growth of the face [256]. Later in 1968, Moss proposed the nasal septum as a passive structure that serves a supportive role for the other craniofacial structures [151]. Here, I provide evidence that during the early phases of facial development, ectopic nasal septum mineralization affects the growth of the midface.

I performed an *in vivo* reporter assay to determine *Mgp* promoter activity in the developing craniofacial complex. For this purpose, I used a *Cre* transgenic line in which the gene encoding *Cre* recombinase was ‘knocked in’ at the *Mgp* locus by placing it directly under the control of the endogenous *Mgp* promoter and its regulatory elements [248]. I found strong *Mgp* promoter activity in the cranial vault sutures, cranial base synchondroses and in the nasal septum. It is interesting to note that despite the high level of *Mgp* expression in both SOS and ISS, only the SOS growth plates in *Mgp*^{-/-} mice showed mild mineralization irregularities, while the ISS growth plates remained unaffected. In addition, the cranial sutures were also not abnormally mineralized in these mice.

In order to investigate whether MGP acts locally to prevent abnormal nasal septum mineralization, we generated *Mgp*^{-/-};*Col2a1-Mgp* mice, which express MGP in the cartilaginous tissues only. Ectopic nasal septum mineralization was fully prevented in the *Mgp*^{-/-};*Col2a1-Mgp*

mice, together with the midface hypoplasia seen in *Mgp*^{-/-} controls, which establishes that MGP acts locally to prevent ectopic calcification [65].

During endochondral bone development, growth plate cartilage mineralization is a normal process that requires chondrocyte hypertrophy, hallmarked by type X collagen expression, and the release of matrix vesicles. Interestingly, chondrocyte hypertrophy and matrix vesicles appear not to be a prerequisite for ectopic mineralization of the cartilaginous ECM in the nasal septum of MGP-deficient mice. Khavandgar *et al.* reported a similar nonchondrogenic ectopic mineralization event in the arteries of MGP-deficient mice [258]. Based on this observation, I conclude that the initiation of ECM mineralization in the MGP-deficient nasal septum does not require cellular differentiation (nor release of abundant matrix vesicles), but happens spontaneously by calcium phosphate precipitation. As is the case in blood vessels, whether any particular ECM protein promotes this mineral precipitation in the absence of MGP is yet to be determined.

Analyses of the deposited mineral in the calcified nasal septum of MGP-deficient mice indicate that the mineral is primarily amorphous (noncrystalline) calcium phosphate. This finding indicates that MGP normally influences the early stages of calcium phosphate precipitation. At this point it is not known which structural features in MGP are essential for this function. Considering that osteocalcin, a Gla protein related to MGP, does not show any anti-mineralization function, the anti-mineralization function of MGP may not be solely attributable to the post-translational gamma-carboxylation of its glutamic acid residues.

My experimental data revealed an increased apoptosis in the MGP-deficient septal chondrocytes, which may explain, at least in part, the observed shortening of the nasal septum in

these mice. Hayano *et al* found that augmented BMP-SMAD signalling leads to apoptosis in the developing nasal cartilage through p53 upregulation [259]. A second hypothesis that can explain the increased apoptosis in the nasal septum of *Mgp*^{-/-} mice is the local increase of P_i caused by the solubilization of the early phase metastable mineral forms in the cartilaginous ECM. Inorganic phosphate has been shown to be a major regulator of apoptosis of hypertrophic chondrocytes in the developing endochondral bones [260]. As reported here, I found the presence of amorphous calcium phosphate precipitates in the calcified nasal septum. The unstable nature of this transient phase may allow the minerals to be readily dissolved, increasing the local P_i levels inducing apoptosis of the neighbouring cells.

Lastly, I found that systemic regulation of P_i levels in the serum is sufficient to prevent nasal septum mineralization in *Mgp*^{-/-};*Hyp* double mutant mice. This finding has a substantial clinical implication in that it demonstrates that nasal septum mineralization and craniofacial malformations can be modulated by systemic factors. Future preventive interventions can be developed based on this finding.

At this point an interesting question can be raised: *Is MGP a common link in craniofacial anomalies caused by abnormal cartilage calcification?* In fact, most of the abnormalities seen in Keutel syndrome are also common in Chondrodysplasia Punctata and Warfarin Embryopathy [3, 263, 264]. Although it is known that the inactivation of arylsulfatase E leads (ARSE) to Chondrodysplasia Punctata, the actual substrate and function of this enzyme is still unknown [144]. It has been suggested that mutation in ARSE leads to impaired vitamin K metabolism, which in turn inhibits the gammaglutamyl-carboxylation of Gla proteins including MGP [265].

Although it was reported that warfarin, a commonly used anti-coagulant, may inhibit ARSE *in vitro* [264], the primary pharmacological target of warfarin *in vivo* is the vitamin K epoxide reductase (VKORC1), an enzyme that recycles oxidized vitamin K1 to its reduced form after it has participated in the gamma-carboxylation of the Gla proteins. This explains the prevalence of Keutel syndrome-like craniofacial abnormalities in the babies born to pregnant mothers treated with warfarin or similar blood thinning agents [144, 266, 267]. Further supporting the pathophysiological link between gammacarboxylation and MGP, it was recently reported that patients with mutations in the gene encoding the gammaglutamyl-carboxylase (GGCX) are also often characterized by midface hypoplasia [255]. For example, Watzka et al reported the phenotypes of 9 patients with GGCX gene mutations, where 5 out of 9 patients showed midface hypoplasia [255].

In a genetic experiment, Murshed *et al.* demonstrated that transgenic overexpression of *Mgp* in bone results in mild impairment of bone mineralization. However, a mutant form of *Mgp* lacking the conserved Gla-residues did not cause any mineralization defect [65]. This observation further confirms the predicted role of the Gla-residues in MGP's function. While the genetic mutations in Keutel syndrome and several related disorders are now well-established, the mechanism of action of the proteins coded by these genes and their linked pathways in the developing skeleton still need to be elucidated. It is however apparent, that the loss of functional MGP is the common cause of all these syndromes.

5.2. Implications and Future directions

The current study has opened up new areas of research to further understand the mode of action of MGP and its role in vertebrate development and health. Future work in this regard may have important clinical implications for the treatment and/or management of diseases associated with ectopic calcification. Some implications of the above findings and possible future studies, have been discussed below:

- The data presented here further establishes that not all kind of soft tissue calcification can be grouped together as ectopic bone/cartilage formation. However, this does not rule out the possibility that some soft tissue calcification events, particularly in the vascular tissues, require an induction of the chondrogenic/osteogenic pathways [161]. A systematic comparison of the determinants regulating different types of vascular calcification may help finding the cures for calcification caused by different etiology.
- The bone loss in elderly have been linked to ectopic calcification. It has been suggested that the loss of bone mass, as a result of increased bone resorption, may lead to the mobilization of minerals from bone to the calcification-prone ectopic sites. However, in MGP-deficient mice, we did not observe this. Although there was a loss of bone mass as well as deposition of minerals in the blood vessels, we showed that the vascular calcification trait is responsible for the low bone mass in MGP-deficient mice [64], not

vice versa. Whether vascular calcification affects the bone mass in Keutel syndrome patients and/or other diseases associated with vascular calcification need to be examined.

- This study suggests that in addition to craniosynostosis and premature fusion of the cranial base synchondroses, abnormal development of the nasal septum due to its calcification during the early stages of facial development may lead to midface hypoplasia [191]. This observation provides support to the view of Scott, who originally proposed that the nasal septum acts as a critical growth center during the mid-face development. Whether other syndromes associated with abnormal cartilage calcification show similar facial anomalies remain to be seen. More importantly, whether the regulation of MGP expression and/or post translational modifications have been affected in these diseases need to be examined.

- We show that it is possible to prevent or delay the initiation and progression of vascular calcification in MGP-deficient mice by reducing the systemic levels of P_i or by decreasing the elastin content in the arteries. While these findings are exciting, it will be challenging to use them directly as therapeutic approaches. Novel therapeutic strategies to reduce the P_i levels locally in the soft tissues or selective drugs blocking the mineral nucleation sites on the elastic lamina might be proven as a viable approach to prevent the initiation and/or progression of ectopic mineralization.

- We have demonstrated that the local expression of *Mgp* in the cartilaginous tissues or reduction of the P_i levels in the circulation can completely prevent nasal septum calcification and can correct the craniofacial malformations in MGP-deficient mice [191].

These findings have a substantial clinical implication. Local delivery of anti-mineralization peptides or pharmacologic agents at the calcifying soft tissues may be an effective way to prevent facial anomalies without major surgical interventions. Considering its highly hydrophobic nature, intact MGP may not be an attractive molecule as a drug. Therefore, identifying MGP peptide(s) with the anti-mineralization properties will be critical in this regard.

- Despite the fact that MGP has emerged as a critical regulator of midface development and a strong inhibitor of vascular calcification, its mechanism of action is still unknown. As mentioned before, mouse MGP has 4 conserved glutamic acid residues which are post-translationally converted to Gla-residues. Further genetic experiments will be needed to directly examine the role these Gla-residues in soft tissue calcification *in vivo*. MGP undergoes an additional post-translational modification in its N-terminal region. *In vitro* studies using synthetic peptides suggested that three conserved serine residues (S3, S6 and S9) need to be phosphorylated to prevent the growth of the mineral crystals [9]. As is the case with the Gla-residues, the role of these conserved residues in the prevention of soft tissue calcification must be investigated *in vivo*. Finally, it will be interesting to investigate whether these post-translational events have distinct roles in the prevention of ectopic calcification at different phases of initiation and progression of the mineralization process and whether they have any cooperative effect on MGP's anti-mineralization function.

- The *Mgp*^{-/-} mice show a severe ectopic calcification of the nasal septum and a mild premature calcification of the spheno-occipital synchondrosis (SOS), without any signs of craniosynostosis [191]. This mouse model clearly demonstrates that midface hypoplasia can occur without the involvement of the cranial sutures. However, this model also showed a mild pathology of the SOS. Although cephalometric analyses suggested no significant contribution of this pathology to the midface hypoplasia, this needs to be confirmed in a model carrying an isolated pathology of nasal septum calcification and/or isolated premature closure of the SOS. Further studies of the mouse models of midface hypoplasia may reveal such isolated phenotypes.

- Genetically modified animal models have become indispensable tools for modern biomedical research aimed to understand and manage human diseases. However, the question remains whether long snouted animals like rodents represent the best models to study craniofacial development. Until recently, technological barriers prevented wide spread genetic modifications in more relevant animal models (e.g. primates). The development of new technologies of gene-editing such as CRISPR-Cas9 will represent an invaluable tool not just for generating suitable animal models with candidate human mutations resulting from genome-wide sequence analysis, but also for the treatment of such conditions.

Conclusion

MGP-deficient mice are a unique tool not only to understand the pathophysiology of Keutel syndrome, but also to study the molecular mechanisms of soft tissue calcification. Indeed, our study of these mice provided deeper insights on the role of MGP in the prevention of soft tissue calcification. More specifically, we show that 1) serum P_i levels and the matrix protein elastin are critical determinants for vascular calcification caused by MGP deficiency, 2) prevention of arterial calcification corrects the low bone mass phenotype in MGP-deficient mice, and finally, 3) MGP deficiency calcifies the cartilaginous nasal septum and impairs its growth, causing midface hypoplasia. Taken together, this study further reinforces the role of MGP in fundamental biological processes.

References

1. Keutel, J., G. Jorgensen, and P. Gabriel, *A new autosomal recessive syndrome peripheral pulmonary stenoses, brachytelephalangism, neural hearing loss and abnormal cartilage calcifications-ossification*. Birth Defects Orig. Artic Ser. VIII, 1972. **5**: p. 60-68.
2. Fryns, J.P., et al., *Calcification of cartilages, brachytelephalangy and peripheral pulmonary stenosis. Confirmation of the Keutel syndrome*. Eur J Pediatr, 1984. **142**(3): p. 201-3.
3. Munroe, P.B., et al., *Mutations in the gene encoding the human matrix Gla protein cause Keutel syndrome*. Nat Genet, 1999. **21**(1): p. 142-4.
4. Khosroshahi, H.E., et al., *Long term follow-up of four patients with Keutel syndrome*. Am J Med Genet A, 2014. **164A**(11): p. 2849-56.
5. Meier, M., et al., *Tracheobronchial stenosis in Keutel syndrome*. European Respiratory Journal, 2001. **17**(3): p. 566-569.
6. Ayyildiz, P., et al., *Keutel Syndrome: A Case Report With Aortic Calcification*. Firat Tip Dergisi, 2012. **17**(3): p. 167-169.
7. Price, P.A., M.R. Urist, and Y. Otawara, *Matrix Gla protein, a new gamma-carboxyglutamic acid-containing protein which is associated with the organic matrix of bone*. Biochem Biophys Res Commun, 1983. **117**(3): p. 765-71.
8. Price, P.A. and M.K. Williamson, *Primary structure of bovine matrix Gla protein, a new vitamin K-dependent bone protein*. J Biol Chem, 1985. **260**(28): p. 14971-5.
9. Schurgers, L.J., et al., *Post-translational modifications regulate matrix Gla protein function: importance for inhibition of vascular smooth muscle cell calcification*. J Thromb Haemost, 2007. **5**(12): p. 2503-11.
10. Weston, B.W. and P.E. Monahan, *Familial deficiency of vitamin K-dependent clotting factors*. Haemophilia, 2008. **14**(6): p. 1209-13.
11. Luo, G., et al., *Spontaneous calcification of arteries and cartilage in mice lacking matrix GLA protein*. Nature, 1997. **386**(6620): p. 78-81.
12. Speer, M.Y. and C.M. Giachelli, *Regulation of cardiovascular calcification*. Cardiovasc Pathol, 2004. **13**(2): p. 63-70.
13. Shanahan, C.M., et al., *Arterial calcification in chronic kidney disease: key roles for calcium and phosphate*. Circ Res, 2011. **109**(6): p. 697-711.
14. Kramer, C.K., et al., *Coronary artery calcium score prediction of all cause mortality and cardiovascular events in people with type 2 diabetes: systematic review and meta-analysis*. BMJ, 2013. **346**: p. f1654.
15. Valdivielso, J.M., *[Vascular calcification: types and mechanisms]*. Nefrologia, 2011. **31**(2): p. 142-7.
16. Murshed, M., et al., *Unique coexpression in osteoblasts of broadly expressed genes accounts for the spatial restriction of ECM mineralization to bone*. Genes Dev, 2005. **19**(9): p. 1093-104.
17. Murshed, M. and M.D. McKee, *Molecular determinants of extracellular matrix mineralization in bone and blood vessels*. Curr Opin Nephrol Hypertens, 2010. **19**(4): p. 359-65.

18. Vattikuti, R. and D.A. Towler, *Osteogenic regulation of vascular calcification: an early perspective*. Am J Physiol Endocrinol Metab, 2004. **286**(5): p. E686-96.
19. Doherty, T.M., et al., *Genetic determinants of arterial calcification associated with atherosclerosis*. Mayo Clin Proc, 2004. **79**(2): p. 197-210.
20. Towler, D.A. and L.L. Demer, *Thematic series on the pathobiology of vascular calcification: an introduction*. Circ Res, 2011. **108**(11): p. 1378-80.
21. Stewart, B.F., et al., *Clinical factors associated with calcific aortic valve disease. Cardiovascular Health Study*. J Am Coll Cardiol, 1997. **29**(3): p. 630-4.
22. O'Brien, K.D., *Epidemiology and genetics of calcific aortic valve disease*. J Investig Med, 2007. **55**(6): p. 284-91.
23. Cohen, G.F. and N.S. Vyas, *Sodium thiosulfate in the treatment of calciphylaxis*. J Clin Aesthet Dermatol, 2013. **6**(5): p. 41-4.
24. Shao, J.S., J. Cai, and D.A. Towler, *Molecular mechanisms of vascular calcification: lessons learned from the aorta*. Arterioscler Thromb Vasc Biol, 2006. **26**(7): p. 1423-30.
25. Bachra, B.N. and H.R. Fischer, *Recalcification of decalcified bone collagen in vitro as a model for biologic calcification*. Calcif Tissue Res, 1968: p. Suppl:7.
26. Eicher, E.M., et al., *Hypophosphatemia: mouse model for human familial hypophosphatemic (vitamin D-resistant) rickets*. Proc Natl Acad Sci U S A, 1976. **73**(12): p. 4667-71.
27. Henthorn, P.S., et al., *Different missense mutations at the tissue-nonspecific alkaline phosphatase gene locus in autosomal recessively inherited forms of mild and severe hypophosphatasia*. Proc Natl Acad Sci U S A, 1992. **89**(20): p. 9924-8.
28. *A gene (PEX) with homologies to endopeptidases is mutated in patients with X-linked hypophosphatemic rickets. The HYP Consortium*. Nat Genet, 1995. **11**(2): p. 130-6.
29. Fedde, K.N., et al., *Alkaline phosphatase knock-out mice recapitulate the metabolic and skeletal defects of infantile hypophosphatasia*. J Bone Miner Res, 1999. **14**(12): p. 2015-26.
30. de Oliveira, R.B., et al., *Vascular calcification in chronic kidney disease: a review*. J Bras Nefrol, 2013. **35**(2): p. 147-61.
31. Reynolds, J.L., et al., *Human vascular smooth muscle cells undergo vesicle-mediated calcification in response to changes in extracellular calcium and phosphate concentrations: a potential mechanism for accelerated vascular calcification in ESRD*. J Am Soc Nephrol, 2004. **15**(11): p. 2857-67.
32. Barros, N.M., et al., *Proteolytic processing of osteopontin by PHEX and accumulation of osteopontin fragments in Hyp mouse bone, the murine model of X-linked hypophosphatemia*. J Bone Miner Res, 2013. **28**(3): p. 688-99.
33. Shimada, T., et al., *Cloning and characterization of FGF23 as a causative factor of tumor-induced osteomalacia*. Proc Natl Acad Sci U S A, 2001. **98**(11): p. 6500-5.
34. Urakawa, I., et al., *Klotho converts canonical FGF receptor into a specific receptor for FGF23*. Nature, 2006. **444**(7120): p. 770-4.
35. Bai, X., et al., *Transgenic mice overexpressing human fibroblast growth factor 23 (R176Q) delineate a putative role for parathyroid hormone in renal phosphate wasting disorders*. Endocrinology, 2004. **145**(11): p. 5269-79.
36. Lampropoulos, C.E., I. Papaioannou, and D.P. D'Cruz, *Osteoporosis--a risk factor for cardiovascular disease?* Nat Rev Rheumatol, 2012. **8**(10): p. 587-98.

37. Golub, E.E., *Role of matrix vesicles in biomineralization*. Biochim Biophys Acta, 2009. **1790**(12): p. 1592-8.
38. Goldberg, M., et al., *Dentin: structure, composition and mineralization*. Front Biosci (Elite Ed), 2011. **3**: p. 711-35.
39. Li, X., H.Y. Yang, and C.M. Giachelli, *Role of the sodium-dependent phosphate cotransporter, Pit-1, in vascular smooth muscle cell calcification*. Circ Res, 2006. **98**(7): p. 905-12.
40. Crouthamel, M.H., et al., *Sodium-Dependent Phosphate Cotransporters and Phosphate-Induced Calcification of Vascular Smooth Muscle Cells: Redundant Roles for PiT-1 and PiT-2*. Arterioscler Thromb Vasc Biol, 2013. **33**(11): p. 2625-32.
41. Rautiainen, S., et al., *The role of calcium in the prevention of cardiovascular disease--a review of observational studies and randomized clinical trials*. Curr Atheroscler Rep, 2013. **15**(11): p. 362.
42. Block, G.A., et al., *Association of serum phosphorus and calcium x phosphate product with mortality risk in chronic hemodialysis patients: a national study*. Am J Kidney Dis, 1998. **31**(4): p. 607-17.
43. Arnold, W.V. and A. Fertala, *Skeletal diseases caused by mutations that affect collagen structure and function*. Int J Biochem Cell Biol, 2013. **45**(8): p. 1556-67.
44. Yang, X., et al., *ATF4 is a substrate of RSK2 and an essential regulator of osteoblast biology; implication for Coffin-Lowry Syndrome*. Cell, 2004. **117**(3): p. 387-98.
45. Maurice, P., et al., *Elastin fragmentation and atherosclerosis progression: the elastokine concept*. Trends Cardiovasc Med, 2013. **23**(6): p. 211-21.
46. Khavandgar, Z., et al., *Elastin haploinsufficiency impedes the progression of arterial calcification in MGP-deficient mice*. J Bone Miner Res, 2013.
47. Fleisch, H. and S. Bisaz, *Mechanism of calcification: inhibitory role of pyrophosphate*. Nature, 1962. **195**: p. 911.
48. Terkeltaub, R.A., *Inorganic pyrophosphate generation and disposition in pathophysiology*. Am J Physiol Cell Physiol, 2001. **281**(1): p. C1-C11.
49. Okawa, A., et al., *Mutation in Npps in a mouse model of ossification of the posterior longitudinal ligament of the spine*. Nat Genet, 1998. **19**(3): p. 271-3.
50. Nakamura, I., et al., *Association of the human NPPS gene with ossification of the posterior longitudinal ligament of the spine (OPLL)*. Hum Genet, 1999. **104**(6): p. 492-7.
51. Ho, A.M., M.D. Johnson, and D.M. Kingsley, *Role of the mouse ank gene in control of tissue calcification and arthritis*. Science, 2000. **289**(5477): p. 265-70.
52. Johnson, K., et al., *Chondrogenesis mediated by PPi depletion promotes spontaneous aortic calcification in NPP1^{-/-} mice*. Arterioscler Thromb Vasc Biol, 2005. **25**(4): p. 686-91.
53. Narisawa, S., N. Frohlander, and J.L. Millan, *Inactivation of two mouse alkaline phosphatase genes and establishment of a model of infantile hypophosphatasia*. Dev Dyn, 1997. **208**(3): p. 432-46.
54. Hesse, L., et al., *Tissue-nonspecific alkaline phosphatase and plasma cell membrane glycoprotein-1 are central antagonistic regulators of bone mineralization*. Proc Natl Acad Sci U S A, 2002. **99**(14): p. 9445-9.
55. Rutsch, F., et al., *Mutations in ENPP1 are associated with 'idiopathic' infantile arterial calcification*. Nat Genet, 2003. **34**(4): p. 379-81.

56. Lomashvili, K.A., W. Khawandi, and W.C. O'Neill, *Reduced plasma pyrophosphate levels in hemodialysis patients*. J Am Soc Nephrol, 2005. **16**(8): p. 2495-500.
57. O'Neill, W.C., M.K. Sigrist, and C.W. McIntyre, *Plasma pyrophosphate and vascular calcification in chronic kidney disease*. Nephrol Dial Transplant, 2010. **25**(1): p. 187-91.
58. Hackeng, T.M., et al., *Total chemical synthesis of human matrix Gla protein*. Protein Sci, 2001. **10**(4): p. 864-70.
59. Price, P.A., S.A. Faus, and M.K. Williamson, *Warfarin causes rapid calcification of the elastic lamellae in rat arteries and heart valves*. Arterioscler Thromb Vasc Biol, 1998. **18**(9): p. 1400-7.
60. Booth, S.L., *Skeletal functions of vitamin K-dependent proteins: not just for clotting anymore*. Nutr Rev, 1997. **55**(7): p. 282-4.
61. Teebi, A.S., et al., *Keutel syndrome: further characterization and review*. Am J Med Genet, 1998. **78**(2): p. 182-7.
62. Schinke, T., M.D. McKee, and G. Karsenty, *Extracellular matrix calcification: where is the action?* Nat Genet, 1999. **21**(2): p. 150-1.
63. El-Maadawy, S., et al., *Cartilage formation and calcification in arteries of mice lacking matrix Gla protein*. Connect Tissue Res, 2003. **44 Suppl 1**: p. 272-8.
64. Marulanda, J., et al., *Prevention of arterial calcification corrects the low bone mass phenotype in MGP-deficient mice*. Bone, 2013.
65. Murshed, M., et al., *Extracellular matrix mineralization is regulated locally; different roles of two gla-containing proteins*. J Cell Biol, 2004. **165**(5): p. 625-30.
66. O'Young, J., et al., *Matrix Gla protein inhibits ectopic calcification by a direct interaction with hydroxyapatite crystals*. J Am Chem Soc, 2011. **133**(45): p. 18406-12.
67. Price, P.A. and J.E. Lim, *The inhibition of calcium phosphate precipitation by fetuin is accompanied by the formation of a fetuin-mineral complex*. J Biol Chem, 2003. **278**(24): p. 22144-52.
68. Jahnke-Dechent, W., et al., *Fetuin-A regulation of calcified matrix metabolism*. Circ Res, 2011. **108**(12): p. 1494-509.
69. Stenvinkel, P., et al., *Low fetuin-A levels are associated with cardiovascular death: Impact of variations in the gene encoding fetuin*. Kidney Int, 2005. **67**(6): p. 2383-92.
70. Marechal, C., et al., *Serum fetuin-A levels are associated with vascular calcifications and predict cardiovascular events in renal transplant recipients*. Clin J Am Soc Nephrol, 2011. **6**(5): p. 974-85.
71. Li, Q., et al., *Pseudoxanthoma elasticum: clinical phenotypes, molecular genetics and putative pathomechanisms*. Exp Dermatol, 2009. **18**(1): p. 1-11.
72. Jiang, Q., et al., *Overexpression of fetuin-a counteracts ectopic mineralization in a mouse model of pseudoxanthoma elasticum (abcc6(-/-))*. J Invest Dermatol, 2010. **130**(5): p. 1288-96.
73. Baud'huin, M., et al., *RANKL, RANK, osteoprotegerin: key partners of osteoimmunology and vascular diseases*. Cell Mol Life Sci, 2007. **64**(18): p. 2334-50.
74. Heymann, M.F., et al., *Role of the OPG/RANK/RANKL triad in calcifications of the atheromatous plaques: comparison between carotid and femoral beds*. Cytokine, 2012. **58**(2): p. 300-6.
75. Bucay, N., et al., *osteoprotegerin-deficient mice develop early onset osteoporosis and arterial calcification*. Genes Dev, 1998. **12**(9): p. 1260-8.

76. Mizuno, A., et al., *Severe osteoporosis in mice lacking osteoclastogenesis inhibitory factor/osteoprotegerin*. *Biochem Biophys Res Commun*, 1998. **247**(3): p. 610-5.
77. Panizo, S., et al., *RANKL increases vascular smooth muscle cell calcification through a RANK-BMP4-dependent pathway*. *Circ Res*, 2009. **104**(9): p. 1041-8.
78. Yao, Y., A. Shahbazian, and K.I. Bostrom, *Proline and gamma-carboxylated glutamate residues in matrix Gla protein are critical for binding of bone morphogenetic protein-4*. *Circ Res*, 2008. **102**(9): p. 1065-74.
79. Orita, Y., et al., *Role of osteoprotegerin in arterial calcification: development of new animal model*. *Arterioscler Thromb Vasc Biol*, 2007. **27**(9): p. 2058-64.
80. Olesen, M., et al., *No influence of OPG and its ligands, RANKL and TRAIL, on proliferation and regulation of the calcification process in primary human vascular smooth muscle cells*. *Mol Cell Endocrinol*, 2012. **362**(1-2): p. 149-56.
81. Kiechl, S., et al., *Osteoprotegerin is a risk factor for progressive atherosclerosis and cardiovascular disease*. *Circulation*, 2004. **109**(18): p. 2175-80.
82. Ozkok, A., et al., *Osteoprotegerin/RANKL axis and progression of coronary artery calcification in hemodialysis patients*. *Clin J Am Soc Nephrol*, 2012. **7**(6): p. 965-73.
83. Moe, S.M., et al., *Medial artery calcification in ESRD patients is associated with deposition of bone matrix proteins*. *Kidney Int*, 2002. **61**(2): p. 638-47.
84. Moe, S.M., et al., *Uremia induces the osteoblast differentiation factor Cbfa1 in human blood vessels*. *Kidney Int*, 2003. **63**(3): p. 1003-11.
85. Shao, J.S., et al., *Msx2 promotes cardiovascular calcification by activating paracrine Wnt signals*. *J Clin Invest*, 2005. **115**(5): p. 1210-20.
86. Yao, Y., et al., *Inhibition of bone morphogenetic proteins protects against atherosclerosis and vascular calcification*. *Circ Res*, 2010. **107**(4): p. 485-94.
87. Speer, M.Y., et al., *Smooth muscle cells give rise to osteochondrogenic precursors and chondrocytes in calcifying arteries*. *Circ Res*, 2009. **104**(6): p. 733-41.
88. Zebboudj, A.F., M. Imura, and K. Bostrom, *Matrix GLA protein, a regulatory protein for bone morphogenetic protein-2*. *J Biol Chem*, 2002. **277**(6): p. 4388-94.
89. Lomashvili, K.A., et al., *Matrix Gla protein metabolism in vascular smooth muscle and role in uremic vascular calcification*. *J Biol Chem*, 2011. **286**(33): p. 28715-22.
90. Basalyga, D.M., et al., *Elastin degradation and calcification in an abdominal aorta injury model: role of matrix metalloproteinases*. *Circulation*, 2004. **110**(22): p. 3480-7.
91. Wang, S.S., et al., *Disruption of the aortic elastic lamina and medial calcification share genetic determinants in mice*. *Circ Cardiovasc Genet*, 2009. **2**(6): p. 573-82.
92. Morris, C.A. and C.B. Mervis, *Williams syndrome and related disorders*. *Annu Rev Genomics Hum Genet*, 2000. **1**: p. 461-84.
93. Proudfoot, D., et al., *Apoptosis regulates human vascular calcification in vitro: evidence for initiation of vascular calcification by apoptotic bodies*. *Circ Res*, 2000. **87**(11): p. 1055-62.
94. Dai, X.Y., et al., *Phosphate-induced autophagy counteracts vascular calcification by reducing matrix vesicle release*. *Kidney Int*, 2013. **83**(6): p. 1042-51.
95. Garcia, J.H. and H. Khang-Loon, *Carotid atherosclerosis. Definition, pathogenesis, and clinical significance*. *Neuroimaging Clin N Am*, 1996. **6**(4): p. 801-10.
96. Maw, T.T. and L. Fried, *Chronic kidney disease in the elderly*. *Clin Geriatr Med*, 2013. **29**(3): p. 611-24.

97. Taal, M.W., *Chronic kidney disease in general populations and primary care: diagnostic and therapeutic considerations*. Curr Opin Nephrol Hypertens, 2013. **22**(6): p. 593-8.
98. Schurgers, L.J., et al., *The circulating inactive form of matrix gla protein is a surrogate marker for vascular calcification in chronic kidney disease: a preliminary report*. Clin J Am Soc Nephrol, 2010. **5**(4): p. 568-75.
99. Pai, A.S. and C.M. Giachelli, *Matrix remodeling in vascular calcification associated with chronic kidney disease*. J Am Soc Nephrol, 2010. **21**(10): p. 1637-40.
100. Chen, N.X. and S.M. Moe, *Arterial calcification in diabetes*. Curr Diab Rep, 2003. **3**(1): p. 28-32.
101. Sinha, A. and N.R. Vyavahare, *High-glucose levels and elastin degradation products accelerate osteogenesis in vascular smooth muscle cells*. Diab Vasc Dis Res, 2013. **10**(5): p. 410-9.
102. Rachner, T.D., S. Khosla, and L.C. Hofbauer, *Osteoporosis: now and the future*. Lancet, 2011. **377**(9773): p. 1276-87.
103. Otero, J.E., et al., *Severe skeletal toxicity from protracted etidronate therapy for generalized arterial calcification of infancy*. J Bone Miner Res, 2013. **28**(2): p. 419-30.
104. Edouard, T., et al., *Efficacy and safety of 2-year etidronate treatment in a child with generalized arterial calcification of infancy*. Eur J Pediatr, 2011. **170**(12): p. 1585-90.
105. Osako, M.K., et al., *Estrogen inhibits vascular calcification via vascular RANKL system: common mechanism of osteoporosis and vascular calcification*. Circ Res, 2010. **107**(4): p. 466-75.
106. Hofbauer, L.C., et al., *Vascular calcification and osteoporosis--from clinical observation towards molecular understanding*. Osteoporos Int, 2007. **18**(3): p. 251-9.
107. Finger, R.P., et al., *Pseudoxanthoma elasticum: genetics, clinical manifestations and therapeutic approaches*. Surv Ophthalmol, 2009. **54**(2): p. 272-85.
108. Nitschke, Y. and F. Rutsch, *Genetics in arterial calcification: lessons learned from rare diseases*. Trends Cardiovasc Med, 2012. **22**(6): p. 145-9.
109. Campens, L., et al., *Characterization of cardiovascular involvement in pseudoxanthoma elasticum families*. Arterioscler Thromb Vasc Biol, 2013. **33**(11): p. 2646-52.
110. Karsenty, G., *The complexities of skeletal biology*. Nature, 2003. **423**(6937): p. 316-8.
111. Karsenty, G., H.M. Kronenberg, and C. Settembre, *Genetic control of bone formation*. Annu Rev Cell Dev Biol, 2009. **25**: p. 629-48.
112. Mackie, E.J., L. Tatarczuch, and M. Mirams, *The skeleton: a multi-functional complex organ: the growth plate chondrocyte and endochondral ossification*. J Endocrinol, 2011. **211**(2): p. 109-21.
113. Eaton, R.H. and D.W. Moss, *Kinetic studies on the orthophosphatase and iorganic pyrophosphatase activities of human alkaline phsophatase*. Enzymologia, 1968. **35**(3): p. 168-78.
114. Raggatt, L.J. and N.C. Partridge, *Cellular and molecular mechanisms of bone remodeling*. J Biol Chem, 2010. **285**(33): p. 25103-8.
115. Park, J.H., N.K. Lee, and S.Y. Lee, *Current Understanding of RANK Signaling in Osteoclast Differentiation and Maturation*. Mol Cells, 2017. **40**(10): p. 706-713.
116. Li, J., et al., *RANK is the intrinsic hematopoietic cell surface receptor that controls osteoclastogenesis and regulation of bone mass and calcium metabolism*. Proc Natl Acad Sci U S A, 2000. **97**(4): p. 1566-71.

117. Aliprantis, A.O., et al., *NFATc1 in mice represses osteoprotegerin during osteoclastogenesis and dissociates systemic osteopenia from inflammation in cherubism*. J Clin Invest, 2008. **118**(11): p. 3775-89.
118. Ducy, P. and G. Karsenty, *Two distinct osteoblast-specific cis-acting elements control expression of a mouse osteocalcin gene*. Mol Cell Biol, 1995. **15**(4): p. 1858-69.
119. Ducy, P., et al., *Osf2/Cbfa1: a transcriptional activator of osteoblast differentiation*. Cell, 1997. **89**(5): p. 747-54.
120. Gao, Y., et al., *Molecular cloning, structure, expression, and chromosomal localization of the human Osterix (SP7) gene*. Gene, 2004. **341**: p. 101-10.
121. Nakashima, K., et al., *The novel zinc finger-containing transcription factor osterix is required for osteoblast differentiation and bone formation*. Cell, 2002. **108**(1): p. 17-29.
122. Xiao, G., et al., *Cooperative interactions between activating transcription factor 4 and Runx2/Cbfa1 stimulate osteoblast-specific osteocalcin gene expression*. J Biol Chem, 2005. **280**(35): p. 30689-96.
123. Lee, B., et al., *Missense mutations abolishing DNA binding of the osteoblast-specific transcription factor OSF2/CBFA1 in cleidocranial dysplasia*. Nat Genet, 1997. **16**(3): p. 307-10.
124. Lapunzina, P., et al., *Identification of a frameshift mutation in Osterix in a patient with recessive osteogenesis imperfecta*. Am J Hum Genet, 2010. **87**(1): p. 110-4.
125. Biancalana, V., et al., *Confirmation and refinement of the genetic localization of the Coffin-Lowry syndrome locus in Xp22.1-p22.2*. Am J Hum Genet, 1992. **50**(5): p. 981-7.
126. Rice, J.S., M.K. Williamson, and P.A. Price, *Isolation and sequence of the vitamin K-dependent matrix Gla protein from the calcified cartilage of the soupfin shark*. J Bone Miner Res, 1994. **9**(4): p. 567-76.
127. Laroche, M., et al., *Osteoporosis and ischemic cardiovascular disease*. Joint Bone Spine, 2017. **84**(4): p. 427-432.
128. Vassalle, C. and A. Mazzone, *Bone loss and vascular calcification: A bi-directional interplay?* Vascul Pharmacol, 2016. **86**: p. 77-86.
129. Nakahara, T., et al., *Fibroblast growth factor 23 inhibits osteoblastic gene expression and induces osteoprotegerin in vascular smooth muscle cells*. Atherosclerosis, 2016. **253**: p. 102-110.
130. Tunon-Le Pouttel, D., et al., *Association of matrix Gla protein gene functional polymorphisms with loss of bone mineral density and progression of aortic calcification*. Osteoporos Int, 2014. **25**(4): p. 1237-46.
131. WHO, R.M.o.C.A., *Craniofacial anomalies and associated birth defects*. Global registry and database on craniofacial anomalies, 2001.
132. Wang, Y., et al., *Racial/Ethnic differences in survival of United States children with birth defects: a population-based study*. J Pediatr, 2015. **166**(4): p. 819-826 e2.
133. Hur, D.J., et al., *A novel MGP mutation in a consanguineous family: review of the clinical and molecular characteristics of Keutel syndrome*. Am J Med Genet A, 2005. **135**(1): p. 36-40.
134. Lefebvre, M., et al., *Severe X-linked chondrodysplasia punctata in nine new female fetuses*. Prenat Diagn, 2015. **35**(7): p. 675-84.
135. Couly, G.F., P.M. Coltey, and N.M. Le Douarin, *The triple origin of skull in higher vertebrates: a study in quail-chick chimeras*. Development, 1993. **117**(2): p. 409-29.

136. Szabo-Rogers, H.L., et al., *New directions in craniofacial morphogenesis*. Dev Biol, 2010. **341**(1): p. 84-94.
137. Sant'Anna, L.B. and D.O. Tosello, *Fetal alcohol syndrome and developing craniofacial and dental structures--a review*. Orthod Craniofac Res, 2006. **9**(4): p. 172-85.
138. Wei, X. and K.K. Sulik, *Pathogenesis of craniofacial and body wall malformations induced by ochratoxin A in mice*. Am J Med Genet, 1993. **47**(6): p. 862-71.
139. Twigg, S.R. and A.O. Wilkie, *New insights into craniofacial malformations*. Hum Mol Genet, 2015. **24**(R1): p. R50-9.
140. Wagner, E.F. and G. Karsenty, *Genetic control of skeletal development*. Curr Opin Genet Dev, 2001. **11**(5): p. 527-32.
141. Suzuki, A., et al., *Molecular mechanisms of midfacial developmental defects*. Dev Dyn, 2016. **245**(3): p. 276-93.
142. Hirasawa, T. and S. Kuratani, *Evolution of the vertebrate skeleton: morphology, embryology, and development*. Zoological Lett, 2015. **1**: p. 2.
143. Neskey, D., J.A. Eloy, and R.R. Casiano, *Nasal, septal, and turbinate anatomy and embryology*. Otolaryngol Clin North Am, 2009. **42**(2): p. 193-205, vii.
144. Weaver, K.N., et al., *Keutel syndrome: report of two novel MGP mutations and discussion of clinical overlap with arylsulfatase E deficiency and relapsing polychondritis*. Am J Med Genet A, 2014. **164A**(4): p. 1062-8.
145. Patel, N. and J.A. Fearon, *Treatment of the syndromic midface: a long-term assessment at skeletal maturity*. Plast Reconstr Surg, 2015. **135**(4): p. 731e-42e.
146. Cielo, C.M. and C.L. Marcus, *Obstructive sleep apnoea in children with craniofacial syndromes*. Paediatr Respir Rev, 2015. **16**(3): p. 189-96.
147. Hall, B.K. and D.S. Precious, *Cleft lip, nose, and palate: the nasal septum as the pacemaker for midfacial growth*. Oral Surg Oral Med Oral Pathol Oral Radiol, 2013. **115**(4): p. 442-7.
148. Scott, J.H., *Growth at facial sutures*. American Journal of Orthodontics, 1956. **42**(5): p. 381-387.
149. Kvinnsland, S., *Partial resection of the cartilaginous nasal septum in rats; its influence on growth*. Angle Orthod, 1974. **44**(2): p. 135-40.
150. Wong, K.K., S. Filatov, and D.J. Kibblewhite, *Septoplasty retards midfacial growth in a rabbit model*. Laryngoscope, 2010. **120**(3): p. 450-3.
151. Moss, M.L., et al., *The passive role of nasal septal cartilage in mid-facial growth*. Plast Reconstr Surg, 1968. **41**(6): p. 536-42.
152. Copray, J.C., *Growth of the nasal septal cartilage of the rat in vitro*. J Anat, 1986. **144**: p. 99-111.
153. Al Dayeh, A.A., et al., *Real-time monitoring of the growth of the nasal septal cartilage and the nasofrontal suture*. Am J Orthod Dentofacial Orthop, 2013. **143**(6): p. 773-83.
154. Delaire, J. and D. Precious, *Influence of the nasal septum on maxillonasal growth in patients with congenital labiomaxillary cleft*. Cleft Palate J, 1986. **23**(4): p. 270-7.
155. Dai, J., et al., *Postnatal Development of the Spheno-occipital Synchondrosis: A Histological Analysis*. J Craniofac Surg, 2017.
156. Lajeunie, E., et al., *FGFR2 mutations in Pfeiffer syndrome*. Nat Genet, 1995. **9**(2): p. 108.
157. Schell, U., et al., *Mutations in FGFR1 and FGFR2 cause familial and sporadic Pfeiffer syndrome*. Hum Mol Genet, 1995. **4**(3): p. 323-8.

158. Wilkie, A.O., et al., *Apert syndrome results from localized mutations of FGFR2 and is allelic with Crouzon syndrome*. Nat Genet, 1995. **9**(2): p. 165-72.
159. Meyers, G.A., et al., *Fibroblast growth factor receptor 3 (FGFR3) transmembrane mutation in Crouzon syndrome with acanthosis nigricans*. Nat Genet, 1995. **11**(4): p. 462-4.
160. Goldstein, J.A., et al., *Earlier evidence of spheno-occipital synchondrosis fusion correlates with severity of midface hypoplasia in patients with syndromic craniosynostosis*. Plast Reconstr Surg, 2014. **134**(3): p. 504-10.
161. Marulanda, J., S. Alqarni, and M. Murshed, *Mechanisms of vascular calcification and associated diseases*. Curr Pharm Des, 2014. **20**(37): p. 5801-10.
162. Wang, C.E., et al., *Extensive calcifications in portal venous system in a patient with hepatocarcinoma*. World J Gastroenterol, 2014. **20**(43): p. 16377-80.
163. Shanahan, C.M., et al., *Arterial Calcification in Chronic Kidney Disease: Key Roles for Calcium and Phosphate*. Circulation Research, 2011. **109**(6): p. 697-711.
164. Meyer, W.W., *The mode of calcification in atherosclerotic lesions*. Adv Exp Med Biol, 1977. **82**: p. 786-92.
165. Yogamundi Moon, J., *Factors affecting arterial calcification associated with atherosclerosis. A review*. Atherosclerosis, 1972. **16**(1): p. 119-26.
166. Teebi, A.S., et al., *Keutel syndrome: Further characterization and review*. American Journal of Medical Genetics, 1998. **78**(2): p. 182-187.
167. Murshed, M., et al., *Extracellular matrix mineralization is regulated locally; different roles of two gla-containing proteins*. The Journal of Cell Biology, 2004. **165**(5): p. 625-630.
168. Yao, Y., et al., *Matrix Gla protein deficiency causes arteriovenous malformations in mice*. J Clin Invest, 2011. **121**(8): p. 2993-3004.
169. Speer, M.Y., et al., *Inactivation of the osteopontin gene enhances vascular calcification of matrix Gla protein-deficient mice: evidence for osteopontin as an inducible inhibitor of vascular calcification in vivo*. J Exp Med, 2002. **196**(8): p. 1047-55.
170. Khavandgar, Z., et al., *Elastin Haploinsufficiency Impedes the Progression of Arterial Calcification in MGP-Deficient Mice*. Journal of Bone and Mineral Research, 2014. **29**(2): p. 327-337.
171. Abedin, M., Y. Tintut, and L.L. Demer, *Vascular calcification: mechanisms and clinical ramifications*. Arterioscler Thromb Vasc Biol, 2004. **24**(7): p. 1161-70.
172. Wuthier, R.E. and G.F. Lipscomb, *Matrix vesicles: structure, composition, formation and function in calcification*. Front Biosci (Landmark Ed), 2011. **16**: p. 2812-902.
173. Khavandgar, Z., et al., *A cell-autonomous requirement for neutral sphingomyelinase 2 in bone mineralization*. J Cell Biol, 2011. **194**(2): p. 277-89.
174. Kapustin, A.N., et al., *Vascular smooth muscle cell calcification is mediated by regulated exosome secretion*. Circ Res, 2015. **116**(8): p. 1312-23.
175. Giachelli, C.M., *The emerging role of phosphate in vascular calcification*. Kidney Int, 2009. **75**(9): p. 890-7.
176. Magalhaes, L.P., et al., *Predictive Factors of One-Year Mortality in a Cohort of Patients Undergoing Urgent-Start Hemodialysis*. PLoS One, 2017. **12**(1): p. e0167895.
177. Merhi, B., et al., *Serum Phosphorus and Risk of Cardiovascular Disease, All-Cause Mortality, or Graft Failure in Kidney Transplant Recipients: An Ancillary Study of the FAVORIT Trial Cohort*. Am J Kidney Dis, 2017. **70**(3): p. 377-385.

178. Li, S.S., et al., *Seven novel and six de novo PHEX gene mutations in patients with hypophosphatemic rickets*. *Int J Mol Med*, 2016. **38**(6): p. 1703-1714.
179. Strom, T.M., et al., *Pex gene deletions in Gy and Hyp mice provide mouse models for X-linked hypophosphatemia*. *Hum Mol Genet*, 1997. **6**(2): p. 165-71.
180. Liu, S., et al., *Regulation of fibroblastic growth factor 23 expression but not degradation by PHEX*. *J Biol Chem*, 2003. **278**(39): p. 37419-26.
181. Li, J., et al., *Smpd3 Expression in both Chondrocytes and Osteoblasts Is Required for Normal Endochondral Bone Development*. *Mol Cell Biol*, 2016. **36**(17): p. 2282-99.
182. Razali, N.N., T.T. Hwu, and K. Thilakavathy, *Phosphate homeostasis and genetic mutations of familial hypophosphatemic rickets*. *J Pediatr Endocrinol Metab*, 2015. **28**(9-10): p. 1009-17.
183. Hirano, E., et al., *Functional rescue of elastin insufficiency in mice by the human elastin gene: implications for mouse models of human disease*. *Circ Res*, 2007. **101**(5): p. 523-31.
184. Gourgas, O., et al., *Multidisciplinary Approach to Understand Medial Arterial Calcification*. *Arterioscler Thromb Vasc Biol*, 2017.
185. Morris, M.D. and G.S. Mandair, *Raman assessment of bone quality*. *Clin Orthop Relat Res*, 2011. **469**(8): p. 2160-9.
186. Cosmidis, J., et al., *Characterization of Ca-phosphate biological materials by scanning transmission X-ray microscopy (STXM) at the Ca L2,3-, P L2,3- and C K-edges*. *Acta Biomater*, 2015. **12**: p. 260-9.
187. Nudelman, F., et al., *The role of collagen in bone apatite formation in the presence of hydroxyapatite nucleation inhibitors*. *Nat Mater*, 2010. **9**(12): p. 1004-9.
188. Khavandgar, Z. and M. Murshed, *Sphingolipid metabolism and its role in the skeletal tissues*. *Cell Mol Life Sci*, 2015. **72**(5): p. 959-69.
189. Li, Q., et al., *Mutant Enpp1asj mice as a model for generalized arterial calcification of infancy*. *Dis Model Mech*, 2013. **6**(5): p. 1227-35.
190. Sheen, C.R., et al., *Pathophysiological role of vascular smooth muscle alkaline phosphatase in medial artery calcification*. *J Bone Miner Res*, 2015. **30**(5): p. 824-36.
191. Marulanda, J., et al., *Matrix Gla protein deficiency impairs nasal septum growth, causing midface hypoplasia*. *J Biol Chem*, 2017. **292**(27): p. 11400-11412.
192. Lu, X. and M.C. Hu, *Klotho/FGF23 Axis in Chronic Kidney Disease and Cardiovascular Disease*. *Kidney Dis (Basel)*, 2017. **3**(1): p. 15-23.
193. Yamada, S. and C.M. Giachelli, *Vascular calcification in CKD-MBD: Roles for phosphate, FGF23, and Klotho*. *Bone*, 2017. **100**: p. 87-93.
194. Sarmiento-Dias, M., et al., *Fibroblast growth factor 23 is associated with left ventricular hypertrophy, not with uremic vasculopathy in peritoneal dialysis patients*. *Clin Nephrol*, 2016. **85**(3): p. 135-41.
195. Grabner, A., et al., *Activation of Cardiac Fibroblast Growth Factor Receptor 4 Causes Left Ventricular Hypertrophy*. *Cell Metab*, 2015. **22**(6): p. 1020-32.
196. Lim, K., et al., *Vascular Klotho deficiency potentiates the development of human artery calcification and mediates resistance to fibroblast growth factor 23*. *Circulation*, 2012. **125**(18): p. 2243-55.
197. Kruger, T., et al., *Warfarin induces cardiovascular damage in mice*. *Arterioscler Thromb Vasc Biol*, 2013. **33**(11): p. 2618-24.

198. Tani, T., et al., *Development of a novel chronic kidney disease mouse model to evaluate the progression of hyperphosphatemia and associated mineral bone disease*. Sci Rep, 2017. **7**(1): p. 2233.
199. Piontkivska, H., et al., *Multi-species sequence comparison reveals dynamic evolution of the elastin gene that has involved purifying selection and lineage-specific insertions/deletions*. BMC Genomics, 2004. **5**(1): p. 31.
200. Iguchi, A., et al., *Effect of ferric citrate hydrate on FGF23 and PTH levels in patients with non-dialysis-dependent chronic kidney disease with normophosphatemia and iron deficiency*. Clin Exp Nephrol, 2017.
201. Boskey, A.L., *Amorphous calcium phosphate: the contention of bone*. J Dent Res, 1997. **76**(8): p. 1433-6.
202. Kim, K.M. and B.F. Trump, *Amorphous calcium precipitations in human aortic valve*. Calcif Tissue Res, 1975. **18**(2): p. 155-60.
203. Kavukcuoglu, N.B., et al., *Connective tissue mineralization in Abcc6^{-/-} mice, a model for pseudoxanthoma elasticum*. Matrix Biol, 2012. **31**(4): p. 246-52.
204. LeGeros, R.Z., *Formation and transformation of calcium phosphates: relevance to vascular calcification*. Z Kardiol, 2001. **90 Suppl 3**: p. 116-24.
205. Mahamid, J., et al., *Mapping amorphous calcium phosphate transformation into crystalline mineral from the cell to the bone in zebrafish fin rays*. Proc Natl Acad Sci U S A, 2010. **107**(14): p. 6316-21.
206. Danilevicius, C.F., J.B. Lopes, and R.M.R. Pereira, *Bone metabolism and vascular calcification*. Brazilian Journal of Medical and Biological Research, 2007. **40**(4): p. 435-442.
207. Aronow, W.S., *Osteoporosis, osteopenia, and atherosclerotic vascular disease*. Archives of Medical Science, 2011. **1**: p. 21-26.
208. Kovacic, J.C., et al., *Inverse relationship between body mass index and coronary artery calcification in patients with clinically significant coronary lesions*. Atherosclerosis, 2012. **221**(1): p. 176-182.
209. Murshed, M. and M.D. McKee, *Molecular determinants of extracellular matrix mineralization in bone and blood vessels*. Current Opinion in Nephrology and Hypertension, 2010. **19**(4): p. 359-365.
210. Hofbauer, L.C., et al., *Vascular calcification and osteoporosis—from clinical observation towards molecular understanding*. Osteoporosis International, 2006. **18**(3): p. 251-259.
211. Niederhoffer, N., et al., *Calcification of Medial Elastic Fibers and Aortic Elasticity*. Hypertension, 1997. **29**(4): p. 999-1006.
212. Stanford, W., B.H. Thompson, and R.M. Weiss, *Coronary artery calcification: clinical significance and current methods of detection*. American Journal of Roentgenology, 1993. **161**(6): p. 1139-1146.
213. Niskanen, L., et al., *Aortic and lower limb artery calcification in type 2 (non-insulin-dependent) diabetic patients and non-diabetic control subjects A five year follow-up study*. Atherosclerosis, 1990. **84**(1): p. 61-71.
214. Sage, A.P., Y. Tintut, and L.L. Demer, *Regulatory mechanisms in vascular calcification*. Nature Reviews Cardiology, 2010. **7**(9): p. 528-536.
215. O'Young, J., et al., *Matrix Gla Protein Inhibits Ectopic Calcification by a Direct Interaction with Hydroxyapatite Crystals*. Journal of the American Chemical Society, 2011. **133**(45): p. 18406-18412.

216. Spronk, H.M.H., et al., *Matrix Gla Protein Accumulates at the Border of Regions of Calcification and Normal Tissue in the Media of the Arterial Vessel Wall*. Biochemical and Biophysical Research Communications, 2001. **289**(2): p. 485-490.
217. Cranenburg, E.C.M., et al., *Uncarboxylated matrix Gla protein (ucMGP) is associated with coronary artery calcification in haemodialysis patients*. Thrombosis and Haemostasis, 2009.
218. Schurgers, L.J., et al., *The Circulating Inactive Form of Matrix Gla Protein Is a Surrogate Marker for Vascular Calcification in Chronic Kidney Disease: A Preliminary Report*. Clinical Journal of the American Society of Nephrology, 2010. **5**(4): p. 568-575.
219. Hur, D.J., et al., *A novel MGP mutation in a consanguineous family: Review of the clinical and molecular characteristics of Keutel syndrome*. American Journal of Medical Genetics Part A, 2005. **135A**(1): p. 36-40.
220. El-Maadawy, S., et al., *Cartilage Formation and Calcification in Arteries of Mice Lacking Matrix Gla Protein*. Connective Tissue Research, 2003. **44**(1): p. 272-278.
221. Yao, Y., et al., *Matrix Gla protein deficiency causes arteriovenous malformations in mice*. Journal of Clinical Investigation, 2011. **121**(8): p. 2993-3004.
222. Lee, N.K., et al., *Endocrine Regulation of Energy Metabolism by the Skeleton*. Cell, 2007. **130**(3): p. 456-469.
223. Oury, F., et al., *Endocrine Regulation of Male Fertility by the Skeleton*. Cell, 2011. **144**(5): p. 796-809.
224. Luo, G., et al., *The matrix Gla protein gene is a marker of the chondrogenesis cell lineage during mouse development*. Journal of Bone and Mineral Research, 2009. **10**(2): p. 325-334.
225. Li, D.Y., et al., *Elastin is an essential determinant of arterial morphogenesis*. Nature, 1998. **393**(6682): p. 276-80.
226. Starcher, B.C. and D.W. Urry, *Elastin coacervate as a matrix for calcification*. Biochemical and Biophysical Research Communications, 1973. **53**(1): p. 210-216.
227. Pai, A., et al., *Elastin Degradation and Vascular Smooth Muscle Cell Phenotype Change Precede Cell Loss and Arterial Medial Calcification in a Uremic Mouse Model of Chronic Kidney Disease*. The American Journal of Pathology, 2011. **178**(2): p. 764-773.
228. Ducy, P., et al., *Increased bone formation in osteocalcin-deficient mice*. Nature, 1996. **382**(6590): p. 448-52.
229. Szulc, P., et al., *Serum undercarboxylated osteocalcin correlates with hip bone mineral density in elderly women*. J Bone Miner Res, 1994. **9**(10): p. 1591-5.
230. Taylor, B.C., et al., *Matrix Gla protein and osteopontin genetic associations with coronary artery calcification and bone density: the CARDIA study*. Hum Genet, 2005. **116**(6): p. 525-8.
231. Ducy, P., et al., *A Cbfa1-dependent genetic pathway controls bone formation beyond embryonic development*. Genes & Development, 1999. **13**(8): p. 1025-1036.
232. Li, J., et al., *Lithium chloride attenuates BMP-2 signaling and inhibits osteogenic differentiation through a novel WNT/GSK3- independent mechanism*. Bone, 2011. **48**(2): p. 321-331.
233. Sider, K.L., J. Song, and J.E. Davies, *A new bone vascular perfusion compound for the simultaneous analysis of bone and vasculature*. Microscopy Research and Technique, 2009: p. NA-NA.

234. WHO, R.M.o.C.A., *Craniofacial anomalies and associated birth defects*. Global registry and database on craniofacial anomalies, 2000.
235. Lefebvre, M., et al., *Severe X-linked chondrodysplasia punctata in nine new female fetuses*. Prenat Diagn, 2015.
236. Starling, L.D., et al., *Fetal warfarin syndrome*. BMJ Case Rep, 2012. **2012**.
237. Martelli, H., Jr., et al., *Apert syndrome: report of a case with emphasis on craniofacial and genetic features*. Pediatr Dent, 2008. **30**(6): p. 464-8.
238. Mehndiratta, S., et al., *Fetotoxicity of warfarin anticoagulation*. Arch Gynecol Obstet, 2010. **282**(3): p. 335-7.
239. Sarnat, B.G. and M.R. Wexler, *Rabbit snout growth after resection of central linear segments of nasal septal cartilage*. Acta Otolaryngol, 1967. **63**(5): p. 467-78.
240. Cielo, C.M. and C.L. Marcus, *Obstructive sleep apnoea in children with craniofacial syndromes*. Paediatr Respir Rev, 2014.
241. Forte, A.J., et al., *Analysis of midface retrusion in Crouzon and Apert syndromes*. Plast Reconstr Surg, 2014. **134**(2): p. 285-93.
242. Chokdeemboon, C., et al., *FGFR1 and FGFR2 mutations in Pfeiffer syndrome*. J Craniofac Surg, 2013. **24**(1): p. 150-2.
243. Paliga, J.T., et al., *Premature closure of the spheno-occipital synchondrosis in Pfeiffer syndrome: a link to midface hypoplasia*. J Craniofac Surg, 2014. **25**(1): p. 202-5.
244. Howe, A.M., J.K. Hawkins, and W.S. Webster, *The growth of the nasal septum in the 6-9 week period of foetal development--Warfarin embryopathy offers a new insight into prenatal facial development*. Aust Dent J, 2004. **49**(4): p. 171-6.
245. Tie, J.K. and D.W. Stafford, *Structural and functional insights into enzymes of the vitamin K cycle*. J Thromb Haemost, 2016. **14**(2): p. 236-47.
246. Meier, M., et al., *Tracheobronchial stenosis in Keutel syndrome*. Eur Respir J, 2001. **17**(3): p. 566-9.
247. Luo, G., et al., *The matrix Gla protein gene is a marker of the chondrogenesis cell lineage during mouse development*. J Bone Miner Res, 1995. **10**(2): p. 325-34.
248. Borrás, T., M.H. Smith, and L.K. Buie, *A Novel Mgp-Cre Knock-In Mouse Reveals an Anticalcification/Antistiffness Candidate Gene in the Trabecular Meshwork and Peripapillary Scleral Region*. Invest Ophthalmol Vis Sci, 2015. **56**(4): p. 2203-14.
249. Ayyildiz, P., et al., *Keutel Syndrome: A Case Report With Aortic Calcification* Firat Tip Dergisi, 2012. **17**(3): p. 167-169.
250. Palhazı, P., R.K. Daniel, and A.M. Kosins, *The osseocartilaginous vault of the nose: anatomy and surgical observations*. Aesthet Surg J, 2015. **35**(3): p. 242-51.
251. Laurita, J., et al., *The Muenke syndrome mutation (FgfR3P244R) causes cranial base shortening associated with growth plate dysfunction and premature perichondrial ossification in murine basicranial synchondroses*. Dev Dyn, 2011. **240**(11): p. 2584-96.
252. Rosenberg, P., et al., *The role of the cranial base in facial growth: experimental craniofacial synostosis in the rabbit*. Plast Reconstr Surg, 1997. **99**(5): p. 1396-407.
253. Nah, H.D., et al., *Phenotype profile of a genetic mouse model for Muenke syndrome*. Childs Nerv Syst, 2012. **28**(9): p. 1483-93.
254. Tie, J.K., et al., *Characterization of vitamin K-dependent carboxylase mutations that cause bleeding and nonbleeding disorders*. Blood, 2016. **127**(15): p. 1847-55.
255. Watzka, M., et al., *Bleeding and non-bleeding phenotypes in patients with GGcX gene mutations*. Thromb Res, 2014. **134**(4): p. 856-65.

256. Scott, J., *Growth at facial sutures*. Am J Orthod Dentofacial Orthop, 1956. **42**(5): p. 381-387.
257. Anderson, H.C., *Matrix vesicles and calcification*. Curr Rheumatol Rep, 2003. **5**(3): p. 222-6.
258. Khavandgar, Z., et al., *Elastin haploinsufficiency impedes the progression of arterial calcification in MGP-deficient mice*. J Bone Miner Res, 2014. **29**(2): p. 327-37.
259. Hayano, S., et al., *Augmented BMP signaling in the neural crest inhibits nasal cartilage morphogenesis by inducing p53-mediated apoptosis*. Development, 2015. **142**(7): p. 1357-67.
260. Mansfield, K., R. Rajpurohit, and I.M. Shapiro, *Extracellular phosphate ions cause apoptosis of terminally differentiated epiphyseal chondrocytes*. J Cell Physiol, 1999. **179**(3): p. 276-86.
261. Eimar, H., et al., *Craniofacial and Dental Defects in the Colla1Jrt/+ Mouse Model of Osteogenesis Imperfecta*. J Dent Res, 2016. **95**(7): p. 761-8.
262. Lee, E.R., et al., *Neoepitopes reveal the features of type II collagen cleavage and the identity of a collagenase involved in the transformation of the epiphyses anlagen in development*. Dev Dyn, 2009. **238**(6): p. 1547-63.
263. Wainwright, H. and P. Beighton, *Warfarin embryopathy: fetal manifestations*. Virchows Arch, 2010. **457**(6): p. 735-9.
264. Franco, B., et al., *A cluster of sulfatase genes on Xp22.3: mutations in chondrodysplasia punctata (CDPX) and implications for warfarin embryopathy*. Cell, 1995. **81**(1): p. 15-25.
265. Herman, T.E. and M.J. Siegel, *Warfarin-induced brachytelephalangic chondrodysplasia punctata*. J Perinatol, 2010. **30**(6): p. 437-8.
266. Rost, S., et al., *Mutations in VKORC1 cause warfarin resistance and multiple coagulation factor deficiency type 2*. Nature, 2004. **427**(6974): p. 537-41.
267. Howe, A.M., et al., *Binder's syndrome due to prenatal vitamin K deficiency: a theory of pathogenesis*. Aust Dent J, 1992. **37**(6): p. 453-60.

Appendix I: Other papers published

In addition to the publications described before, I have also collaborated and coauthored the following articles during my doctoral studies:

1. Gourgas O, **Marulanda J**, Zhang P, Murshed M, Cerruti M. Structural and Chemical Characterization of Mineral Deposits in Calcified Aortas from MGP-Deficient Mice, a Model of Vascular Calcification. *Arteriosclerosis, Thrombosis and Vascular Biology*. 2017.
2. Dhaliwal J, **Marulanda J**, Li J, Alebrahim S, Feine JS, Murshed M. In vitro comparison of two titanium dental implant surface treatments: 3M™ESPE™ MDIs versus Ankylos®. *International Journal of Implant Dentistry*. 2017 Dec;3(1):27.
3. Alebrahim S, Khavandgar Z, **Marulanda J**, Murshed M. Inducible transient expression of Smpd3 prevents early lethality in fro/fro mice. *Genesis*. 2014 May;52(5):408-16.